THE EFFECT OF GENERAL IMPERFECTIONS

ON THE

BUCKLING OF CYLINDRICAL SHELLS

Thesis by

Johann Arbocz

In Partial Fulfillment of the Requirements

For the Degree of

Doctor of Philosophy

California Institute of Technology

Pasadena, California

1968

(Submitted May 1, 1968)

ACKNOWLEDGMENT

ABSTRACT

An experimental and theoretical investigation of the effect of general imperfections on the buckling load of a circular cylindrical shell under axial compression was carried out.

A non-contact probe has been used to make complete imperfection surveys on electroformed copper shells before and during the loading process up to the buckling load. The data recording process has been fully automated and the data reduction was done on an IBM 7094. Three-dimensional plots were obtained of the measured initial imperfection surfaces and of the growth of these imperfections under increasing axial load. The modal components of the measured imperfection surfaces were also obtained.

The theoretical solution located the limit points of the post-buckled states. A simplified imperfection model was used consisting of one axisymmetric and one asymmetric component. For global buckling the correlation between the theoretical buckling loads and the experimental values was found to be good.

iv

TABLE OF CONTENTS

TABLE OF CONTENTS (Cont'd)

TABLE OF CONTENTS (Cont'd)

LIST OF TABLES

LIST OF FIGURES

LIST OF FIGURES (Cont'd)

LIST OF FIGURES (Cont'd)

LIST OF SYMBOLS

λ	Nondimensional loading parameter $\left(\lambda = \sqrt{3(1-\nu^2)}\dfrac{R}{t}\dfrac{\sigma}{E}\right)$
ν	Poisson's Ratio
R	Shell radius
t	Shell thickness
σ	Axial stress
E	Young's Modulus
δ	Displacement of pick-up from conducting surface
V	Pick-up output voltage
X_1, Y_1	Coordinates locating origin of the best fit cylinder reference axis
ϵ_1, ϵ_2	Small angles in radians denoting the inclination of the best fit reference axis ($\epsilon_1 = \pi/2 - \alpha$; $\epsilon_2 = \pi/2 - \beta$ when using notation of Fig. 18)
$\overline{w}, \overline{W}$	Radial imperfection from perfect circular cylinder
x, y	Axial and circumferential coordinates on middle surface of shell, respectively
$\overline{x}, \overline{y}$	Nondimensional coordinates ($\overline{x} = \dfrac{2\pi x}{L}$, $\overline{y} = \dfrac{y}{R}$)
L	Length of the shell
A_{ij}	Coefficient of $\cos i\overline{y} \cdot \cos j\overline{x}$
B_{ij}	Coefficient of $\sin i\overline{y} \cdot \cos j\overline{x}$
C_{ij}	Coefficient of $\cos i\overline{y} \cdot \sin j\overline{x}$
D_{ij}	Coefficient of $\sin i\overline{y} \cdot \sin j\overline{x}$

LIST OF SYMBOLS (Cont'd)

Δ_i Nondimensional growth of initial imperfection after application of the ith load increment

$\overline{\xi}_i$ Nondimensional initial imperfection amplitude

η Nondimensional number indicating size of imperfection growth

ξ_i Nondimensional radial displacement amplitude

w, W Radial displacement

f, F Airy stress function

i, k Axial wave numbers

ℓ Circumferential wave number

$K_1, K_2, \ldots K_{10}$ Constants defined in Appendix A

$A, B, \ldots J$ Constants defined in Appendix A

$\alpha, \alpha_A, \alpha_1, \alpha_2, \alpha_3, \beta$ Mode shape parameters defined on page 35

C_1, C_2, C_3, C_4 Constants defined on page 37

I. INTRODUCTION

The stability of cylindrical shells under axial compression has been studied in the past both theoretically and experimentally by several investigators. Previously reported experimental studies (Ref. 1) showed that, when compared with the results predicted by the linearized small deflection theories of buckling, the experimental values were much lower and the data had a large scatter band. In the past decade the following five factors found acceptance as an explanation of the discrepancy between theory and experiments:

1. Initial geometrical imperfections of the order of a fraction of the wall thickness.

2. Nonuniformity of load distribution around the shell circumference.

3. Influence of boundary conditions.

4. Effect of prebuckling deformation caused by edge constraints.

5. Nuclei of plastic strain.

The influence of the load distribution on the buckling load is unknown. Little is known about the effect of the nuclei of plastic strain. However the influence of the boundary conditions and the effect of prebuckling deformations caused by edge constraints has been extensively investigated (Refs. 2, 3, 4, 5, and 6). Whereas for certain end conditions the solution of the linear buckling equations predicts buckling at $\lambda = 0.5$, for the clamped boundary conditions which are encountered almost exclusively in experiments the solution predicts buckling at

λ = 1.0. Including the effect of prebuckling deformations due to the edge constraints will lower the buckling load to only about λ = 0.85. Thus initial geometrical imperfections have come to be accepted as the main degrading factor in the load carrying capacity of cylindrical shells under axial compression. Since the pioneering paper by Donnell in 1934 (Ref. 7) there have been many refinements in the theoretical solutions (Refs. 8, 9, 10, 11, 12, and 13). Experimental studies, however, seem to have suffered under the very difficult task of accurately recording imperfections of the order of only fractions of the wall thicknesses.

The purpose of the work described in the main part of this thesis was to determine the effect of general initial imperfections on the buckling load of cylindrical shells under axial compression. This was done by carrying out complete imperfection surveys on the cylindrical shells before and during the loading process up to the buckling load. Also by tracing the growth of the initial imperfections during the loading process prior to buckling it was hoped to isolate those modal components which furnished the mechanism by which the initial imperfections reduced the buckling load.

II. EXPERIMENTAL PROGRAM

The following sections contain a description of the instrumentation designed to carry out the imperfection measurements, an outline of the check-out procedure used to assure the proper functioning of the individual components of the experimental set-up and a brief discussion about the fabrication of the test specimens and the procedure used to carry out the buckling tests. An outline of the imperfection measurements and a discussion of the data reduction process is also included.

1. Test Equipment

a. Traversing Mechanism

The specifications of the experimental program called for a scanning device that would be adequate to pick-up and record imperfections of only fractions of the test specimen's wall thickness of 0.004 in. In addition the scanning device had to travel both in the axial and in the circumferential directions in order to record a complete surface map of the shell being tested. The numbers[1], [2] etc. used in the following section refer to part numbers listed in Fig. 1.

The scanning device was built around an inductance-type, non-contacting pick-up which measured the air gap between the end of the pick-up and the conducting copper surface of the shell. The pick-up was installed in a movable support[3] which in turn was fixed to a long shaft[2] protruding inside the shell being tested. The 22 in. long, 1-3/8 in. diameter stainless steel shaft was ground on a cylindrical grinder to a straightness of less than 0.0001 in. total indicator reading.

This shaft was supported by two bronze bearings, which were pressed into an aluminum alloy supporting ring[1] and then lapped to fit the shaft. For better adjustment, the bronze bearings were partially split and could be tightened or loosened by fine thread set screws. The shaft could be moved axially in and out by means of a leadscrew[5] which was supported in a self-aligning bearing[66] pressed into the end-piece[4]. This in turn, was supported by the outer shell[12] consisting of a 5 in. diameter aluminum alloy tube. The leadscrew was driven by the axial motor[72] installed on the rear plate[17] of the end-cap[16]. The shaft was driven in the circumferential direction by the circumferential motor[71] installed at the rear side of a supporting plate[6] which traveled back and forth with the shaft in the axial direction. Whenever the shaft was driven in the circumferential direction the axial drive had to be disengaged in order to avoid moving the shaft axially because of the advancing or retreating nut on the leadscrew. The disengagement was accomplished by de-energizing a magnetic coupling[70]. The circumferential position of the pick-up was determined by the print control consisting of a microswitch which was triggered by the switching disk[9] which had 48 uniformly spaced notches machined into it. The traversing sequence which consisted of a circumferential scan followed by an axial advance was controlled by strategically spaced microswitches. It will be described in more detail in the section on the Model Control Unit. Figure 1 shows the assembly drawing of the traversing mechanism, and the partially assembled scanning mechanism can be seen in Fig. 2.

A schematic layout of the shell buckling experiment measuring imperfections is shown in Fig. 3. The following sections contain a detailed description of the individual components of the overall system.

b. Model Control Unit

As mentioned earlier, during the imperfection measurements, the shaft of the traversing device supporting the noncontact probe was driven alternatingly in the axial and circumferential directions by small electric motors. The control of this automatic sequence was accomplished by a series of relays controlled by microswitches. Figure 4 shows a schematic layout of the model control unit. To start the automatic scanning sequence the shaft had to be in the home position. Only then did pressing of the start button energize relay[2]. Energizing the relay made power available to the circumferential motor which started rotating the shaft in the counterclockwise direction. At the same time, relay[6] was energized, opening the clutch between the axial motor and the leadscrew to avoid a simultaneous axial advance. Upon completing its circumferential scan, the circular cam riding on the shaft tripped one of the circumferential limit switches. This stopped the circumferential motor, de-energized relay[6] which engaged the clutch between the axial motor and the leadscrew. At the same time relay[2] was also de-energized creating a pulse that operated relay[3], that latched relay[4], making power available to the axial motor which started advancing the shaft of the scanning device. Upon completing the preset axial advance the incremental switch was tripped stopping the axial motor and de-activating

relay[4]. This resulted in a pulse on relay[1], which latched relay[2] starting the circumferential motor in the clockwise direction, and the whole sequence was repeated. The automatic scanning with intermittent circumferential scans and axial advances continued until the shaft completed its full axial advance tripping the upper axial limit switch which stopped the sequence. The circumferential and the axial position of the noncontact probe was monitored by the output of two helipots. One helipot was driven by the circumferential motion, the other by the axial motion of the shaft. The output of the circumferential position indicator helipot was also used to drive the x-axis of the xy-plotter which recorded the pick-up signal directly on the y-axis of the graph paper.

The control of the traversing device could also be switched from automatic to manual. Then the circumferential and axial motion were controlled by separate 3-position switches eliminating the automatic sequencing. The completion of a full circumferential scan, or the full travel in the axial direction was determined by the limit switches.

c. Pick-up System

The pick-up circuit shown on Fig. 5 consisted of two inductance-type pick-ups, an oscillator, a differential amplifier and a demodulator. The pick-ups consisted of a coil with a powdered iron core excited by a 100 KHz signal generated by the oscillator. The impedance of the coils to this signal changed as their electromagnetic fields were disturbed by the eddy currents generated in the external

conducting surfaces. The reference pick-up was preset during the calibration of the active pick-up and its setting remained the same for any given test. By determining the change in impedance of the coil of the active pick-up the position of the external shell surface could be measured quite accurately. This was done by first amplifying the voltage across the active pick-up's coil 100 times on the differential amplifier, then demodulating this AC signal. The output of the demodulator, consisting of a DC voltage was then read on the digital voltmeter and recorded on cards by an IBM 526 card punch. Using the reference pick-up and the differential amplifier increased the sensitivity of the system to 1.0 volt per 0.001 in. as compared to a sensitivity of 0.25 volt per 0.001 in. if the active pick-up was used alone.

    d.   Data Control Unit

As can be seen from Fig. 3, the same digital voltmeter was used to read the strain gages on the load cell and the demodulated DC signal of the pick-up used to measure the imperfections of the test shell. To control the sequence of the signals fed to the digital voltmeter, a data control unit was built which included a 26 channel stepping switch circuit. Twenty-four channels were connected to the strain gages on the load cell, the 25th channel indicated the voltage of the power source used to energize the strain gage circuits, the 26th channel was the home position. It read the demodulated DC signal of the imperfection measuring pick-up. Using the stepping switch made it possible to read the strain gages automatically at a preset rate.

Channel 26 of the data control unit also included an adjustable time delay circuit. This circuit became necessary because of the finite sampling time required by the Cimron digital voltmeter. Thus when using channel 26 the punch signal from the circular cam trapped the output of the pick-up at that particular instant in the time delay circuit. This would allow time for the digital voltmeter to sample this signal and to come to an essentially constant reading. At the end of the preset time delay the circuit activated the card punch recording the last reading of the digital voltmeter.

e. Digital Voltmeter

The digital voltmeter used for the tests was made by Cimron Division of Lear Siegler Inc., Trademark Cimron, Model P9400B with a DC preamplifier mode 6812B. Balance time for a full scale change in the 5 digits was 300 milliseconds.

f. Card Punch

Recording of the data was done on an IBM 526 card punch with a capability of 15 characters per second. The format used to record the data was 9F8.4 with the last 8 columns used to record the run number and the card number. The run number was dialed in through a parameter board and the number of cards used was monitored on a card counter connected to the card punch.

2. Check-out of the Test Equipment

a. Scans of Known Contours

In checking out the pick-up system, a surface of known contour was scanned with the pick-up and its output was recorded by

the DVM card punch system, giving the recorded data in terms of

voltages. Later this data was converted into displacements on an

IBM 7094 by means of the pick-up's calibration curve. The shape of

the contour obtained by the pick-up measurements was then cross-

plotted with the shape of the contour as measured very accurately by

micrometer on an optical comparator. Figure 6 shows a cross-plot

of pick-up measurements vs. micrometer measurements. The

agreement between the two readings was excellent except for the

regions adjacent to the sharp step where the pick-up measurements

deviated from the exact shape due to the integrating feature of the

pick-up. The width of this region was approximately equal to the

diameter of the pick-up.

Since the scanning of the shells with the pick-up was to be done

continuously it was necessary to verify that the output of the digital

voltmeter, which was recorded in set intervals automatically on cards,

represented the true shape of the measured shell surface. The verifi-

cation was done by scanning a carefully machined surface of known

contour with the pick-up moving at constant speed and recording the

output of the pick-up by the DVM card punch system. A sample of

these data is shown in Fig. 7. The agreement between the pick-up

measurements and the measurements made with a micrometer was

once again very good except fot the regions close to sharp corners

where the integrating property of the pick-up smoothed out the shape

of the scanned surface.

b. Circumferential Time Delay Check-Out

During the circumferential scans a circular cam rotating with the shaft triggered a microswitch at every 7.5° (See Fig. 1 for details). This was the signal to the Model Control Unit to record the readings of the Digital Voltmeter on cards by the IBM card punch. The intermittent counterclockwise and clockwise circumferential motion resulted initially in misalignments of identical circumferential stations measured at different axial positions. This was caused by the fact that the circular cam triggered the microswitch at different positions depending upon whether it was moving clockwise or counterclockwise. This problem was solved by placing an adjustable time delay into the punch control circuit. Figure 8 explains in detail the triggering sequence with and without the time delay.

Proper adjustment of the time delay circuit was achieved with the help of an xy-plotter. The x-axis was driven by the circumferential position indicator helipot, whereas the y-axis was connected across the punch relay. Thus every punch was registered as a square wave on the graph paper. Using the graphs of the counterclockwise and clockwise scans done side by side the deviations from the planned exact punch locations were read off without any difficulty. Figure 9 shows a picture of the counterclockwise and clockwise punch signals. With the help of these graphs it was possible to compute the deviations of the actual punch signals from the planned exact punch locations. It was found that the punch intervals were kept as 7.5° ± 0.5°.

c. Hysteresis and Repeatability of the Measured Data

For the checkout of the system as a whole a thick-walled

aluminum cylinder was used. This cylinder was machined out of

standard thick-walled aluminum tubing and was precision honed so

that its deviations from roundness and its deviations from the mean

diameter combined were less than 0.0005 in. total indicator reading.

Basically it should not have mattered whether the circumfer-

ential scanning at any one axial station was done clockwise or

counterclockwise. However due to friction in the bronze bearings

and play in the overall mechanical system it was expected that a

certain amount of hysteresis would exist between the counterclockwise

and clockwise scans at any one axial station. Figure 10 shows plots

of the pick-up output during counterclockwise and clockwise circum-

ferential scans at three different axial stations. The maximum

deviation at any one point between the clockwise and counterclockwise

scans was less than 0.0003 in. , for most part of the plot less than

0.0001 in. It should be remarked here that originally, before making

the bronze bearings adjustable the hysteresis between the clockwise

and counterclockwise outputs was of the order of 0.001 in.

The final checkout of the system as a whole consisted of the

complete surface scan of the near perfect thick-walled aluminum

cylinder. The data were punched on cards, ran through the data re-

duction program and it was found that the maximum amplitude of any

one of the computed harmonics was less than 0.0006 in. This was in

good agreement with the previously mentioned tolerances of fabrication of this cylinder.

This complete surface scan was repeated at a later date and the reduced data compared with the results of the first scan. Repeatability was found to be very good. Table I gives some data on these measurements.

3. Fabrication of the Test Specimen

The cylindrical shells used for this testing program were fabricated by electroforming on wax mandrels. This process was used previously in other investigations (Ref. 14). About an inch thick layer of wax was first cast on water cooled mandrels. After the wax had hardened it was machined to the desired dimensions on a lathe and spray painted with a silver paint thinned with Toluene. The plating was carried out in a Copper Fluoborate bath. Because of previous experience, copper was retained as the plating material. The plating time was about 20 minutes per 0.001 in. of plate. After the plating was completed, the mandrel was rinsed thoroughly and the shell cut to the desired length while it was still on the mandrel. After the cutting operation the shell was then removed from the mandrel by melting out the wax. The excess wax and silver paint was removed from the finished shells with benzene. For a more detailed description of the plating process see references 14 and 15.

a. Wall Thickness

The average thickness of the test shells was determined before the buckling tests by weighing the shells. The specific gravity

used in the calculation of the thickness was 8.9. The thickness varia-
tion along the generator of the shells was determined by cutting strips
out of the first test specimens and determining their thickness by a
comparator. The thickness variation was found to be less than $\pm$ 2
per cent of the nominal value (See also Ref. 14).

   b.   Material Properties

   Tests to determine the material properties of the plated copper
were carried out in uniaxial tension. This was done by utilizing long
strips of the plated copper which were soldered into 1/8 in. thick
plates that were in turn clamped into the jaws of an Instron testing
machine. The strips had length to width ratios of about 80. The head
displacement of the testing machine was used as the measure of strain
and the load read from the Instron load cell.

   A determination of Poisson's ratio for each shell was not
attempted since its influence in the reduction of the buckling data is
of secondary importance. A value of 0.3 was used for this purpose.

   4.   Test Procedure

   The buckling tests were carried out in the controlled end-
displacement type testing machine shown in Fig. 11. By the use of
matched pairs of high precision thrust bearings the axial elastic
displacement under load of the testing machine was kept to a mini-
mum thus making the testing machine rigid in comparison with the
test specimen. The relative displacement of the two end plates of the
testing machine was controlled by four loading screws, which could
be adjusted independently to give the proper load distribution on the

shell, or turned simultaneously to increase the load up to the critical value. One complete turn of the screws gave a displacement of 0.025 in. Figure 12 shows the details of these displacement controlling screws. The springs shown in Fig. 11 were used to preload the testing machine when installing the test specimen in the machine and securing it to the upper end plate of the testing machine. The testing was carried out when the machine was in the position shown in Fig. 11. The end plate with the gear drive rested on pins and the opposite end rested on a set of rollers. By this arrangement the frictional torque produced when turning the gears was transmitted through the pins into the base plate on which the testing machine rested, and the test specimen was loaded by axial compression only.

a. Load Cell

During the buckling tests the load distribution was monitored and the total load was obtained by means of the load cell shown in Fig. 13. It consisted of a seamless, electroformed copper cylinder which was 0.015 in. thick, 3.00 in. long and 8.00 in. in diameter. Twenty-four foil type strain gages from Micro-Measurements Inc., Serial No. Ma-09-500BH-120 with extra stable characteristics were mounted on the cylinder equally spaced around the circumference. The ones on the inside were directly opposite to those on the outside. It has been shown in reference 14 that the strain measured by this type of arrangement represented very accurately the actual strain in the test shell. The load cell was secured to the end plate of the testing machine with a thin layer of Devcon. Devcon is a plastic-like

material in a putty state which hardens in several hours after the addition of a hardening agent.

b.   Calibration of the Pick-up

To carry out the imperfection measurements the traversing mechanism was installed in the position shown in Fig. 14 with the shaft protruding through the hole in the end-plate inside the load cell. To carry out the calibration of the pick-up which was installed in a movable support at the end of the protruding shaft, a short shell was cast with Cerrolow into the load cell as shown in Fig. 14.   Then the pick-up was moved vertically away from the surface of the shell 0.001 in. at a time recording the reading of the digital voltmeter each time.   Figure 15 shows a typical calibration curve with the working range and the preset position of the pick-up so indicated. Upon completion of the calibration the pick-up was preset to a position about at the center of the working range.   Next the shaft was retracted into the load cell, the short calibration shell was removed and the load cell was ready for the installment of the test shell.

c.   Installing the Test Shell

The test shell was fastened into an end ring with a low melting point alloy Cerrolow and its other end was secured to the load cell in the same manner.   After this operation was completed the end ring was secured to the upper end-plate by a thin layer of Devcon.   Upon hardening of the Devcon the cylinder was ready for testing.   Figure 16 shows the complete cylindrical shell testing configuration.

d. Initial Imperfection Measurements

After the installment of the test specimen was completed a full automatic imperfection scan of the shell was performed. The data was recorded both by the IBM card punch and by the xy-plotter. The imperfection measurements on the shells A7, A8, A9, and A10 were carried out with a pick-up 5/8 in. in diameter, whereas shell A12 was scanned with a smaller pick-up only 1/4 in. in diameter. Because of the integrating properties of the pick-up the axial increments were preset to be 0.50 in. for the large pick-up. In order to avoid unwanted edge effects the initial axial station was located 0.50 in. from the end of the shell which was cast into the load cell. The automatic scanning sequence was started with a counterclockwise circumferential scan at the initial axial station followed by an axial advance of 0.50 in. This was followed by a clockwise circumferential scan and the automatic sequence continued with intermittent axial advances and circumferential scans until the full length of the shell was covered. Shells A7, A8, A9, and A10 were 8.00 in. long, so 14 axial advances of 0.50 in. each were used. That put the last axial station 0.50 in. from the end ring thus avoiding the picking up of any unwanted edge effects. On shell A12 due to the smaller pick-up 30 axial advances of 0.24 in. each were used. Upon completion of the initial imperfection measurements the shaft of the scanning device was run back to its initial position.

e. Monitoring of the Strain Gages

Before carrying out the buckling tests the gages on the load cell were connected to a 24 channel bridge box which contained 24 Wheatstone bridge circuits. In order to minimize the effect of temperature changes an additional 24 strain gages were installed on a dummy cylinder and connected to the same bridge box where they formed one of the branches of the individual Wheatstone bridge circuits. The initial zero reading could be adjusted individually through differential shunt balances. The output of the bridge was monitored by a Cimron Digital Voltmeter. By using the stepping switch unit connected between the bridge and the digital voltmeter the readings of the 24 strain gages were recorded automatically by means of an IBM card punch. The total compressive load was computed by averaging the readings of all gages and using a previously determined calibration factor. The calibration of the load cell was carried out using a very accurate Schaevitz dynamometer-type load ring.

f. Buckling Procedure

Upon completion of the initial imperfection measurements the cylindrical shells were initially loaded to about one-sixth of the expected buckling load and the circumferential load distribution was made as uniform as possible by individually adjusting the four loading screws of the testing machine. This was followed by another complete automatic scanning of the shell surface. The duration of one automatic scan was about 1/2 hour. The strain gages were read before and after the completion of the scan and the load was taken as

the average of the two readings. The axial load was then increased

in small increments by turning the four loading screws simultane-

ously. After each loading the load distribution was adjusted again.

Also after each load increment another complete scan of the shell

surface was performed. Thus any change in the shell surface due to

the increase in loading was recorded. This was carried out up to

about two-thirds of the expected buckling load. After this point the

load distribution was no longer adjusted so as to prevent buckling

occurring during one of the adjustments. The load was increased in

small increments, each load increment followed by a complete scan

of the shell surface and the strain gages were monitored until buckling

occurred. It should be noted here that due to the working range of

0.125 in. of the pick-up used for the imperfection measurements, it

was possible to get a complete scan of the postbuckling shapes of the

shells tested.

5. Data Reduction - Main Program

As described in the previous sections the imperfection

measurements were carried out by scanning the surface of the test

shells by an inductance-type pick-up. The output of the pick-up was

monitored on a digital voltmeter whose readings were recorded at

preset intervals by an IBM 526 card punch on cards. Thus, upon

completion of each buckling test, there was a set of cards containing

the displacement pick-up calibration data in volts and displacements

and a set of cards containing the shell displacements given in volts

for each scan completed. These displacements were referred to the

end of the pick-up. The shell displacements were given in volts because they consisted of the readings of the digital voltmeter recorded at preset intervals.

The data reduction of the experimental measurements was done on an IBM 7094 digital computer. Figure 17 shows a flow chart of the main data reduction program. By using an overlay technique it could handle up to 29 x 97 = 2813 experimental points.

a. Best Fit Polynomial to Pick-up Calibration Data

The first step in the data reduction program consisted of fitting a best fit polynomial of the form

$$\delta = \sum_{n=o}^{N} a_n V^n$$

to the working range of the pick-up's calibration data. Figure 15 shows the calibration data of the pick-up used on shell A7 and the corresponding best fit polynomial curve.

The unknown coefficients a_n of the polynomial representation were determined by the Method of Least Squares and stored in a common block for later use. As a measure of the accuracy of the best fit approximation, the Xi-squared error was also computed. It was found that the best possible approximation, that is the approximation for which the Xi-squared error was the least, was obtained for $N = 16$.

Next the data reduction program converted the voltage readings of the initial imperfection scan into displacements in inches

using the polynomial representation of the calibration curve obtained in the previous step. These displacements were also stored in a common block for later use.

Upon completing the conversion of the data of the initial imperfection scan link[1] was erased from the core except for the results stored in common blocks.

b.   Definition of the "Perfect" Cylinder

In the experimental set up shown in Fig. 1 a certain misalignment of the shell center line with that of the traversing device was expected. Thus it was necessary to remove from the measured imperfection data the effects of such a misalignment. Also before the harmonic components of the measured imperfection surface could be computed it was necessary to define what was considered the perfect shell. This was accomplished by finding the best fit cylinder to the data of the initial imperfection scan. This was done by the Method of Least Squares by first computing the sum of the squares of the normal distances from the measured points in space to the surface of the assumed best fit cylinder.

$$S = \sum_{i=1}^{N} d_i^2 = \sum_{i=1}^{N} (R_i - R)^2 = f(X_1, Y_1, \epsilon_1, \epsilon_2, R)$$

(See Fig. 18)

Minimizing S with respect to the unknown parameters $X_1, Y_1, \epsilon_1, \epsilon_2$ and R yielded five simultaneous, nonlinear algebraic equations in the five unknowns. Assuming that $X_1, Y_1, \epsilon_1, \epsilon_2$ were small, these

equations were linearized and solved to determine the new reference axis system and to define the perfect cylinder.

In link[2] the data reduction program computed X_1, Y_1, ϵ_1, ϵ_2, R and stored them in a common block. Next it took the measured displacements reduced by link[1] which originally were referred to the end of the scanning pick-up from the common block and recomputed them with respect to the newly found best fit cylinder of radius R. Then the measured displacements, which now represented deviations from the perfect cylinder, were stored in the same common block. Upon completion of this step, link[2] was erased from the core except for the results stored in common blocks.

c. Finding the Harmonic Components of the Measured Imperfection Surface

Three different Fourier representations were used for the measured imperfection surfaces. The full wave representation in the axial direction involved the determination of four sets of harmonic components:

$$\overline{w}(x, y) = \sum_{m=o}^{N} \sum_{n=o}^{N} A_{mn} \cos m \frac{y}{R} \cos \frac{2n\pi x}{L} +$$

$$\sum_{m=1}^{N} \sum_{n=o}^{N} B_{mn} \sin m \frac{y}{R} \cos \frac{2n\pi x}{L} +$$

$$\sum_{m=o}^{N} \sum_{n=1}^{N} C_{mn} \cos m \frac{y}{R} \sin \frac{2n\pi x}{L} + \sum_{m=1}^{N} \sum_{n=1}^{N} D_{mn} \sin m \frac{y}{R} \sin \frac{2n\pi x}{L}$$

where

$$A_{mn} = \frac{2}{\pi L} \int_0^L \int_0^{2\pi R} \overline{w}(x, y) \cos m \frac{y}{R} \cos \frac{2n\pi x}{L} \, dy \, dx$$

$$B_{mn} = \frac{2}{\pi L} \int_0^L \int_0^{2\pi R} \overline{w}(x, y) \sin m \frac{y}{R} \cos \frac{2n\pi x}{L} \, dy \, dx$$

$$C_{mn} = \frac{2}{\pi L} \int_0^L \int_0^{2\pi R} \overline{w}(x, y) \cos m \frac{y}{R} \sin \frac{2n\pi x}{L} \, dy \, dx$$

$$D_{mn} = \frac{2}{\pi L} \int_0^L \int_0^{2\pi R} \overline{w}(x, y) \sin m \frac{y}{R} \sin \frac{2n\pi x}{L} \, dy \, dx$$

The half wave cosine representation in the axial direction involved the determination of two sets of harmonic components:

$$\overline{w}(x, y) = \sum_{m=o}^{N} \sum_{n=o}^{N} A_{mn} \cos m \frac{y}{R} \cos \frac{n\pi x}{L}$$

$$+ \sum_{m=1}^{N} \sum_{n=o}^{N} B_{mn} \sin m \frac{y}{R} \cos \frac{n\pi x}{L}$$

where

$$A_{mn} = \frac{1}{\pi L} \int_{-L}^{L} \int_{0}^{2\pi R} \overline{w}(x, y) \cos m \frac{y}{R} \cos \frac{n\pi x}{L} \, dy \, dx$$

$$B_{mn} = \frac{1}{\pi L} \int_{-L}^{L} \int_{0}^{2\pi R} \overline{w}(x, y) \sin m \frac{y}{R} \cos \frac{n\pi x}{L} \, dy \, dx$$

Finally the half wave sine representation in the axial direction also involved the determination of two sets of harmonic components:

$$\overline{w}(x, y) = \sum_{m=0}^{N} \sum_{n=1}^{N} C_{mn} \cos m \frac{y}{R} \sin \frac{n\pi x}{L} + \sum_{m=1}^{N} \sum_{n=1}^{N} D_{mn} \sin m \frac{y}{R} \sin \frac{n\pi x}{L}$$

where

$$C_{mn} = \frac{1}{\pi L} \int_{-L}^{L} \int_{0}^{2\pi} \overline{w}(x, y) \cos m \frac{y}{R} \sin \frac{n\pi x}{L} \, dy \, dx$$

$$D_{mn} = \frac{1}{\pi L} \int_{-L}^{L} \int_{0}^{2\pi} \overline{w}(x, y) \sin m \frac{y}{R} \sin \frac{n\pi x}{L} \, dy \, dx$$

Separate subroutines were written for the different Fourier representations. The double integrals involved in the determination of the required coefficients were carried out numerically using the trapesoidal rule. Before returning to the main program each sub-routine not only printed out the computed Fourier coefficients but also

punched them on cards. In addition, upon return to the main pro-
gram, the measured displacements representing the deviations from
the defined perfect cylinder were printed out and punched on cards.

After the data reduction of the initial imperfection measure-
ments was completed, the program returned to read in the data of the
second full scan. The data reduction of the second and of all the
subsequent full scans was done using the polynomial representation of
the pick-up calibration obtained during the data reduction of the
initial imperfection scan. However the position of the best fit cylinder
and with it the definition of the perfect cylinder were recomputed for
each scan.

Thus upon completion of the data reduction of the buckling test
of a shell by the layered main program the following output has been
obtained:

1. A list of the location of the best fit or perfect
   shell at each load level.

2. The measured shell displacements representing
   deviations from the perfect shell at each load
   level both listed and punched on cards.

3. The coefficients of any one of the three Fourier
   representations at each load level both listed
   and punched on cards.

6. <u>Data Reduction - Auxiliary Programs</u>

The output from the main data reduction program was examin-
ed in different ways.

a. Three-Dimensional Plots

The cards containing the measured deviations from the perfect shell at different load levels were used as the input to a plotting program. When the proper values were assigned to the built in flags this program prepared three-dimensional plots of the imperfection scans at different load levels by offsetting the origin of the successive circumferential scans by the proper amount along both the x- and y-axis. The same program was also used to prepare three-dimensional plots of the growth of imperfections at increasing load levels. This was done by subtracting from the measured shell surface at each load level the measured initial imperfections of the shell before calling the plotting subroutine. The three-dimensional plots were enhanced by using additional points computed by an Aitken interpolation routine.

b. Computing the Growth of Harmonic Components

The cards containing the computed coefficients of the chosen Fourier representation of the measured shell surfaces at each load level were used as the input to an auxiliary program that computed the growth of each of the coefficients with increasing loading. This was done by subtracting from the coefficients at each load level the corresponding coefficients from the initial scan.

7. Test Results

As stated in the introduction, the purpose of this experimental study was to determine the effect of initial imperfections on the buckling load of cylindrical shells under axial compression and to

find the mechanism by which imperfections reduce the load carrying capacity of the shells. The instrumentation was designed and built to detect such initial imperfections and to trace their growth during the loading process prior to buckling. The results of buckling tests on five cylindrical shells are reported here.

By using electroformed copper shells it was felt that the size of the unintended initial imperfections would be minimized. However all five shells had initial imperfections that were greater than the wall thicknesses of the respective shells as can be seen from Fig. 19 through Fig. 23 which show the initial surveys of shells A7, A8, A9, A10, and A12. The principal Fourier coefficients of these initial surveys, defined as the components whose amplitudes exceeded 5 per cent of the respective wall thicknesses, are summarized in Table II. Table III shows the variation of the "perfect" cylinder with load increments for the five shells tested.

Figures 24 through 26 show the growth of prebuckling deformation of shell A7 at different load levels prior to local buckling. Figure 27 shows the local buckling pattern of shell A7. It confirmed the visual observation made at the time of the buckling test which showed that the local buckling pattern consisted of two isolated waves on the central portion of the shell. The location of these initial buckles coincided with the most pronounced growth of the pre-buckling deformation just prior to the occurrence of the local buckling as shown in Fig. 26. Also at the location of the initial buckles there were very pronounced localized defects in the test

specimen as can be seen from the initial scan of shell A7, shown in Fig. 19.

Figures 28 through 31 show the growth of prebuckling deformations at the last load level prior to buckling for shells A8, A9, A10, and A12. Figure 32 shows the local buckling pattern of shell A10. Figures 33 through 37 show the postbuckling patterns of the five shells tested. It should be mentioned here that for better three-dimensional effect these figures should be observed at a rather shallow angle of incidence.

As stated previously, the load distribution was adjusted to be as uniform as possible with the four loading screws of the testing machine. The ajustment was done by equalizing the strain in the load cell at the 45°, 135°, 225°, and 315° position. Detailed results of the buckling tests for shells A7, A8, A9, A10, and A12 are summarized in Table IV. It includes the maximum variation in load distribution near buckling which was kept to about 20 per cent. Figures 38 and 39 show the load distribution on the five shells at the last load level before buckling.

Shells A7 and A10 failed initially in isolated localized buckles. These localized waves caused the load distribution to fall off in their neighborhood without appreciably affecting the load distribution over the rest of the circumference of the shell. After the initial local buckling the load was increased until general collapse occurred without attempting to adjust the load distribution. General collapse occurred in the same manner as for the other three shells A8, A9,

and A12 which did not have any initial local buckling, but at a lower

value of axial loading.

General collapse consisted of a snap-through which is

characteristic of this type of test. In all cases the postbuckling state

consisted of 2 to 3 rows of buckles that extended completely around

the circumference. The number of circumferential waves is noted in

Table IV.

The three-dimensional plots representing the growth of the

prebuckling deformations showed at a glance the general deformation

pattern of the shells before buckling. As seen from Fig. 26 and Figs.

28 through 31 there was a very pronounced growth of an imperfection

whose half wave length in the axial direction was approximately equal

to the length of the shell. The number of circumferential waves of

this predominant imperfection mode was approximately equal to the

number of circumferential waves in the postbuckled shape. However,

the wave length in the axial direction in the postbuckled shape was

considerably shorter than the length of the shell as can be seen from

Figs. 33 through 37.

In an attempt to isolate the "critical modal components" -

defined as those modal components which showed exponential growth

close to the critical load - harmonic analyses of the measured

imperfection surfaces were carried out at each load level. In order

to obtain the mathematical representation that would describe "best"

the measured imperfection surfaces different axial expansions were

used. Thus the Fourier coefficients of the full wave, the half wave

sine and the half wave cosine axial representations were calculated.

This involved the computation of approximately 1,400 Fourier

coefficients for each complete scan. Detailed investigation of the

rate of growth of these coefficients with increasing loading revealed

that the consideration should be restricted to coefficients with a

growth in excess of one per cent of the respective wall thicknesses

at the load level just before buckling. This would include all the

coefficients which approach exponential growth at the experimental

buckling load. Only about 40 of the computed Fourier coefficients

showed significant growth rate and only about 20 of these showed

exponential growth. All the coefficients that were investigated are

summarized in Table V. Figures 40 through 44 show the rate of

growth of three such "critical modal components" for shells A7, A8,

A9, A10, and A12 respectively. As can be seen from these figures

most of these curves representing the experimentally measured

growth rates approach a horizontal tangent at the experimental buck-

ling load. The same characteristic curves were obtained for some

of the other coefficients. However, most of the coefficients that

approach a horizontal tangent at the experimental buckling load had

similar circumferential and axial wave numbers.

III.   COMPARISON WITH THEORY

By tracing the growth of individual modal components of the measured imperfection surfaces during the loading process prior to buckling it was discovered that for each shell tested several different modal components seemed to approach a horizontal tangent at about the experimental buckling load.   It was, however, impossible to ascertain the exact value of loading at the respective points of horizontal tangency just from observation of the given experimental data.

In considering the available theoretical methods it was found that none of them were quite general enough to be used directly with the measured experimental values.   Koiter (Ref. 9) has presented an analytical procedure for obtaining the role of imperfections in imperfection sensitive structures.   Later, working with an imperfection in the form of the radial displacement component of the axisymmetric buckling mode $\overline{W} = \mu \cos(q_o x/R)$, he was able to show (Ref. 10) that such an imperfection would reduce the buckling load of a cylindrical shell under axial compression to as low as one-third of the classical value for values of μ only a fraction of the shell thickness.   However, he considered axisymmetric imperfections only.

In general, any radial imperfection pattern of the shell can be represented by a double Fourier series in the axial and circumferential coordinates.   Thus in an effort to gain insight into the effects of the nonlinear interactions of several buckling modes an approximate solution of the nonlinear Donnell type shell equations was obtained with the initial radial imperfection being represented by only three

terms of the double Fourier series, one axisymmetric and two

asymmetric ones. The approximate solution of the full nonlinear

equations was obtained as follows:

1. The compatibility equation was solved exactly for

the stress function F in terms of the assumed radial

displacement W and the measured imperfection $\overline{W}$.

This guaranteed that a kinematically admissible

displacement field would be associated with the solution

of the second equation, the condition of equilibrium.

2. The equation of equilibrium was solved approxi-

mately by substituting therein F, W, and $\overline{W}$ and then

applying the Galerkin procedure.

It should be mentioned here that a similar method of solution has been

used by Hutchinson (Ref. 12). However he restricted his imper-

fections to the form of a linear buckling mode of the cylindrical shell.

In the following solution this restriction was removed.

1. <u>Donnell's Shell Equations</u>

Assuming that the radial displacement W is positive outward

and that the membrane stress resultants can be obtained from an

Airy stress function F as $N_x = F,_{yy}$, $N_y = F,_{xx}$ and $N_{xy} = -F,_{xy}$,

then Donnell's equations for an imperfection cylindrical shell (Ref. 13)

can be written as:

$$\frac{1}{Et} \nabla^4 F - \frac{1}{R} W,_{xx} + \frac{1}{2} L (W, W + 2\overline{W}) = 0 \qquad (1.1)$$

$$\frac{Et^3}{12(1-\nu^2)} \nabla^4 W + \frac{1}{R} F,_{xx} - L(F, W+\overline{W}) = 0 \qquad (1.2)$$

where the nonlinear operator L is defined by

$$L(S, T) = S,_{xx} T,_{yy} - 2S,_{xy} T,_{xy} + S,_{yy} T,_{xx} \qquad (1.3)$$

and ∇^4 is the two-dimensional biharmonic operator. See Fig. 45 for notation.

2. Nonlinear Buckling Equations

The solution assumes initial imperfection shapes represented by

$$\overline{W} = \overline{\xi}_1 t \cos i\overline{x} + \overline{\xi}_2 t \cos k\overline{x} \cdot \cos \ell\overline{y} + \overline{\xi}_3 t \sin k\overline{x} \cdot \cos \ell\overline{y} \qquad (2.1)$$

The equilibrium state of the axially loaded cylinder will be expressed as:

$$W = \frac{\nu}{E} \sigma t + w \qquad (2.2)$$

$$F = -\frac{1}{2} \sigma t y^2 + f \qquad (2.3)$$

where the terms added to w and f constitute the membrane pre-buckling solution for the perfect shell. Further, w will be assumed as

$$w = \xi_1 t \cos i\overline{x} + \xi_2 t \cos k\overline{x} \cdot \cos \ell\overline{y} + \xi_3 t \sin k\overline{x} \cdot \cos \ell\overline{y} \qquad (2.4)$$

In the following approximate solution the effect of boundary conditions will be neglected. Although in some instances the shell buckling may be characterized by certain end conditions, as has been shown by Hoff (Ref. 5) and Kobayashi (Ref. 6), in this solution only the effect of initial imperfections on the buckling load is of interest.

Substituting the assumed form of W and $\overline{W}$ into the compatibility equation (1.1) yields

$$\frac{1}{Et} (F,_{xxxx} + 2F,_{xxyy} + F,_{yyyy}) = K_1 \cos 2k\overline{x} + K_2 \cos i\overline{x} + K_3 \cos 2\ell\overline{y} \tag{2.5}$$

$$+ K_4 \sin 2k\overline{x} + K_5 \cos k\overline{x} \cdot \cos \ell\overline{y} + K_6 \sin k\overline{x} \cdot \cos \ell\overline{y}$$

$$+ K_7 \cos(i+k)\overline{x} \cdot \cos \ell\overline{y} + K_8 \cos(i-k)\overline{x} \cdot \cos \ell\overline{y}$$

$$+ K_9 \sin(i+k)\overline{x} \cdot \cos \ell\overline{y} + K_{10} \sin(i-k)\overline{x} \cdot \cos \ell\overline{y}$$

where the constants K_1, K_2, ..., K_{10} are defined in Appendix A.

Since the boundary conditions of the finite shell will be neglected, therefore only a particular solution of equation (2.5) needs to be considered. To obtain such a particular solution let

$$F = -\frac{1}{2} \sigma t y^2 + f_p \tag{2.6}$$

where

$$f_p = A \cos 2k\overline{x} + B \cos i\overline{x} + C \cos 2\ell\overline{y} + D \sin 2k\overline{x} + E \cos k\overline{x} \cdot \cos \ell\overline{y}$$

$$+ F \sin k\overline{x} \cdot \cos \ell\overline{y} + G \cos(i+k)\overline{x} \cdot \cos \ell\overline{y} + H \cos(i-k)\overline{x} \cdot \cos \ell\overline{y} \;,$$

$$+ I \sin(i+k)\overline{x} \cdot \cos \ell\overline{y} + J \sin(i-k)\overline{x} \cdot \cos \ell\overline{y}$$

$$(2.7)$$

The unknown coefficients A, B, ..., J are determined by substituting the assumed F into equation (2.5) and equating coefficients of like terms. They are written out in detail in Appendix A.

Substituting the assumed form for W, $\overline{W}$ and the computed particular solution for F as given by equations (2.1), (2.2) and (2.3) into the equilibrium equation (1.2) yields the "error" $\mathcal{E}_N = \mathcal{E}_N$ $(\xi_1, \xi_2, \xi_3, \overline{x}, \overline{y})$. Using Galerkin's idea of minimization of the "error" with respect to a set of functions leads to a system of three nonlinear algebraic equations in the three unknowns ξ_1, ξ_2, ξ_3. Here these equations are obtained from the following integrals

$$\int_0^{2\pi} \int_0^{2\pi} \mathcal{E}_N(\xi_1, \xi_2, \xi_3, \overline{x}, \overline{y}) \cdot \cos i\overline{x} \, d\overline{x} \, d\overline{y} = 0 \qquad (2.8)$$

$$\int_0^{2\pi} \int_0^{2\pi} \mathcal{E}_N(\xi_1, \xi_2, \xi_3, \overline{x}, \overline{y}) \cdot \cos k\overline{x} \cdot \cos \ell\overline{y} \, d\overline{x} \, d\overline{y} = 0 \qquad (2.9)$$

$$\int_0^{2\pi} \int_0^{2\pi} \mathcal{E}_N(\xi_1, \xi_2, \xi_3, \bar{x}, \bar{y}) \cdot \sin k\bar{x} \cdot \cos \ell\bar{y} \, d\bar{x} \, d\bar{y} = 0 \qquad (2.10)$$

Imposing the restriction $k = \frac{i}{2}$, carrying out the indicated integrations and introducing the following nondimensional parameters

$$\alpha_A^2 = i^2 \frac{Rt}{2c} \left(\frac{2\pi}{L}\right)^2 \qquad\qquad \alpha_2^2 = (i-k)^2 \frac{Rt}{2c}\left(\frac{2\pi}{L}\right)^2$$

$$\alpha^2 = k^2 \frac{Rt}{2c}\left(\frac{2\pi}{L}\right)^2 \qquad\qquad \alpha_3^2 = \frac{i^4}{k^2} \frac{Rt}{2c}\left(\frac{2\pi}{L}\right)^2$$

$$\qquad\qquad\qquad\qquad\qquad\qquad\qquad\qquad\qquad (2.11)$$

$$\alpha_1^2 = (i+k)^2 \frac{Rt}{2c}\left(\frac{2\pi}{L}\right)^2 \qquad\qquad \beta^2 = \ell^2 \frac{Rt}{2c}\left(\frac{1}{R}\right)^2$$

$$\lambda = c \frac{R}{t} \frac{\sigma}{E} \qquad\qquad\qquad c = \sqrt{3(1-\nu^2)}$$

yields the following equilibrium equations:

$$\xi_1 \left\{ \frac{1}{2}\left(\alpha_A^2 + \frac{1}{\alpha_A^2}\right) - \lambda \right\} + \frac{c}{16}\left\{ \frac{\beta^2}{\alpha^2} \right\} \left[\bar{\xi}_2 \xi_2 - \bar{\xi}_3 \xi_3 + \frac{1}{2}(\xi_2^2 - \xi_3^2) \right]$$

$$+ \frac{c}{4}\left\{ \frac{\alpha^2 \beta^2}{(\alpha^2 + \beta^2)^2} \right\} \left[(\xi_2 + \bar{\xi}_2)\xi_2 - (\xi_3 + \bar{\xi}_3)\xi_3 \right] \qquad (2.12)$$

$$+ \frac{c}{2}\left\{ \frac{\alpha_A^2 \beta^4}{(\alpha_1^2 + \beta^2)^2} + \frac{\alpha_A^2 \beta^4}{(\alpha_2^2 + \beta^2)^2} \right\} \left\{ (\xi_2 + \bar{\xi}_2)\left[(\xi_1 + \bar{\xi}_1)\xi_2 + \bar{\xi}_2 \xi_1 \right] \right.$$

$$+ (\xi_3 + \bar{\xi}_3)\left. \left[(\xi_1 + \bar{\xi}_1)\xi_3 + \bar{\xi}_3 \xi_1 \right] \right\} = \lambda \bar{\xi}_1$$

$$\xi_2 \left\{ \frac{1}{2} \left[\frac{(\alpha^2+\beta^2)^2}{\alpha^2} + \frac{\alpha^2}{(\alpha^2+\beta^2)^2} \right] - \lambda \right\} + 2c \left\{ \frac{\alpha^2\beta^2}{(\alpha^2+\beta^2)^2} \right\} \left[2(\xi_1 + \overline{\xi}_1)\xi_2 + \overline{\xi}_2\xi_1 \right]$$

$$+ \frac{c}{2} \left\{ \frac{\beta^2}{\alpha^2} \right\} (\xi_2 + \overline{\xi}_2)\xi_1 + \frac{c^2}{4} \left\{ \frac{\beta^4}{\alpha^2} \right\} \left\{ (\xi_3 + \overline{\xi}_3) \left[(\xi_2 + \overline{\xi}_2)\xi_3 + \overline{\xi}_3\xi_2 \right] \right.$$

$$\left. + (\xi_2 + \overline{\xi}_2) \left[\overline{\xi}_2\xi_2 - \overline{\xi}_3\xi_3 + \frac{1}{2}(\xi_2^2 - \xi_3^2) \right] \right\} \tag{2.13}$$

$$+ \frac{c^2}{4} \left\{ \alpha^2 \right\} \left[\overline{\xi}_2\xi_2 + \overline{\xi}_3\xi_3 + \frac{1}{2}(\xi_2^2 + \xi_3^2) \right] (\xi_2 + \overline{\xi}_2)$$

$$+ \frac{c^2}{2} \left\{ \frac{\alpha_3^2\beta^4}{(\alpha_1^2+\beta^2)^2} + \frac{\alpha_3^2\beta^4}{(\alpha_2^2+\beta^2)^2} \right\} \left[(\xi_1 + \overline{\xi}_1)\xi_2 + \overline{\xi}_2\xi_1 \right] (\xi_1 + \overline{\xi}_1) = \lambda \overline{\xi}_2$$

$$\xi_3 \left\{ \frac{1}{2} \left[\frac{(\alpha^2+\beta^2)^2}{\alpha^2} + \frac{\alpha^2}{(\alpha^2+\beta^2)^2} \right] - \lambda \right\} - 2c \left\{ \frac{\alpha^2\beta^2}{(\alpha^2+\beta^2)^2} \right\} \left[2(\xi_1 + \overline{\xi}_1)\xi_3 + \overline{\xi}_3\xi_1 \right]$$

$$- \frac{c}{2} \left\{ \frac{\beta^2}{\alpha^2} \right\} (\xi_3 + \overline{\xi}_3)\xi_1 - \frac{c^2}{4} \left\{ \frac{\beta^4}{\alpha^2} \right\} \left\{ (\xi_3 + \overline{\xi}_3) \left[\overline{\xi}_2\xi_2 - \overline{\xi}_3\xi_3 + \frac{1}{2}(\xi_2^2 - \xi_3^2) \right] \right.$$

$$\tag{2.14}$$

$$\left. - (\xi_2 + \overline{\xi}_2) \left[(\xi_2 + \overline{\xi}_2)\xi_3 + \overline{\xi}_3\xi_2 \right] \right\} + \frac{c^2}{4} \left\{ \alpha^2 \right\} \left[\overline{\xi}_2\xi_2 + \overline{\xi}_3\xi_3 + \frac{1}{2}(\xi_2^2 + \xi_3^2) \right] (\xi_3 + \overline{\xi}_3)$$

$$+ \frac{c^2}{2} \left\{ \frac{\alpha_3^2\beta^4}{(\alpha_1^2+\beta^2)^2} + \frac{\alpha_3^2\beta^4}{(\alpha_2^2+\beta^2)^2} \right\} \left[(\xi_1 + \overline{\xi}_1)\xi_3 + \overline{\xi}_3\xi_1 \right] (\xi_1 + \overline{\xi}_1) = \lambda \overline{\xi}_3$$

A solution of these "nonlinear equations" would yield the equilibrium configuration of the finite shell as a function of λ. However for $\bar{\xi}_1$ and $\bar{\xi}_2$ small enough the essential character of the shell in the pre-buckling and the immediate postbuckling configuration is retained if the terms of the order $\bar{\xi}\bar{\xi}^2$, $\bar{\xi}^2\xi$ and ξ^3 are omitted from the previous equations. Thus the following system of simplified equations is obtained:

$$\xi_1(C_1-\lambda) + C_2\left[\bar{\xi}_2\xi_2 - \bar{\xi}_3\xi_3 + \frac{1}{2}(\xi_2^2 - \xi_3^2)\right] + C_3\left[(\xi_2 + \bar{\xi}_2)\xi_2 - (\xi_3 + \bar{\xi}_3)\bar{\xi}_3\right] = \lambda\bar{\xi}_1$$

$$(2.15)$$

$$\xi_2(C_4 - \lambda) + 8C_3\left[2(\xi_1 + \bar{\xi}_1)\xi_2 + \bar{\xi}_2\xi_1\right] + 8C_2(\xi_2 + \bar{\xi}_2)\xi_1 = \lambda\bar{\xi}_2 \qquad (2.16)$$

$$\xi_3(C_4 - \lambda) - 8C_3\left[2(\xi_1 + \bar{\xi}_1)\xi_3 + \bar{\xi}_3\xi_1\right] - 8C_2(\xi_3 + \bar{\xi}_3)\xi_1 = \lambda\bar{\xi}_3 \qquad (2.17)$$

where

$$C_1 = \frac{1}{2}\left[\alpha_A^2 + \frac{1}{\alpha_A^2}\right] \qquad\qquad C_2 = \frac{c}{16}\frac{\beta^2}{\alpha^2}$$

$$(2.18)$$

$$C_3 = \frac{c}{4}\frac{\alpha^2\beta^2}{(\alpha^2+\beta^2)^2} \qquad\qquad C_4 = \frac{1}{2}\left[\frac{(\alpha^2+\beta^2)}{\alpha^2} + \frac{\alpha^2}{(\alpha^2+\beta^2)^2}\right]$$

3. <u>Buckling of a Perfect Shell:</u> $\overline{\xi}_1 = \overline{\xi}_2 = \overline{\xi}_3 = 0$

In this case the governing equations become

$$\xi_1(C_1 - \lambda) + (\tfrac{1}{2} C_2 + C_3)(\xi_2^2 - \xi_3^2) = 0 \qquad (3.1)$$

$$\xi_2 \left\{ C_4 - \lambda + 8(C_2 + 2C_3)\xi_1 \right\} = 0 \qquad (3.2)$$

$$\xi_3 \left\{ C_4 - \lambda - 8(C_2 + 2C_3)\xi_1 \right\} = 0 \qquad (3.3)$$

If $C_1 > C_4$, there is no deformation of a perfect shell in the buckling modes ($\xi_1 = \xi_2 = \xi_3 = 0$) until λ reaches C_4. Then the coefficients of ξ_2 and ξ_3 in equations (3.2) and (3.3) vanish and a bifurcation of the solution in the ξ_2 or ξ_3 mode will occur. Since $\overline{\xi}_1 = 0$, ξ_1 can be either positive or negative. Suppose $\xi_3 = 0$, then following bifurcation λ will decrease with deformation occurring in the ξ_2 as well as the negative axisymmetric mode ξ_1. However if $\xi_2 = 0$, then following bifurcation λ will decrease with deformation occurring in the ξ_3 and in the positive axisymmetric mode ξ_1. In either case the maximum value of λ attained is at $\lambda = C_4$.

If $C_1 < C_4$, there is no deformation of a perfect shell in the buckling modes ($\xi_1 = \xi_2 = \xi_3 = 0$) until λ reaches C_1. With λ remaining at C_1, deformation can occur in the axisymmetric mode; and since $\overline{\xi}_1 = 0$, ξ_1 can be either positive or negative. If ξ_1 attains the value $- (C_4 - C_1)/8(C_2 + 2C_3)$ then the coefficient of ξ_2 in equation (3.2) vanishes and a bifurcation of the solution in the ξ_2 mode occurs.

The bifurcated solution corresponds to decreasing values of λ with deformation in both the ξ_1 and ξ_2 modes. Similarly if the axisymmetric deformation is such that ξ_1 attains the value $(C_4 - C_1)/8$ $(C_2 + 2C_3)$ then the coefficient of ξ_3 in equation (3.3) vanishes and λ decreases with deformation in both the ξ_1 and ξ_3 modes. In either case the maximum value of λ attained is at $\lambda = C_1$. The behavior of the perfect shell is shown in Fig. 46.

4.   Buckling of a Shell with Axisymmetric Imperfection:

$$\overline{\xi_1} \neq 0, \overline{\xi_2} = \overline{\xi_3} = 0$$

In this case the governing equations become:

$$\xi_1(C_1 - \lambda) + (\tfrac{1}{2} C_2 + C_3)(\xi_2^2 - \xi_3^2) = \lambda \overline{\xi_1} \qquad (4.1)$$

$$\xi_2 \left\{ C_4 - \lambda + 8(C_2 + 2C_3)\xi_1 + 16 C_3 \overline{\xi_1} \right\} = 0 \qquad (4.2)$$

$$\xi_3 \left\{ C_4 - \lambda - 8(C_2 + 2C_3)\xi_1 - 16 C_3 \overline{\xi_1} \right\} = 0 \qquad (4.3)$$

Now if the imperfection is purely axisymmetric then the prebuckling deformation is also purely axisymmetric. Hence $\xi_2 = \xi_3 = 0$ which satisfies equations (4.2) and (4.3) identically and from equation (4.1)

$$\xi_1 = \frac{\lambda}{C_1 - \lambda} \overline{\xi_1} \qquad (4.4)$$

until there is a bifurcation of the solution in one of the asymmetric modes.

<u>For $\overline{\xi}_1$</u> <u>negative</u> the prebuckling axisymmetric deformation ξ_1 will be negative and bifurcation into the asymmetric mode will occur when the coefficient of ξ_2 in equation (4.2) vanishes. That is when

$$\left\{ C_4 - \lambda + 8(C_2 + 2C_3)\xi_1 + 16\ C_3\ \overline{\xi}_1 \right\} = 0 \qquad (4.5)$$

which is the equation of a straight line in the $\lambda\xi_1$ - plane. Following bifurcation the value of λ decreases with deformation occurring in both the axisymmetric mode ξ_1 and the asymmetric mode ξ_2.

<u>For $\overline{\xi}_1$</u> <u>positive</u> the prebuckling axisymmetric deformation ξ_1 will be positive and bifurcation into the asymmetric mode will occur when the coefficient of ξ_3 in equation (4.3) vanishes. That is when

$$\left\{ C_4 - \lambda - 8(C_2 + 2C_3)\xi_1 - 16C_3\overline{\xi}_1 \right\} = 0 \qquad (4.6)$$

which is the equation of another straight line in the $\lambda\xi_1$ - plane. Following bifurcation the value of λ decreases with deformation occurring in both the axisymmetric mode ξ_1 and the asymmetric mode ξ_3. This behavior of the shell is shown in Fig. 47.

The maximum value of λ_1 denoted by λ_M, occurs at the bifurcation point and can be solved for explicitly by eliminating ξ_1 between equations (4.4) and (4.5). Its value is found to be

$$\lambda_M = \frac{B}{2} - \frac{1}{2} \sqrt{B^2 - 4D} \qquad (4.7)$$

where

$$B = C_1 + C_4 + 8C_2\overline{\xi_1}$$

(4.8)

$$D = C_1(C_4 - 16C_3\overline{\xi_1})$$

5. Buckling of a Shell with Both Axisymmetric and
    Asymmetric Imperfections: $\overline{\xi_1} \neq 0$ and $\overline{\xi_2} \neq 0$,
    $\overline{\xi_3} = 0$ or $\overline{\xi_2} = 0$, $\overline{\xi_3} \neq 0$

If $\overline{\xi_1} \neq 0$, $\overline{\xi_2} \neq 0$ and $\overline{\xi_3} = 0$ then the governing equations become:

$$\xi_1(C_1 - \lambda) + C_2\left[\overline{\xi_2}\xi_2 + \tfrac{1}{2}(\xi_2^2 - \xi_3^2)\right] + C_3\left[(\xi_2 + \overline{\xi_2})\xi_2 - \xi_3^2\right] = \lambda\overline{\xi_1} \quad (5.1)$$

$$\xi_2(C_4 - \lambda) + 8C_3\left[2(\xi_1 + \overline{\xi_1})\xi_2 + \overline{\xi_2}\xi_1\right] + 8C_2(\xi_2 + \overline{\xi_2})\xi_1 = \lambda\overline{\xi_2} \quad (5.2)$$

$$\xi_3\left\{C_4 - \lambda - 16C_3(\xi_1 + \overline{\xi_1}) - 8C_2\xi_1\right\} = 0 \quad (5.3)$$

In this case deformation occurs in both the ξ_1 and ξ_2 modes for any nonzero values of λ. Nonzero values of ξ_3 can occur only if the coefficient of ξ_3 in equation (5.3) vanishes. Assuming that such does not occur then $\xi_3 = 0$. This satisfies equation (5.3) identically and reduces the other two equations to:

$$\xi_1(C_1 - \lambda) + C_2(\overline{\xi_2}\xi_2 + \tfrac{1}{2}\xi_2^2) + C_3(\xi_2 + \overline{\xi_2})\xi_2 = \lambda\overline{\xi_1} \quad (5.4)$$

$$\xi_2(C_4 - \lambda) + 8C_3\left[2(\xi_1 + \overline{\xi}_1)\xi_2 + \overline{\xi}_2\xi_1\right] + 8C_2(\xi_2 + \overline{\xi}_2)\xi_1 = \lambda\overline{\xi}_2 \tag{5.5}$$

The trace of the general solution curve in the $\lambda\xi_2$ - plane can be obtained by eliminating ξ_1 between equations (5.4) and (5.5). This yields

$$A_1\lambda^2 + B_1\lambda + D_1 = 0 \tag{5.6}$$

where

$$A_1 = \xi_2 + \overline{\xi}_2$$

$$B_1 = (C_1 + C_4 - 8C_2\overline{\xi}_1)\xi_2 + C_1\overline{\xi}_2 - 8(C_2 + C_3)\overline{\xi}_1\overline{\xi}_2 \tag{5.7}$$

$$D_1 = \left[C_1C_4 + 16C_1C_3\overline{\xi}_1 - 8(C_2 + C_3)^2\overline{\xi}_2^2\right]\cdot\xi_2$$

$$- (C_2 + 2C_3)\left[12(C_2 + C_3)\overline{\xi}_2\xi_2^2 + 4(C_2 + 2C_3)\xi_2^3\right]$$

But this is just a standard quadratic equation whose solution can be written down immediately as:

$$\lambda = \frac{B_1}{2A_1} \pm \frac{1}{2A_1}\sqrt{B_1^2 - 4A_1D_1} = f(\xi_2, \overline{\xi}_1, \overline{\xi}_2, \alpha, \beta, c) \tag{5.8}$$

Here the negative sign must be used for $\overline{\xi}_2$ positive and the positive sign for $\overline{\xi}_2$ negative.

A maximum value of λ (if it occurs) is associated with $d\lambda/d\xi_2 = 0$. This condition along with equation (5.6) can be used to solve for λ_M. The result is analogous to equation (4.7) but considerably more complicated. Hence it is more convenient to obtain λ_M from the λ vs. ξ_2 plot using equation (5.8). This behavior of the shell is shown in Fig. 48.

If $\overline{\xi_1} \neq 0$, $\overline{\xi_2} = 0$ and $\overline{\xi_3} \neq 0$ then the governing equations become:

$$\xi_1(C_1 - \lambda) + C_2\left[-\overline{\xi_3}\xi_3 + \frac{1}{2}(\xi_2^2 - \xi_3^2)\right] + C_3\left[\xi_2^2 - (\xi_3 + \overline{\xi_3})\xi_3\right] = \lambda\overline{\xi_1}$$

(5.9)

$$\xi_2\left\{C_4 - \lambda + 16C_3(\xi_1 + \overline{\xi_1}) + 8C_2\xi_1\right\} = 0 \qquad (5.10)$$

$$\xi_3(C_4 - \lambda) - 8C_3\left[2(\xi_1 + \overline{\xi_1})\xi_3 + \overline{\xi_3}\xi_1\right] - 8C_2(\xi_3 + \overline{\xi_3})\xi_1 = \lambda\overline{\xi_3} \qquad (5.11)$$

Here deformation occurs in both the ξ_1 and ξ_3 modes for any nonzero value of λ. Nonzero values of ξ_2 can occur only if the coefficient of ξ_2 in equation (5.10) vanishes. Assuming that such does not occur then $\xi_2 = 0$. This satisfies equation (5.10) identically and reduces the other two equations to:

$$\xi_1(C_1 - \lambda) - C_2(\overline{\xi_3}\xi_3 + \frac{1}{2}\xi_3^2) - C_3(\xi_3 + \overline{\xi_3})\xi_3 = \lambda\overline{\xi_1} \qquad (5.12)$$

$$\xi_3(C_4 - \lambda) - 8C_3\left[2(\xi_1 + \overline{\xi_1})\xi_3 + \overline{\xi_3}\xi_1\right] - 8C_2(\xi_3 + \overline{\xi_3})\xi_1 = \lambda\overline{\xi_3} \qquad (5.13)$$

The trace of the general solution curve in the $\lambda \xi_3$ - plane can be obtained by eliminating ξ_1 between equations (5.12) and (5.13). This yields

$$A_2 \lambda^2 + B_2 \lambda + D_2 = 0 \tag{5.14}$$

where

$$A_2 = \xi_3 + \bar{\xi}_3$$

$$B_2 = (C_1 + C_4 + 8C_2\bar{\xi}_1)\xi_3 + C_1\bar{\xi}_3 + 8(C_2 + C_3)\bar{\xi}_1\bar{\xi}_3$$

$$\tag{5.15}$$

$$D_2 = \left[C_1 C_4 - 16 C_1 C_3 \bar{\xi}_1 - 8(C_2 + C_3)^2 \bar{\xi}_2^2 \right] \xi_3$$

$$-(C_2 + 2C_3) \left[12(C_2 + C_3)\bar{\xi}_3 \xi_3^2 + 4(C_2 + 2C_3)\xi_3^3 \right]$$

The solution of this standard quadratic equation can be written down immediately as:

$$\lambda = \frac{B_2}{2A_2} \pm \frac{1}{2A_2} \sqrt{B_2^2 - 4A_2 D_2} = g(\xi_3, \bar{\xi}_1, \bar{\xi}_2, \alpha, \beta, c) \tag{5.16}$$

The negative sign must be used for $\bar{\xi}_3$ positive and the positive sign for $\bar{\xi}_3$ negative.

A maximum value of λ(if it occurs) is associated with $d\lambda/d\xi_3 = 0$. This condition along with equation (5.16) could be used to

solve for λ_M. However, as pointed out earlier, it was found more convenient to obtain λ_M from the λ vs. ξ_3 plot using equation (5.16). This behavior of the shell is shown in Fig. 48.

As expected, the introduction of the additional asymmetric imperfection decreases the load carrying capacity of the shell even further. Thus the λ_M obtained from the λ vs. ξ_2 plot using equation (5.8) or from the λ vs. ξ_3 plot using equation (5.16) for a shell with both axisymmetric and asymmetric imperfections will always be less than the λ_M computed from equation (4.7) for a shell with axisymmetric imperfection only.

6. Numerical Results

Equations (5.8) and (5.16) were programmed on the IBM 7094 and used in the search for the "pair of critical modal components", defined as that combination of one axisymmetric and one asymmetric imperfection component which gave the lowest value for λ_M.

In deriving the buckling equations (2.11) - (2.13) it was necessary to impose the condition $k = i/2$ otherwise all the quadratic terms in ξ_1, ξ_2, and ξ_3 would vanish identically and the resulting buckling equations would describe a system with stable postbuckled states which are known to be insensitive to initial imperfections. Thus choosing an axisymmetric imperfection with wave number i automatically fixed the axial wave number k of the asymmetric imperfection. Then in order to minimize the asymmetric buckling load $\lambda = C_4$ the circumferential wave number ℓ was computed from

$$\alpha^2 + \beta^2 - \alpha = 0 \tag{6.1}$$

or solving for ℓ:

$$\ell = R \sqrt{ k\left(\frac{2\pi}{L}\right)^2 \left(\frac{L}{2\pi} \sqrt{\frac{2c}{Rt}} - k\right) } \tag{6.2}$$

with the restriction that for a positive, nonzero ℓ

$$k < \frac{L}{2\pi} \sqrt{\frac{2c}{Rt}} = {}^i_c\ell \tag{6.3}$$

where

$\quad {}^i_c\ell$ = wave number of the classical axisymmetric buckling

$\qquad$ mode

The computation of the wave numbers is summarized in Table VI for

the shells tested. In actual use ℓ was rounded to the nearest integer.

When combining the harmonic components of the experimen-

tally measured imperfection surfaces into pairs to be used as input

to the computer programs two separate cases had to be considered.

Case a: $\quad \overline{\xi}_1 \neq 0, \overline{\xi}_2 \neq 0, \overline{\xi}_3 = 0$

This resulted in coupling between the ξ_1 and ξ_2 modes and

the input to equation (5.8) consisted of

$$A_{oi} \cdot \cos i\overline{x} \longrightarrow \begin{cases} A_{k\ell} \cdot \cos k\overline{x} \cdot \cos \ell\overline{y} \\[2ex] B_{k\ell} \cdot \cos k\overline{x} \cdot \sin \ell\overline{y} \end{cases} \tag{6.4}$$

or

$$C_{oi} \cdot \sin i\overline{x} \longrightarrow \begin{cases} C_{k\ell} \cdot \sin k\overline{x} \cdot \cos \ell\overline{y} \\[2ex] D_{k\ell} \cdot \sin k\overline{x} \cdot \sin \ell\overline{y} \end{cases} \qquad (6.5)$$

Case b: $\overline{\xi}_1 \neq 0, \overline{\xi}_2 = 0, \overline{\xi}_3 \neq 0$

This resulted in coupling between the ξ_1 and ξ_3 modes and the input to equation (5.16) consisted of

$$A_{oi} \cdot \cos i\overline{x} \longrightarrow \begin{cases} C_{k\ell} \cdot \sin k\overline{x} \cdot \cos \ell\overline{y} \\[2ex] D_{k\ell} \cdot \sin k\overline{x} \cdot \sin \ell\overline{y} \end{cases} \qquad (6.6)$$

of

$$C_{oi} \cdot \sin i\overline{x} \longrightarrow \begin{cases} A_{k\ell} \cdot \cos k\overline{x} \cdot \cos \ell\overline{y} \\[2ex] B_{k\ell} \cdot \cos k\overline{x} \cdot \sin \ell\overline{y} \end{cases} \qquad (6.7)$$

It should be mentioned here that the location of the origin in the circumferential direction was arbitrary. Thus either sine or cosine $\overline{y}$-dependence was admissible.

It was found that for a positive axisymmetric imperfection coupling in the ξ_3 mode would yield a lower value for λ_M then coupling in the ξ_2 mode if both $\overline{\xi}_2$ and $\overline{\xi}_3$ were of the same size. Similarly for a negative axisymmetric imperfection coupling in the ξ_2 mode would result in a lower value for λ_M.

A list of the numerical results for the shells tested is given
in Table VII. The comparison between the results of this simplified
analytical approach and the experimental values is shown in Table
VIII.

IV.   CONCLUSION

Due to the small number of shells tested the results obtained

thus far must be considered only preliminary.   However the follow-

ing conclusions seemed to be warranted:

1.   The initial imperfections of the shells surveyed so far

were characterized by being composed predominantly of lower order

modes (i. e. few circumferential and even fewer axial waves).   The

amplitudes of the higher order modes were in general very small (i. e.

of the order of one per cent of the wall thickness or less).

2.   As can be seen from the three-dimensional plots repres-

enting the growth of the prebuckling deformations just prior to

buckling (Figs. 28 through 31) there was a very pronounced growth of

imperfection components with long axial wave length and short

circumferential wave length for all the shells tested.   The number of

circumferential waves of these dominant components was approxima-

tely equal to the number of circumferential waves in the postbuckled

shape.   The half wave length of the dominant components was equal

to the length of the shell in the axial direction.   However the axial

half wave length of the postbuckled shape was much shorter than the

axial half wave length of the dominant components in the prebuckling

deformation.

3.   There seemed to exist several "critical modal compo-

nents" for every shell tested, all showing the same exponential

growth close to the critical load instead of an isolated "critical

modal component".   In other words the mode of prebuckling

deformation which apparently contributed to the reduction in buckling load of the shells had many Fourier coefficients. Furthermore, some of these components had relatively small initial values. That is, the "critical modal components" were not necessarily predominant in the initial imperfection shape.

4. The failure modes of shell A7 with local buckling in two isolated waves and of shell A10 with one isolated wave at the upper edge seemed to support the claim expressed in reference 15 that local bucklings were caused by some pronounced localized initial imperfections of the test specimens. Upon comparing the local buckling pattern of shell A7 (Fig. 27) with the initial imperfection survey of the same shell (Fig. 19) it was strikingly evident that not only did the initial local buckling occur at the exact location of very pronounced localized initial defects of the test specimen but the same localized defects showed the most pronounced growth rate as can be seen from Fig. 26 just prior to the occurrence of local buckling. Similarly shell A10 also had a very pronounced initial imperfection at the location of the local buckling as can be seen by comparing Fig. 32 showing the local buckling deformation with Fig. 22 showing the initial imperfection survey.

5. The comparison of the analytical results with the experimental values showed good agreement for the cases of global buckling. Apparently the dominant part of the measured imperfection surfaces was adequately approximated by the two terms of the pair of critical modal components.

6.   All the pairs of critical modal components were composed of an axisymmetric imperfection with one full wave in the axial direction and an asymmetric imperfection with one half wave in the axial direction.   This seemed to confirm the conclusions of the visual observation of the growth of the prebuckling deformations where the most degrading imperfections, the ones with the most pronounced growth rate, were of long axial wave length.

REFERENCES

1. Weingarten, V. I.; Morgan, E. T.; and Seide, P.: Final
   Report on Development of Design Criteria for Elastic
   Stability of Thin Shell Structures. STL/TR-60-000-
   19425, Space Technology Laboratories, 1960.

2. Stein, M.: The Effect on the Buckling of Perfect Cylinders of
   Prebuckling Deformations and Stresses Induced by Edge
   Support. Collected Papers on Instability of Shell
   Structures, NASA TN D-1510, 1962, pp. 217-227.

3. Fischer, E.: Uber den Einfluss der Gelenkigen Lagerung auf
   die Stabilität Dunnwandiger Kreiszylinderschalen unter
   Axiallast und Innendruck. Z. Flugwissenschaften, Vol.
   11, 1963, pp. 111-119.

4. Almroth, B. O.: Influence of Edge Conditions on the Stability
   of Axially Compresed Cylindrical Shells. NASA CR-161,
   Feb. 1963.

5. Hoff, N. J.: The Effect of Edge Conditions on the Buckling of
   Thin Walled Circular Shells in Axial Compression.
   Proc. 11th Int. Congress of Appl. Mech.,
   Julius Springer Verlag, Berlin, 1964.

6. Kobayashi, S.: The Influence of the Boundary Conditions on the
   Buckling Load of Cylindrical Shells under Axial
   Compression. GALCIT SM 66-3, March 1966.

7. Donnell, L. M.: A New Theory for the Buckling of Thin

      Cylinders under Axial Compression and Bending. Trans.

      Am. Soc. Mech. Eng., Vol. 56, 1934, p. 795.

8. Donnell, L. M. and Wan, C. C.: Effect of Imperfections on

      Buckling of Thin Cylinders and Columns under Axial

      Compression. Journ. Appl. Mech., Vol. 17, 1950,

      p. 73.

9. Koiter, W. T.: On the Stability of Elastic Equilibrium. Ph. D.

      Thesis, Delft, H. T. Paris, Amsterdam, 1945.

10. Koiter, W. T.: The Effect of Axisymmetric Imperfections on

      the Buckling of Cylindrical Shells under Axial

      Compression. Lockheed Missiles and Space Company,

      6-90-63-86, Sunnyvale, California, Aug. 1963.

11. Koiter, W. T.: Elastic Stability and Postbuckling Behavior.

      Proc. Symposium Nonlinear Problems, (R. E. Langer

      ed.) University of Wisconsin Press, Madison, Wisconsin,

      1963.

12. Hutchinson, J.: Axial Buckling of Pressurized Imperfect

      Cylindrical Shells, AIAA J.,Vol. 3, Aug. 1965, pp.

      1461-1466.

13. Thurston, E. A. and Freeland, M. A.: Buckling of Imperfect

      Cylinders under Axial Compression, NASA CR-541,

      July 1966.

14. Babcock, C. D.: The Buckling of Cylindrical Shells with an Initial Imperfection under Axial Compression Loading. Ph. D. Thesis, California Institute of Technology, 1962.

15. Arbocz, J.: Buckling of Conical Shells under Axial Compression. GALCIT SM 68-6, Feb. 1968.

APPENDIX A

The approximate solution of Donnell's equations for an imperfect cylindrical shell

$$\frac{1}{Et} \nabla^4 F - \frac{1}{R} W,_{xx} + \frac{1}{2} L(W, W + 2\overline{W}) = 0 \tag{1}$$

$$\frac{Et^3}{12(1-\nu^2)} \nabla^4 W + \frac{1}{R} F,_{xx} - L(F, W + \overline{W}) = 0 \tag{2}$$

where the nonlinear operator L is defined by

$$L(S, T) = S,_{xx} T,_{yy} - 2S,_{xy} T,_{xy} + S,_{yy} T,_{xx} \tag{3}$$

assumes that the initial imperfection shape is represented by

$$\overline{W} = \xi_1 t \cos i\overline{x} + \xi_2 t \cos k\overline{x} \cdot \cos \ell \overline{y} + \xi_3 t \sin k\overline{x} \cdot \cos \ell \overline{y} \tag{4}$$

The equilibrium state of the axially loaded cylinder is approximated as:

$$W = \frac{\nu}{E} \sigma t + w \tag{5}$$

$$F = -\frac{1}{2} \sigma t y^2 + f \tag{6}$$

where the terms added to w and f constitute the prebuckling membrane solution for the perfect shell. Further w is assumed as:

$$w = \xi_1 t \cos i\overline{x} + \xi_2 t \cos k\overline{x} \cdot \cos \ell \overline{y} + \xi_3 t \sin k\overline{x} \cdot \cos \ell \overline{y} \tag{7}$$

Substituting the assumed form of W and $\overline{W}$ into the compatibility

equation (1) yields

$$\frac{1}{Et}(F,_{xxxx} + 2F,_{xxyy} + F,_{yyyy}) = K_1\cos 2k\overline{x} + K_2\cos i\overline{x} + K_3\cos 2\ell\overline{y} \quad (8)$$

$$+ K_4\sin 2k\overline{x} + K_5\cos k\overline{x}\cdot\cos\ell\overline{y}$$

$$+ K_6\sin k\overline{x}\cdot\cos\ell\overline{y} + K_7\cos(i+k)\overline{x}\cdot\cos\ell\overline{y}$$

$$+ K_8\cos(i-k)\overline{x}\cdot\cos\ell\overline{y} + K_9\sin(i+k)\overline{x}\cdot\cos\ell\overline{y}$$

$$+ K_{10}\sin(i-k)\overline{x}\cdot\cos\ell\overline{y}$$

where

$$K_1 = -\left(\frac{2\pi}{L}\right)^2\left(\frac{t}{R}\right)^2 k^2\ell^2\left[\overline{\xi}_2\xi_2 - \overline{\xi}_3\xi_3 + \frac{1}{2}(\xi_2^2 - \xi_3^2)\right]$$

$$K_2 = -\left(\frac{2\pi}{L}\right)^2\frac{t}{R}i^2\xi_1$$

$$K_3 = -\left(\frac{2\pi}{L}\right)^2\left(\frac{t}{R}\right)^2 k^2\ell^2\left[\overline{\xi}_2\xi_2 + \overline{\xi}_3\xi_3 + \frac{1}{2}(\xi_2^2 + \xi_3^2)\right]$$

$$K_4 = -\left(\frac{2\pi}{L}\right)^2\left(\frac{t}{R}\right)^2 k^2\ell^2\left[\overline{\xi}_3\xi_2 + (\overline{\xi}_2 + \xi_2)\xi_3\right]$$

$$K_5 = -\left(\frac{2\pi}{L}\right)^2\frac{t}{R}k^2\xi_2$$

$$K_6 = -\left(\frac{2\pi}{L}\right)^2\frac{t}{R}k^2\xi_3$$

$$K_7 = -\left(\frac{2\pi}{L}\right)^2\left(\frac{t}{R}\right)^2\frac{i^2\ell^2}{2}\left[\overline{\xi}_2\xi_1 + (\xi_1+\overline{\xi}_1)\xi_2\right]$$

$$K_8 = -\left(\frac{2\pi}{L}\right)^2\left(\frac{t}{R}\right)^2\frac{i^2\ell^2}{2}\left[\overline{\xi}_2\xi_1 + (\xi_1+\overline{\xi}_1)\xi_2\right]$$

$$K_9 = -\left(\frac{2\pi}{L}\right)^2\left(\frac{t}{R}\right)^2\frac{i^2\ell^2}{2}\left[\overline{\xi}_3\xi_1 + (\xi_1+\overline{\xi}_1)\xi_3\right]$$

$$K_{10} = \left(\frac{2\pi}{L}\right)^2\left(\frac{t}{R}\right)^2\frac{i^2\ell^2}{2}\left[\overline{\xi}_3\xi_1 + (\xi_1+\overline{\xi}_1)\xi_3\right]$$

$$(9)$$

The boundary conditions of the finite shell will be neglected, therefore only a particular solution of equation (8) is needed. To obtain such a particular solution let

$$F = -\frac{1}{2}\sigma t y^2 + f_p \tag{10}$$

where

$$f_p = A\cos 2k\bar{x} + B\cos i\bar{x} + C\cos 2\ell\bar{y} + D\sin 2k\bar{x} + \tilde{E}\cos k\bar{x} \cdot \cos \ell\bar{y}$$

$$+ F\sin k\bar{x} \cdot \cos \ell\bar{y} + G\cos(i+k)\bar{x} \cdot \cos \ell\bar{y} + H\cos(i-k)\bar{x} \cdot \cos \ell\bar{y}$$

$$+ I\sin(i+k)\bar{x} \cdot \cos \ell\bar{y} + J\sin(i-k)\bar{x} \cdot \cos \ell\bar{y}$$

Substituting this expression into equation (2) and equating coefficients of like terms yields:

$$A = Et\left(\frac{L}{2\pi}\right)^4 \frac{1}{(2k)^4} \quad K_1 = -Et\left(\frac{L}{2\pi}\right)^2\left(\frac{t}{R}\right)^2\frac{\ell^2}{16k^2}\left[\xi_2\xi_2 - \xi_3\xi_3 + \frac{1}{2}(\xi_2^2 - \xi_3^2)\right]$$

$$B = Et\left(\frac{L}{2\pi}\right)^4 \frac{1}{i^4}\quad K_2 = -Et\left(\frac{L}{2\pi}\right)^2\frac{t}{R}\frac{1}{i^2}\xi_1$$

$$C = EtR^4\frac{1}{(2\ell)^4}\quad K_3 = -EtR^4\left(\frac{2\pi}{L}\right)^2\left(\frac{t}{R}\right)^2\frac{k^2}{16\ell^2}\left[\xi_2\xi_2 + \xi_3\xi_3 + \frac{1}{2}(\xi_2^2 + \xi_3^2)\right]$$

$$D = Et\left(\frac{L}{2\pi}\right)^4\frac{1}{(2k)^4}\quad K_4 = -Et\left(\frac{L}{2\pi}\right)^2\left(\frac{t}{R}\right)^2\frac{\ell^2}{16k^2}\left[\xi_3\xi_2 + (\xi_2 + \xi_2)\xi_3\right]$$

$$\tilde{E} = Et\left[\left(\frac{2\pi}{L}\right)^2 k^2 + \frac{\ell^2}{R^2}\right]^{-2}\quad K_5 = -Et\left(\frac{2\pi}{L}\right)^2\frac{t}{R}k^2\left[\left(\frac{2\pi}{L}\right)^2 k^2 + \frac{\ell^2}{R^2}\right]^{-2}\xi_2$$

$$F = Et\left[\left(\frac{2\pi}{L}\right)^2 k^2 + \frac{\ell^2}{R^2}\right]^{-2}\quad K_6 = -Et\left(\frac{2\pi}{L}\right)^2\frac{t}{R}k^2\left[\left(\frac{2\pi}{L}\right)^2 k^2 + \frac{\ell^2}{R^2}\right]^{-2}\xi_3$$

$$\tag{11}$$

$$G = Et \left[\left(\frac{2\pi}{L}\right)^2 (i+k)^2 + \frac{\ell^2}{R^2} \right]^{-2} K_7$$

$$= -Et \left(\frac{2\pi}{L}\right)^2 \left(\frac{t}{R}\right)^2 \frac{i^2 \ell^2}{2} \left[\left(\frac{2\pi}{L}\right)^2 (i+k)^2 + \frac{\ell^2}{R^2} \right]^{-2} [\bar{\xi}_2 \xi_1 + (\xi_1 + \bar{\xi}_1)\xi_2]$$

$$H = Et \left[\left(\frac{2\pi}{L}\right)^2 (i-k)^2 + \frac{\ell^2}{R^2} \right]^{-2} K_8$$

$$= -Et \left(\frac{2\pi}{L}\right)^2 \left(\frac{t}{R}\right)^2 \frac{i^2 \ell^2}{2} \left[\left(\frac{2\pi}{L}\right)^2 (i-k)^2 + \frac{\ell^2}{R^2} \right]^{-2} [\bar{\xi}_2 \xi_1 + (\xi_1 + \bar{\xi}_1)\xi_2]$$

$$I = Et \left[\left(\frac{2\pi}{L}\right)^2 (i+k)^2 + \frac{\ell^2}{R^2} \right]^{-2} K_9$$

$$= -Et \left(\frac{2\pi}{L}\right)^2 \left(\frac{t}{R}\right)^2 \frac{i^2 \ell^2}{2} \left[\left(\frac{2\pi}{L}\right)^2 (i+k)^2 + \frac{\ell^2}{R^2} \right]^{-2} [\bar{\xi}_3 \xi_1 + (\xi_1 + \bar{\xi}_1)\xi_3]$$

$$J = Et \left[\left(\frac{2\pi}{L}\right)^2 (i-k)^2 + \frac{\ell^2}{R^2} \right]^{-2} K_{10}$$

$$= Et \left(\frac{2\pi}{L}\right)^2 \left(\frac{t}{R}\right)^2 \frac{i^2 \ell^2}{2} \left[\left(\frac{2\pi}{L}\right)^2 (i-k)^2 + \frac{\ell^2}{R^2} \right]^{-2} [\bar{\xi}_3 \xi_1 + (\xi_1 + \bar{\xi}_1)\xi_3]$$

Substituting the assumed form for W and $\overline{W}$ and the computed particular solution for F as given by equations (4), (7) and (10) into the equilibrium equation (2) yields, after multiplying out, regrouping and simplifying through the use of trigonometric identities the following expression for the ERROR $\mathscr{E}_N$:

$$\left\{ \frac{Et^4}{(12(1-\nu^2)} \left(\frac{2\pi}{L}\right)^2 i^4 \xi_1 - \frac{i^2}{R} B - t^2 i^2 (\xi_1 + \bar{\xi}_1) \sigma \right.$$

$$\left. - \frac{t}{4R^2} i^2 \ell^2 [(\xi_2 + \bar{\xi}_2)(G+H) + (\xi_3 + \bar{\xi}_3)(I-J)] \right\} \cdot \cos i\bar{x}$$

$$+ \left\{ \frac{Et^4}{12(1-\nu^2)} \left[\left(\frac{2\pi}{L}\right)^2 k^2 + \left(\frac{\ell}{R}\right)^2 \right]^2 \left(\frac{L}{2\pi}\right)^2 \xi_2 - \frac{k^2}{R} \widetilde{E} - t^2 k^2 (\xi_2 + \overline{\xi}_2) \sigma \right.$$

$$- \frac{t\ell^2}{2R^2} \left[4k^2 [(\xi_2 + \overline{\xi}_2)(A+C) + (\xi_3 + \overline{\xi}_3)D] \right.$$

$$\left. \left. + i^2 (\xi_1 + \overline{\xi}_1)(G+H) \right] \right\} \cos k\overline{x} \cdot \cos \ell \overline{y}$$

$$+ \left\{ \frac{Et^4}{12(1-\nu^2)} \left[\left(\frac{2\pi}{L}\right)^2 k^2 + \left(\frac{\ell}{R}\right)^2 \right]^2 \left(\frac{L}{2\pi}\right)^2 \xi_3 - \frac{k^2}{R} F - t^2 k^2 (\xi_3 + \overline{\xi}_3) \sigma \right.$$

$$- \frac{t}{2R^2} \ell^2 \left[4k^2 [(\xi_2 + \overline{\xi}_2)D + (\xi_3 + \overline{\xi}_3)(C-A)] \right.$$

$$\left. \left. + i^2 (\xi_1 + \overline{\xi}_1)(I-J) \right] \right\} \sin k\overline{x} \cdot \cos \ell \overline{y}$$

$$+ \left\{ \frac{-4k^2}{R} A - \frac{t}{R^2} k^2 \ell^2 [(\xi_2 + \overline{\xi}_2)\widetilde{E} - (\xi_3 + \overline{\xi}_3)F] \right\} \cos 2k\overline{x}$$

$$+ \left\{ \frac{-(i-k)^2}{R} H - \frac{t}{2R^2} i^2 \ell^2 [(\xi_1 + \overline{\xi}_1)\widetilde{E} + (\xi_2 + \overline{\xi}_2) B] \right\} \cos(i-k)\overline{x} \cdot \cos \ell \overline{y}$$

$$+ \left\{ \frac{-(i-k)^2}{R} J - \frac{t}{2R^2} i^2 \ell^2 [(\xi_1 + \overline{\xi}_1)F + (\xi_2 + \overline{\xi}_2) B] \right\} \sin(i-k)\overline{x} \cdot \cos \ell \overline{y}$$

$$+ \left\{ \frac{-t}{4R^2} i^2 \ell^2 [(\xi_3 + \overline{\xi}_3)(H-G) + (\xi_2 + \overline{\xi}_2)(I+J)] \right\} \sin i\overline{x}$$

$$+ \left\{ \frac{-4k^2}{R} D - \frac{t}{R^2} k^2 \ell^2 [(\xi_2 + \overline{\xi}_2)F + (\xi_3 + \overline{\xi}_3)\widetilde{E}] \right\} \sin 2k\overline{x}$$

$$+ \left\{ \frac{-t}{R^2} k^2 \ell^2 [(\xi_2 + \overline{\xi}_2)\widetilde{E} + (\xi_3 + \overline{\xi}_3)F] \right\} \cos 2\ell \overline{y}$$

$$+ \left\{ \frac{-t}{4R^2} \ell^2 \left[16i^2(\xi_1 + \overline{\xi}_1)C + (2k+i)^2[(\xi_2 + \overline{\xi}_2)G + (\xi_3 + \overline{\xi}_3)I] \right. \right.$$

$$\left. \left. + (2k-i)^2[(\xi_2 + \overline{\xi}_2)H - (\xi_3 + \overline{\xi}_3)J] \right] \right\} \cos i\overline{x} \cdot \cos 2\ell\overline{y}$$

$$+ \left\{ \frac{-t}{4R^2} \ell^2 (2k+i)^2[(\xi_2 + \overline{\xi}_2)G - (\xi_3 + \overline{\xi}_3)I] \right\} \cos(i+2k)\overline{x}$$

$$+ \left\{ \frac{-t}{4R^2} \ell^2 (2k+i)^2[(\xi_2 + \overline{\xi}_2)I + (\xi_3 + \overline{\xi}_3)G] \right\} \sin(i+2k)\overline{x}$$

$$+ \left\{ \frac{-t}{4R^2} \ell^2 \left[(2k+i)^2[(\xi_2 + \overline{\xi}_2)I - (\xi_3 + \overline{\xi}_3)G] \right. \right.$$

$$\left. \left. + (2k-i)^2[(\xi_2 + \overline{\xi}_2)] + (\xi_3 + \overline{\xi}_3)H \right] \right\} \sin i\overline{x} \cdot \cos 2\ell\overline{y}$$

$$+ \left\{ \frac{-(i+k)^2}{R} G - \frac{t}{R^2} \frac{i^2\ell^2}{2} [(\xi_1 + \overline{\xi}_1)\widetilde{E} + (\xi_3 + \overline{\xi}_3)B] \right\} \cos(i+k)\overline{x} \cdot \cos\ell\overline{y}$$

$$+ \left\{ \frac{-(i+k)^2}{R} I - \frac{t}{R^2} \frac{i^2\ell^2}{2} [(\xi_1 + \overline{\xi}_1)F + (\xi_3 + \overline{\xi}_3)B] \right\} \sin(i+k)\overline{x} \cdot \cos\ell\overline{y}$$

$$+ \left\{ \frac{-t}{R^2} 2k^2\ell^2(\xi_3 + \overline{\xi}_3)C \right\} \sin k\overline{x} \cdot \cos 3\ell\overline{y} \tag{12}$$

$$+ \left\{ \frac{-t}{R^2} 2k^2\ell^2(\xi_2 + \overline{\xi}_2)C \right\} \cos k\overline{x} \cdot \cos 3\ell\overline{y}$$

$$+ \left\{ \frac{-t}{4R^2} (2k-i)^2\ell^2[(\xi_2 + \overline{\xi}_2)H + (\xi_3 + \overline{\xi}_3)J] \right\} \cos(2k-i)\overline{x}$$

$$+ \left\{ \frac{-t}{4R^2} (2k-i)^2\ell^2[(\xi_3 + \overline{\xi}_3)H - (\xi_2 + \overline{\xi}_2)J] \right\} \sin(2k-i)\overline{x}$$

$$+ \left\{ \frac{-t}{4R^2} i^2\ell^2[(\xi_2 + \overline{\xi}_2)G - (\xi_3 + \overline{\xi}_3)I] \right\} \cos(2k+i)\overline{x} \cdot \cos 2\ell\overline{y}$$

$$+ \left\{ \frac{-t}{4R^2} i^2 \ell^2 [(\xi_2 + \overline{\xi}_2) I + (\xi_3 + \overline{\xi}_3) G] \right\} \sin(2k+i)\overline{x} \cdot \cos 2\ell\overline{y}$$

$$+ \left\{ \frac{-t}{4R^2} i^2 \ell^2 [(\xi_2 + \overline{\xi}_2) H + (\xi_3 + \overline{\xi}_3) J] \right\} \cos(2k-i)\overline{x} \cdot \cos 2\ell\overline{y}$$

$$+ \left\{ \frac{-t}{4R^2} i^2 \ell^2 [(\xi_3 + \overline{\xi}_3) H - (\xi_2 + \overline{\xi}_2) J] \right\} \sin(2k-i)\overline{x} \cdot \cos 2\ell\overline{y}$$

$$+ \left\{ \frac{-t}{R^2} 2k^2 \ell^2 [(\xi_2 + \overline{\xi}_2) A - (\xi_3 + \overline{\xi}_3) D] \right\} \cos 3k\overline{x} \cdot \cos \ell\overline{y}$$

$$+ \left\{ \frac{-t}{R^2} 2k^2 \ell^2 [(\xi_2 + \overline{\xi}_2) D + (\xi_3 + \overline{\xi}_3) A] \right\} \sin 3k\overline{x} \cdot \cos \ell\overline{y}$$

$$+ \left\{ \frac{-t}{2R^2} i^2 \ell^2 (\xi_1 + \overline{\xi}_1) G \right\} \cos(2i+k)\overline{x} \cdot \cos \ell\overline{y}$$

$$+ \left\{ \frac{-t}{2R^2} i^2 \ell^2 (\xi_1 + \overline{\xi}_1) H \right\} \cos(2i-k)\overline{x} \cdot \cos \ell\overline{y}$$

$$+ \left\{ \frac{-t}{2R^2} i^2 \ell^2 (\xi_1 + \overline{\xi}_1) I \right\} \sin(2i+k)\overline{x} \cdot \cos \ell\overline{y}$$

$$+ \left\{ \frac{-t}{2R^2} i^2 \ell^2 (\xi_1 + \overline{\xi}_1) J \right\} \sin(2i-k)\overline{x} \cdot \cos \ell\overline{y}$$

$$= \mathcal{E}_N (\xi_1, \xi_2, \xi_3, \overline{x}, \overline{y})$$

where the ERROR $\mathcal{E}_N$ is a function of the unknown amplitudes ξ_1, ξ_2 and ξ_3 of the assumed radial displacement W.

Using Galerkin's idea of minimization of the error with respect to a set of given functions leads to a system of three nonlinear algebraic equations in the three unknowns ξ_1, ξ_2, ξ_3. Here these

equations will be obtained from the following integrals:

$$\int_0^{2\pi} \int_0^{2\pi} \mathcal{E}_N(\xi_1, \xi_2, \xi_3, \overline{x}, \overline{y}) \cdot \cos i\overline{x} \, d\overline{x} \, d\overline{y} = 0 \tag{13}$$

$$\int_0^{2\pi} \int_0^{2\pi} \mathcal{E}_N(\xi_1, \xi_2, \xi_3, \overline{x}, \overline{y}) \cdot \cos k\overline{x} \cdot \cos \ell \overline{y} \, d\overline{x} \, d\overline{y} = 0 \tag{14}$$

$$\int_0^{2\pi} \int_0^{2\pi} \mathcal{E}_N(\xi_1, \xi_2, \xi_3, \overline{x}, \overline{y}) \cdot \sin k\overline{x} \cdot \cos \ell \overline{y} \, d\overline{x} \, d\overline{y} = 0 \tag{15}$$

Imposing the restriction k = i/2 and carrying out the indicated

integrations leads to:

$$\frac{Et^4}{12(1-\nu^2)} \left(\frac{2\pi}{L}\right)^2 i^4 \xi_1 \frac{-i^2}{R} B - t^2 i^2 (\xi_1 + \overline{\xi}_1) \sigma$$

$$- \frac{t}{4R^2} i^2 \ell^2 [(\xi_2 + \overline{\xi}_2)(G+H) + (\xi_3 + \overline{\xi}_3)(I-J)]$$

$$\frac{-4k^2}{R} A - \frac{t}{R^2} k^2 \ell^2 [(\xi_2 + \overline{\xi}_2)\widetilde{E} - (\xi_3 + \overline{\xi}_3)F] = 0 \tag{16}$$

$$\frac{Et^4}{(12(1-\nu^2)} \left(\frac{L}{2\pi}\right)^2 \left[\left(\frac{2\pi}{L}\right)^2 k^2 + \left(\frac{\ell}{R}\right)^2\right]^2 \xi_2 - \frac{k^2}{R} \widetilde{E} - t^2 k^2 (\xi_2 + \overline{\xi}_2) \sigma$$

$$- \frac{t}{2R^2} \ell^2 \left[4k^2 [(\xi_2 + \overline{\xi}_2)(A+C) + (\xi_3 + \overline{\xi}_3)D] \right.$$

$$\left. + i^2(\xi_1 + \overline{\xi}_1)(G+H) \right] - \frac{(i-k)^2}{R} H - \frac{t}{2R^2} i^2 \ell^2 [(\xi_1 + \overline{\xi}_1)\widetilde{E} + (\xi_2 + \overline{\xi}_2)B] = 0$$

$$\tag{17}$$

$$\frac{Et^4}{12(1-\nu^2)} \ (\frac{L}{2\pi})^2 \left[(\frac{2\pi}{L})^2 k^2 + (\frac{\ell}{R})^2\right]^2 \xi_3 \ - \ \frac{k^2}{R} \ F - t^2 k^2 (\xi_3 + \overline{\xi}_3) \, \sigma$$

$$- \ \frac{t}{2R^2} \ \ell^2 \left[4k^2[(\xi_2 + \overline{\xi}_2)D + (\xi_3 + \overline{\xi}_3)(C-A)] + i^2(\xi_1 + \overline{\xi}_1)(I-J)\right]$$

$$\underline{- \ \frac{(i-k)^2}{R} \ J} \ - \ \frac{t}{2R^2} \ i^2 \ell^2 [(\xi_1 + \overline{\xi}_1)F + (\xi_3 + \overline{\xi}_3)B] \ = \ 0 \qquad (18)$$

Without the restriction k = i/2 the underlined terms would

vanish because of the orthogonality properties of the respective

trigonometric functions and the resulting equations would contain

only cubic nonlinearities in the unknown amplitudes ξ_1, ξ_2 and ξ_3.

Substituting for the coefficients A, B,...., I and J from

equations (11) and introducing the nondimensional parameters de-

fined in equations (2.11) yields the NONLINEAR BUCKLING EQUA-

TIONS (2.12) - (2.14).

TABLE I

REPEATABILITY CHECKS

Date of Scan	$X_1 \cdot 10^2$ Inches	$Y_1 \cdot 10^2$ Inches	$\epsilon_1 \cdot 10^3$ Radians	$\epsilon_2 \cdot 10^3$ Radians	R Inches
9-21-67	0.156	-0.510	0.143	-1.081	3.9921
9-22-67 10:00 am	0.156	-0.506	0.142	-1.075	3.9919
9-22-67 5:00 pm	0.158	-0.506	0.141	-1.075	3.9919
Average Value	$0.157 \pm 1\%$	$-0.507 \pm 0.5\%$	$0.142 \pm 0.7\%$	$-1.077 \pm 0.3\%$	3.9920

TABLE I (Cont'd)

REPEATABILITY CHECKS

Date of Scan	$A_{1,0} \cdot 10^4$ Inches	$A_{2,0} \cdot 10^3$ Inches	$A_{1,1} \cdot 10^3$ Inches	$B_{2,0} \cdot 10^4$ Inches	$C_{2,1} \cdot 10^3$ Inches
9-21-67	-0.111	0.583	0.108	0.337	-0.150
9-22-67 10:00 am	-0.107	0.570	0.112	0.340	-0.158
9-22-67 5:00 pm	-0.117	0.573	0.115	0.405	-0.159
Average Value	-0.112±5%	0.575±1.3%	0.112+0.5%	0.361±10%	-0.156±4%

TABLE II

PRINCIPAL COMPONENTS OF THE INITIAL IMPERFECTION SURFACE

Shell A7

	$\overline{\xi}$		$\overline{\xi}$		$\overline{\xi}$		$\overline{\xi}$
$A_{2,0}$	-0.402	$B_{2,0}$	-0.241	$A_{2,\frac{1}{2}}$	-0.457	$B_{2,\frac{1}{2}}$	-0.348
$A_{3,0}$	-0.456	$B_{3,0}$	0.150	$A_{3,\frac{1}{2}}$	-0.601	$B_{4,\frac{1}{2}}$	0.129
$A_{4,0}$	0.103	$B_{4,0}$	0.504	$A_{4,\frac{1}{2}}$	0.048	$B_{6,\frac{1}{2}}$	-0.149
$A_{5,0}$	0.193	$B_{5,0}$	0.128	$A_{5,\frac{1}{2}}$	0.073	$B_{8,\frac{1}{2}}$	0.069
$A_{6,0}$	0.114	$B_{6,0}$	-0.165	$A_{7,\frac{1}{2}}$	-0.047	$C_{2,2}\frac{1}{2}$	-0.518
$A_{10,0}$	-0.048	$B_{7,0}$	-0.074	$A_{8,\frac{1}{2}}$	-0.050	$C_{3,\frac{1}{2}}$	-0.586
$A_{0,\frac{1}{2}}$	0.068	$C_{0,1}$	0.068	$A_{2,\frac{3}{2}}$	-0.049	$C_{4,\frac{1}{2}}$	0.136

Note: $\overline{\xi}$ = $\dfrac{\text{Amplitude of the Harmonic}}{\text{Wall Thickness}}$

TABLE II (Cont'd)

PRINCIPAL COMPONENTS OF THE INITIAL IMPERFECTION SURFACE

Shell A7

	$\bar{\xi}$		$\bar{\xi}$		$\bar{\xi}$		$\bar{\xi}$		$\bar{\xi}$
$C_{5,\frac{1}{2}}$	0.242	$C_{2,\frac{5}{2}}$	-0.085	$D_{4,\frac{1}{2}}$	0.644	$D_{6,1}$	-0.108	$D_{2,2}$	-0.126
$C_{6,\frac{1}{2}}$	0.145	$C_{3,\frac{5}{2}}$	-0.099	$D_{5,\frac{1}{2}}$	0.167	$D_{8,1}$	0.049	$D_{4,2}$	0.048
$C_{9,\frac{1}{2}}$	0.051	$C_{2,3}$	-0.103	$D_{6,\frac{1}{2}}$	-0.200	$D_{2,\frac{3}{2}}$	-0.100	$D_{6,2}$	-0.063
$C_{10,\frac{1}{2}}$	-0.073	$C_{2,\frac{7}{2}}$	-0.054	$D_{7,\frac{1}{2}}$	-0.075	$D_{3,\frac{3}{2}}$	0.066	$D_{2,\frac{5}{2}}$	-0.054
$C_{3,1}$	-0.045	$C_{3,\frac{7}{2}}$	-0.062	$D_{13,\frac{1}{2}}$	-0.048	$D_{4,\frac{3}{2}}$	0.200	$D_{4,\frac{5}{2}}$	0.112
$C_{5,1}$	0.056	$D_{2,\frac{1}{2}}$	-0.308	$D_{2,1}$	-0.271	$D_{5,\frac{3}{2}}$	0.047	$D_{6,\frac{5}{2}}$	-0.047
$C_{2,\frac{3}{2}}$	-0.155	$D_{3,\frac{1}{2}}$	0.189	$D_{4,1}$	0.100	$D_{7,\frac{3}{2}}$	-0.056	$D_{2,3}$	-0.079

TABLE II (Cont'd)

PRINCIPAL COMPONENTS OF THE INITIAL IMPERFECTION SURFACE

Shell A8

	$\bar{\xi}$		$\bar{\xi}$		$\bar{\xi}$		$\bar{\xi}$
$A_{2,0}$	-0.611	$A_{0,2}$	-0.199	$C_{0,2}$	0.266	$B_{2,\frac{1}{2}}$	-0.289
$A_{3,0}$	0.655	$A_{0,\frac{5}{2}}$	-0.163	$A_{2,\frac{1}{2}}$	0.796	$B_{3,\frac{1}{2}}$	0.115
$A_{4,0}$	0.128	$A_{0,3}$	-0.080	$A_{3,\frac{1}{2}}$	-0.241	$B_{4,\frac{1}{2}}$	-0.154
$A_{6,0}$	0.086	$B_{2,0}$	0.237	$A_{4,\frac{1}{2}}$	0.131	$B_{6,\frac{1}{2}}$	-0.083
$A_{7,0}$	-0.138	$B_{6,0}$	0.099	$A_{4,1}$	-0.057	$B_{7,\frac{1}{2}}$	0.048
$A_{0,\frac{1}{2}}$	0.653	$B_{10,0}$	-0.054	$A_{2,\frac{3}{2}}$	0.093	$B_{9,\frac{1}{2}}$	-0.055
$A_{0,1}$	0.103	$C_{0,1}$	0.611	$A_{1,2}$	-0.049	$B_{2,1}$	0.065
$A_{0,\frac{3}{2}}$	-0.070	$C_{0,\frac{3}{2}}$	0.231	$A_{1,\frac{5}{2}}$	-0.070	$B_{3,1}$	0.048

TABLE II (Cont'd)

PRINCIPAL COMPONENTS OF THE INITIAL IMPERFECTION SURFACE

Shell A8

	$\bar{\xi}$		$\bar{\xi}$		$\bar{\xi}$		$\bar{\xi}$
$B_{6,1}$	-0.050	$C_{3,1}$	-0.180	$C_{3,3}$	-0.060	$D_{3,1}$	0.087
$B_{2,\frac{5}{2}}$	-0.053	$C_{4,1}$	0.102	$C_{2,\frac{7}{2}}$	-0.094	$D_{4,1}$	-0.113
$C_{2,\frac{1}{2}}$	-0.777	$C_{1,\frac{3}{2}}$	0.051	$D_{2,\frac{1}{2}}$	0.277	$D_{6,1}$	-0.052
$C_{3,\frac{1}{2}}$	0.094	$C_{2,\frac{3}{2}}$	-0.239	$D_{3,\frac{1}{2}}$	-0.073	$D_{9,1}$	-0.048
$C_{4,\frac{1}{2}}$	0.187	$C_{2,2}$	0.292	$D_{6,\frac{1}{2}}$	0.148	$D_{2,2}$	-0.068
$C_{6,\frac{1}{2}}$	0.104	$C_{3,2}$	-0.105	$D_{8,\frac{1}{2}}$	-0.054	$D_{3,2}$	0.058
$C_{7,\frac{1}{2}}$	-0.180	$C_{2,\frac{5}{2}}$	-0.145	$D_{10,\frac{1}{2}}$	-0.068	$D_{4,2}$	-0.057
$C_{2,1}$	0.612	$C_{2,3}$	0.173	$D_{2,1}$	-0.221	$D_{6,2}$	-0.046
						$D_{2,\frac{5}{2}}$	0.075

TABLE II (Cont'd)

PRINCIPAL COMPONENTS OF THE INITIAL IMPERFECTION SURFACE

Shell A9

	$\bar{\xi}$		$\bar{\xi}$		$\bar{\xi}$		$\bar{\xi}$
$A_{2,0}$	-0.153	$B_{2,0}$	0.450	$A_{3,\frac{1}{2}}$	-0.149	$C_{7,\frac{1}{2}}$	-0.062
$A_{3,0}$	0.154	$B_{3,0}$	-0.240	$A_{4,\frac{1}{2}}$	0.094	$C_{9,\frac{1}{2}}$	-0.087
$A_{6,0}$	-0.078	$B_{4,0}$	0.163	$B_{2,\frac{1}{2}}$	-0.402	$C_{2,1}$	-0.183
$A_{7,0}$	-0.047	$B_{5,0}$	0.076	$B_{5,\frac{1}{2}}$	0.078	$C_{3,1}$	-0.115
$A_{9,0}$	-0.061	$B_{7,0}$	-0.086	$C_{2,\frac{1}{2}}$	-0.199	$C_{4,1}$	0.075
$A_{0,\frac{1}{2}}$	0.081	$C_{0,\frac{1}{2}}$	0.056	$C_{3,\frac{1}{2}}$	0.188	$C_{2,\frac{3}{2}}$	-0.057
$A_{0,1}$	-0.047	$C_{0,1}$	0.069	$C_{5,\frac{1}{2}}$	-0.052	$C_{3,\frac{3}{2}}$	0.076
$A_{0,2}$	-0.051	$A_{2,\frac{1}{2}}$	-0.240	$C_{6,\frac{1}{2}}$	-0.103	$C_{2,2}$	-0.092

TABLE II (Cont'd)

PRINCIPAL COMPONENTS OF THE INITIAL IMPERFECTION SURFACE

Shell A9

	$\bar{\xi}$		$\bar{\xi}$
$C_{3,2}$	-0.054	$D_{5,1}$	0.056
$C_{2,3}$	-0.051	$D_{2,\frac{3}{2}}$	0.182
$D_{2,\frac{1}{2}}$	0.570	$D_{3,\frac{3}{2}}$	-0.092
$D_{3,\frac{1}{2}}$	-0.311	$D_{4,\frac{3}{2}}$	0.071
$D_{4,\frac{1}{2}}$	0.205	$D_{2,2}$	-0.145
$D_{5,\frac{1}{2}}$	0.096	$D_{2,\frac{5}{2}}$	0.102
$D_{7,\frac{1}{2}}$	-0.110	$D_{3,\frac{5}{2}}$	-0.050
$D_{8,\frac{1}{2}}$	0.054	$D_{2,3}$	-0.087
$D_{2,1}$	-0.312	$D_{2,\frac{7}{2}}$	0.064

TABLE II (Cont'd)

PRINCIPAL COMPONENTS OF THE INITIAL IMPERFECTION SURFACE

Shell A10

	$\bar{\xi}$		$\bar{\xi}$		$\bar{\xi}$		$\bar{\xi}$
$A_{4,0}$	0.244	$B_{5,0}$	0.112	$B_{2,\frac{1}{2}}$	-0.103	$C_{7,\frac{1}{2}}$	0.056
$A_{6,0}$	-0.166	$B_{6,0}$	-0.073	$B_{3,\frac{1}{2}}$	0.155	$C_{8,\frac{1}{2}}$	0.078
$A_{7,0}$	0.048	$B_{7,0}$	-0.126	$B_{5,\frac{1}{2}}$	-0.130	$C_{9,\frac{1}{2}}$	-0.081
$A_{8,0}$	0.060	$B_{10,0}$	-0.057	$B_{6,\frac{1}{2}}$	-0.063	$C_{2,1}$	0.209
$A_{9,0}$	-0.063	$A_{2,\frac{1}{2}}$	0.267	$B_{8,\frac{1}{2}}$	-0.097	$C_{3,1}$	0.126
$B_{2,0}$	-0.096	$A_{3,\frac{1}{2}}$	0.167	$B_{10,\frac{1}{2}}$	0.062	$C_{7,1}$	0.048
$B_{3,0}$	-0.399	$A_{7,\frac{1}{2}}$	0.059	$C_{4,\frac{1}{2}}$	0.308	$C_{8,1}$	-0.050
$B_{4,0}$	-0.102	$A_{8,\frac{1}{2}}$	-0.064	$C_{6,\frac{1}{2}}$	-0.215	$C_{4,\frac{3}{2}}$	0.104

TABLE II (Cont'd)

PRINCIPAL COMPONENTS OF THE INITIAL IMPERFECTION SURFACE

Shell A10

	$\bar{\xi}$		$\bar{\xi}$		$\bar{\xi}$
$C_{6,\frac{3}{2}}$	-0.061	$D_{5,\frac{1}{2}}$	0.143	$D_{8,1}$	-0.074
$C_{2,2}$	0.094	$D_{6,\frac{1}{2}}$	-0.093	$D_{10,1}$	0.047
$C_{3,2}$	0.065	$D_{7,\frac{1}{2}}$	-0.155	$D_{3,\frac{3}{2}}$	-0.159
$C_{4,\frac{5}{2}}$	0.059	$D_{10,\frac{1}{2}}$	-0.065	$D_{7,\frac{3}{2}}$	-0.058
$C_{2,3}$	0.057	$D_{2,1}$	-0.077	$D_{3,2}$	0.055
$D_{2,\frac{1}{2}}$	-0.127	$D_{3,1}$	0.120	$D_{5,2}$	-0.049
$D_{3,\frac{1}{2}}$	-0.509	$D_{5,1}$	-0.098	$D_{3,\frac{5}{2}}$	-0.087
$D_{4,\frac{1}{2}}$	-0.128	$D_{6,1}$	-0.049	$D_{3,\frac{7}{2}}$	-0.057

TABLE II (Cont'd)

PRINCIPAL COMPONENTS OF THE INITIAL IMPERFECTION SURFACE

Shell A12

	$\bar{\xi}$		$\bar{\xi}$		$\bar{\xi}$		$\bar{\xi}$
$A_{2,0}$	0.076	$B_{4,0}$	0.215	$A_{4,\frac{1}{2}}$	-0.150	$B_{3,\frac{1}{2}}$	-0.318
$A_{3,0}$	0.235	$B_{5,0}$	-0.295	$A_{5,\frac{1}{2}}$	-0.111	$B_{4,\frac{1}{2}}$	-0.098
$A_{4,0}$	0.190	$B_{6,0}$	0.070	$A_{6,\frac{1}{2}}$	0.114	$B_{5,\frac{1}{2}}$	0.302
$A_{6,0}$	-0.053	$B_{7,0}$	0.256	$A_{7,\frac{1}{2}}$	0.166	$B_{6,\frac{1}{2}}$	0.047
$A_{7,0}$	-0.130	$B_{8,0}$	0.089	$A_{10,\frac{1}{2}}$	-0.051	$B_{7,\frac{1}{2}}$	-0.113
$A_{8,0}$	0.102	$B_{10,0}$	-0.046	$A_{9,1}$	0.052	$B_{8,\frac{1}{2}}$	-0.054
$B_{2,0}$	0.286	$A_{2,\frac{1}{2}}$	0.145	$A_{3,\frac{3}{2}}$	-0.074	$B_{9,\frac{1}{2}}$	-0.089
$B_{3,0}$	0.229	$A_{3,\frac{1}{2}}$	-0.639	$B_{2,\frac{1}{2}}$	-0.448	$B_{11,\frac{1}{2}}$	0.060

TABLE II (Cont'd)

PRINCIPAL COMPONENTS OF THE INITIAL IMPERFECTION SURFACE

Shell A12

	$\bar{\xi}$		$\bar{\xi}$		$\bar{\xi}$		$\bar{\xi}$
$B_{2,\frac{3}{2}}$	-0.052	$C_{3,1}$	-0.498	$C_{2,2}$	0.054	$C_{3,6}$	-0.072
$C_{2,\frac{1}{2}}$	0.102	$C_{4,1}$	-0.118	$C_{3,2}$	-0.248	$C_{3,7}$	-0.058
$C_{3,\frac{1}{2}}$	0.292	$C_{5,1}$	-0.088	$C_{4,2}$	-0.058	$D_{2,\frac{1}{2}}$	0.365
$C_{4,\frac{1}{2}}$	0.242	$C_{6,1}$	0.087	$C_{6,2}$	0.047	$D_{3,\frac{1}{2}}$	0.288
$C_{6,\frac{1}{2}}$	-0.065	$C_{7,1}$	0.128	$C_{7,2}$	0.067	$D_{4,\frac{1}{2}}$	0.276
$C_{7,\frac{1}{2}}$	-0.154	$C_{3,\frac{3}{2}}$	0.107	$C_{3,3}$	-0.163	$D_{5,\frac{1}{2}}$	-0.386
$C_{8,\frac{1}{2}}$	0.131	$C_{4,\frac{3}{2}}$	0.080	$C_{3,4}$	-0.119	$D_{6,\frac{1}{2}}$	0.087
$C_{2,1}$	0.113	$C_{7,\frac{3}{2}}$	-0.071	$C_{3,5}$	-0.091	$D_{7,\frac{1}{2}}$	0.334

TABLE II (Cont'd)

PRINCIPAL COMPONENTS OF THE INITIAL IMPERFECTION SURFACE

Shell A12

	$\bar{\xi}$		$\bar{\xi}$		$\bar{\xi}$		$\bar{\xi}$
$D_{8,\frac{1}{2}}$	0.117	$D_{2,\frac{3}{2}}$	0.118	$D_{2,\frac{5}{2}}$	0.072	$D_{2,\frac{7}{2}}$	0.050
$D_{9,\frac{1}{2}}$	0.058	$D_{3,\frac{3}{2}}$	0.103	$D_{3,\frac{5}{2}}$	0.061	$D_{5,\frac{7}{2}}$	-0.046
$D_{2,1}$	-0.349	$D_{4,\frac{3}{2}}$	0.087	$D_{4,\frac{5}{2}}$	0.053	$D_{2,4}$	-0.084
$D_{3,1}$	-0.247	$D_{5,\frac{3}{2}}$	-0.110	$D_{5,\frac{5}{2}}$	-0.065	$D_{3,4}$	-0.059
$D_{4,1}$	-0.076	$D_{7,\frac{3}{2}}$	0.097	$D_{7,\frac{5}{2}}$	0.057	$D_{5,4}$	0.054
$D_{5,1}$	0.240	$D_{2,2}$	-0.173	$D_{2,3}$	-0.114	$D_{2,5}$	-0.064
$D_{7,1}$	-0.091	$D_{3,2}$	-0.126	$D_{3,3}$	-0.080	$D_{3,5}$	-0.046
$D_{9,1}$	-0.069	$D_{5,2}$	0.114	$D_{5,3}$	0.074	$D_{2,6}$	-0.050

TABLE III

VARIATION OF THE BEST FIT ("PERFECT") CYLINDER

WITH LOAD INCREMENTS

Shell A7	$\frac{P}{P_{c\ell}}$ %	$X_1 \cdot 10^2$ Inches	$Y_1 \cdot 10^2$ Inches	$\epsilon_1 \cdot 10^2$ Radians	$\epsilon_2 \cdot 10^2$ Radians	R Inches
1	-3.9	-0.501	-0.055	-0.218	0.120	4.0047
2	6.1	-0.504	-0.054	-0.217	0.119	4.0046
3	11.0	-0.502	-0.053	-0.219	0.119	4.0048
4	18.8	-0.506	-0.052	-0.219	0.118	4.0048
5	23.0	-0.511	-0.050	-0.221	0.119	4.0049
6	27.0	-0.523	-0.041	-0.219	0.118	4.0051
7	32.5	-0.516	-0.040	-0.220	0.118	4.0053
8	38.2	-0.517	-0.039	-0.219	0.118	4.0054

TABLE III (Cont'd)

VARIATION OF THE BEST FIT ("PERFECT") CYLINDER

WITH LOAD INCREMENTS

Shell A7	$\frac{P}{P_{cl}}$ %	$X_1 \cdot 10^2$	$Y_1 \cdot 10^2$	$\epsilon_1 \cdot 10^2$	$\epsilon_2 \cdot 10^2$	
		Inches	Inches	Radians	Radians	Inches
9	45.1	-0.513	-0.039	-0.221	0.118	4.0059
10	53.9	-0.520	-0.041	-0.223	0.118	4.0060
11	** 55.3	-0.485	-0.035	-0.222	0.118	4.0058
12	* 59.7	-0.271	0.107	-0.271	0.065	4.0040

*   Buckling Pattern

**   Initial Local Buckling Pattern

TABLE III (Cont'd)

VARIATION OF THE BEST FIT ("PERFECT") CYLINDER

WITH LOAD INCREMENTS

Shell A8	$\dfrac{P}{P_{c\ell}}$ %	$X_1 \cdot 10^2$	$Y_1 \cdot 10^2$	$\epsilon_1 \cdot 10^2$	$\epsilon_2 \cdot 10^2$	R
		Inches	Inches	Radians	Radians	Inches
1	-2.4	-0.757	0.304	-0.266	0.109	4.0036
2	4.7	-0.766	0.307	-0.265	0.110	4.0033
3	11.0	-0.776	0.318	-0.267	0.111	4.0034
4	20.5	-0.782	0.325	-0.268	0.111	4.0034
5	27.4	-0.782	0.325	-0.269	0.112	4.0034
6	33.9	-0.784	0.324	-0.270	0.112	4.0034
7	42.0	-0.784	0.323	-0.270	0.111	4.0035
8	48.5	-0.786	0.322	-0.271	0.111	4.0036

TABLE III (Cont'd)

VARIATION OF THE BEST FIT ("PERFECT") CYLINDER

WITH LOAD INCREMENTS

Shell A8	$\frac{P}{P_{c\ell}}$ %	$X_1 \cdot 10^2$	$Y_1 \cdot 10^2$	$\epsilon_1 \cdot 10^2$	$\epsilon_2 \cdot 10^2$	R
		Inches	Inches	Radians	Radians	Inches
9	56.4	-0.788	0.321	-0.271	0.110	4.0037
10	63.7	-0.789	0.321	-0.271	0.110	4.0038
11	* 65.8	-0.789	0.286	-0.269	0.108	4.0010

* Buckling Pattern

TABLE III (Cont'd)

VARIATION OF THE BEST FIT ("PERFECT") CYLINDER

WITH LOAD INCREMENTS

Shell A9	$\frac{P}{P_{c\ell}} \%$	$X_1 \cdot 10^2$ Inches	$Y_1 \cdot 10^2$ Inches	$\epsilon_1 \cdot 10^2$ Radians	$\epsilon_2 \cdot 10^2$ Radians	R Inches
1	-4.5	-0.594	0.346	-0.213	0.101	4.0007
2	4.2	-0.599	0.348	-0.210	0.100	4.0007
3	11.8	-0.602	0.349	-0.210	0.100	4.0009
4	20.9	-0.603	0.350	-0.209	0.101	4.0010
5	28.6	-0.604	0.352	-0.209	0.101	4.0012
6	36.0	-0.605	0.353	-0.209	0.101	4.0012
7	43.5	-0.605	0.353	-0.209	0.101	4.0012
8	50.4	-0.605	0.354	-0.208	0.101	4.0012
9	57.1	-0.607	0.355	-0.207	0.101	4.0015
10	61.4	-0.605	0.355	-0.208	0.102	4.0015

TABLE III (Cont'd)

VARIATION OF THE BEST FIT ("PERFECT") CYLINDER

WITH LOAD INCREMENTS

Shell A9	$\frac{P}{P_{c\ell}}$ %	$X_1 \cdot 10^2$ Inches	$Y_1 \cdot 10^2$ Inches	$\epsilon_1 \cdot 10^2$ Radians	$\epsilon_2 \cdot 10^2$ Radians	R Inches
11	65.6	-0.605	0.355	-0.209	0.102	4.0016
12	69.1	-0.604	0.354	-0.209	0.101	4.0016
13	72.2	-0.604	0.353	-0.209	0.101	4.0015
14	* 73.6	-0.680	0.307	-0.210	0.102	3.9989

82

* Buckling Pattern

TABLE III (Cont'd)

VARIATION OF THE BEST FIT ("PERFECT") CYLINDER

WITH LOAD INCREMENTS

Shell A10	$\frac{P}{P_{c\ell}}$ %	$X_1 \cdot 10^2$ Inches	$Y_1 \cdot 10^2$ Inches	$\epsilon_1 \cdot 10^2$ Radians	$\epsilon_2 \cdot 10^2$ Radians	R Inches
1	-1.2	0.324	-0.599	-0.025	-0.062	4.0186
2	7.2	0.324	-0.599	-0.025	-0.062	4.0186
3	14.9	0.323	-0.600	-0.025	-0.063	4.0186
4	28.8	0.323	-0.602	-0.025	-0.064	4.0187
5	42.9	0.321	-0.606	-0.026	-0.065	4.0189
6	** 54.1	0.316	-0.597	-0.023	-0.073	4.0190
7	* 56.8	0.275	-0.594	0.009	-0.054	4.0170

*   Buckling Pattern

**   Initial Local Buckling Pattern

TABLE III (Cont'd)

VARIATION OF THE BEST FIT ("PERFECT") CYLINDER

WITH LOAD INCREMENTS

Shell A12	$\frac{P}{P_{c\ell}}\%$	$X_1 \cdot 10^2$	$Y_1 \cdot 10^2$	$\epsilon_1 \cdot 10^2$	$\epsilon_2 \cdot 10^2$	R
		Inches	Inches	Radians	Radians	Inches
1	-5.3	0.348	-0.615	-0.057	-0.042	4.0087
2	8.1	0.349	-0.622	-0.058	-0.041	4.0088
3	24.0	0.344	-0.614	-0.058	-0.044	4.0089
4	38.2	0.337	-0.607	-0.059	-0.046	4.0091
5	50.5	0.338	-0.622	-0.062	-0.045	4.0093
6	60.4	0.335	-0.627	-0.062	-0.044	4.0094
7	* 67.3	0.375	-0.601	-0.076	-0.050	4.0062

* Buckling Pattern

84

TABLE IV

SUMMARY OF BUCKLING TESTS

Shell	$E \cdot 10^{-6}$ lb/in^2	$t \cdot 10^3$ inches	$\dfrac{P}{P_{c\ell}}$	$\dfrac{\sigma_{max} - \sigma_{min}}{\sigma_{ave}}$ %	m	Remarks
A7	15.1	4.494	0.553/0.597	28.9	13	Local Buckling with 2 isolated dimples in the middle
A8	15.2	4.640	0.658	22.0	13	
A9	14.7	4.540	0.736	17.0	13	
A10	14.9	4.740	0.554/0.568	10.1	17	Local Buckling with 1 isolated dimple at the upper boundary
A12	15.2	4.740	0.673	10.1	13	

Nominal Dimensions for all shells: R = 4.003 in.

L = 8.00 in.

Except Shell A12   L = 8.20 in.

TABLE V

SUMMARY OF "CRITICAL" FOURIER COEFFICIENTS

Shell A7	Δ_9	$\bar{\xi}$	η
$A_{2,0}$	0.056	-0.402	-0.14
$A_{6,0}$	-0.015	0.114	-0.13
$A_{9,0}$	0.026	0.031	0.84
$A_{12,0}$	0.011	0.005	2.20
$B_{2,0}$	-0.024	-0.241	0.10
$B_{6,0}$	-0.011	-0.165	0.07
$B_{7,0}$	0.019	-0.074	-0.26
$B_{13,0}$	-0.018	-0.026	0.69
$C_{0,1}$	-0.045	0.068	-0.66
$C_{0,2}$	-0.016	0.013	-1.23

Note: $\bar{\xi} = \dfrac{\text{Initial Amplitude of the Harmonic}}{\text{Wall Thickness}}$

$\eta = \Delta_9 / \bar{\xi}$

TABLE V (Cont'd)

SUMMARY OF "CRITICAL" FOURIER COEFFICIENTS

Shell A7	Δ_9	$\bar{\xi}$	η
$A_{8,\frac{1}{2}}$	0.012	-0.050	-0.24
$A_{11,\frac{1}{2}}$	0.014	0.029	0.48
$A_{15,\frac{1}{2}}$	0.022	0.011	2.00
$A_{9,1}$	-0.020	-0.028	0.71
$A_{10,1}$	0.012	0.029	0.41
$A_{18,2}$	-0.012	-0.006	2.00
$B_{2,\frac{1}{2}}$	0.012	-0.348	-0.03
$B_{11,\frac{1}{2}}$	0.014	0.036	0.39
$B_{12,\frac{1}{2}}$	-0.021	-0.0001	210.0
$B_{14,\frac{1}{2}}$	0.028	0.008	3.50
$B_{1,1}$	-0.018	0.013	-1.38
$B_{13,1}$	0.016	0.035	0.46
$B_{15,1}$	-0.011	-0.013	0.85

TABLE V (Cont'd)

SUMMARY OF "CRITICAL" FOURIER COEFFICIENTS

Shell A7	Δ_9	$\bar{\xi}$	η
$C_{2,\frac{1}{2}}$	0.072	-0.518	-0.14
$C_{6,\frac{1}{2}}$	-0.019	0.145	-0.13
$C_{8,\frac{1}{2}}$	0.015	0.150	0.10
$C_{9,\frac{1}{2}}$	0.042	0.051	0.82
$C_{10,\frac{1}{2}}$	-0.015	-0.073	0.21
$C_{8,1}$	0.012	0.033	-0.36
$C_{11,1}$	0.016	0.033	0.48
$C_{15,1}$	0.024	0.016	1.50
$C_{2,\frac{3}{2}}$	0.019	0.155	-0.12
$C_{2,\frac{5}{2}}$	0.013	-0.085	-0.15

TABLE V (Cont'd)

SUMMARY OF "CRITICAL" FOURIER COEFFICIENTS

Shell A7	Δ_9	$\bar{\xi}$	η
$D_{2,\frac{1}{2}}$	-0.029	-0.308	0.09
$D_{3,\frac{1}{2}}$	-0.011	0.189	-0.06
$D_{6,\frac{1}{2}}$	-0.016	-0.200	0.08
$D_{7,\frac{1}{2}}$	0.027	-0.075	-0.36
$D_{13,\frac{1}{2}}$	-0.029	-0.048	0.60
$D_{11,1}$	0.015	0.036	0.42
$D_{12,1}$	-0.022	-0.036	0.61
$D_{14,1}$	0.033	0.020	1.65
$D_{2,\frac{3}{2}}$	-0.011	-0.100	0.11
$D_{15,\frac{3}{2}}$	-0.010	-0.012	0.83

TABLE V (Cont'd)

SUMMARY OF "CRITICAL" FOURIER COEFFICIENTS

Shell A8	Δ_9	$\bar{\xi}$	η
$A_{2,0}$	-0.023	-0.611	0.04
$A_{5,0}$	0.013	-0.038	-0.34
$A_{8,0}$	-0.024	0.006	-4.00
$A_{12,0}$	0.014	-0.002	-7.00
$A_{13,0}$	0.024	-0.018	-1.33
$A_{0,\frac{1}{2}}$	0.014	0.653	0.02
$A_{0,1}$	0.013	0.103	0.12
$B_{2,0}$	-0.026	0.024	-1.08
$B_{3,0}$	-0.020	-0.042	0.48
$B_{8,0}$	-0.012	-0.045	0.27
$B_{10,0}$	0.013	-0.054	-0.24
$B_{12,0}$	-0.028	0.004	-7.00
$B_{13,0}$	0.014	0.007	2.00
$C_{0,1}$	0.011	0.611	0.02

TABLE V (Cont'd)

SUMMARY OF "CRITICAL" FOURIER COEFFICIENTS

Shell A8	Δ_9	$\overline{\xi}$	η
$A_{9,\frac{1}{2}}$	-0.012	0.010	-1.20
$A_{10,\frac{1}{2}}$	0.014	0.014	1.00
$A_{8,1}$	0.012	0.024	0.50
$A_{12,1}$	-0.013	-0.007	1.86
$A_{13,1}$	-0.024	-0.023	1.05
$B_{4,\frac{1}{2}}$	0.017	-0.154	-0.11
$B_{11,\frac{1}{2}}$	0.018	0.025	0.72
$B_{12,1}$	0.023	0.013	1.76
$B_{13,1}$	-0.012	-0.016	0.75
$B_{16,1}$	-0.011	-0.003	3.66

TABLE V (Cont'd)

SUMMARY OF "CRITICAL" FOURIER COEFFICIENTS

Shell A8	Δ_9	$\bar{\xi}$	η
$C_{2,\frac{1}{2}}$	-0.031	-0.777	0.04
$C_{5,\frac{1}{2}}$	0.017	-0.035	-0.48
$C_{8,\frac{1}{2}}$	-0.036	-0.005	7.20
$C_{10,\frac{1}{2}}$	-0.015	-0.014	1.07
$C_{11,\frac{1}{2}}$	-0.011	-0.001	11.00
$C_{12,\frac{1}{2}}$	0.024	0.0001	240.0
$C_{13,\frac{1}{2}}$	0.041	-0.013	-3.15
$C_{9,1}$	-0.011	0.004	-2.75
$C_{10,1}$	0.015	0.015	1.00
$C_{1,\frac{3}{2}}$	0.010	0.051	0.20
$C_{13,\frac{3}{2}}$	-0.011	-0.022	0.50
$C_{2,\frac{3}{2}}$	-0.011	-0.239	0.05

TABLE V (Cont'd)

SUMMARY OF "CRITICAL" FOURIER COEFFICIENTS

Shell A8	Δ_9	$\overline{\xi}$	η
$D_{2,\frac{1}{2}}$	-0.036	0.277	-0.13
$D_{3,\frac{1}{2}}$	-0.028	-0.073	0.38
$D_{5,\frac{1}{2}}$	0.010	0.040	0.25
$D_{6,\frac{1}{2}}$	0.015	0.148	0.10
$D_{7,\frac{1}{2}}$	0.011	-0.024	-0.46
$D_{8,\frac{1}{2}}$	-0.016	-0.054	0.30
$D_{10,\frac{1}{2}}$	0.020	-0.068	-0.29
$D_{12,\frac{1}{2}}$	-0.046	-0.0004	115.0
$D_{13,\frac{1}{2}}$	0.022	0.016	1.38

TABLE V (Cont'd)

SUMMARY OF "CRITICAL" FOURIER COEFFICIENTS

Shell A8	Δ_9	$\bar{\xi}$	η
$D_{4,1}$	0.013	-0.113	-0.11
$D_{9,1}$	-0.011	-0.048	0.23
$D_{11,1}$	0.020	0.012	1.67
$D_{14,1}$	0.011	-0.009	-1.22
$D_{14,\frac{3}{2}}$	-0.014	0.008	-1.75
$D_{15,\frac{3}{2}}$	0.011	0.002	5.50
$D_{16,\frac{3}{2}}$	-0.010	·0.008	1.25

TABLE V (Cont'd)

SUMMARY OF "CRITICAL" FOURIER COEFFICIENTS

Shell A9	Δ_{12}	$\overline{\xi}$	η
$A_{8,0}$	-0.020	-0.004	5.00
$A_{9,0}$	-0.038	-0.061	0.62
$A_{10,0}$	-0.026	-0.001	26.00
$A_{11,0}$	-0.023	-0.002	11.50
$B_{6,0}$	-0.015	-0.005	3.00
$B_{10,0}$	0.015	-0.005	-3.00
$C_{0,1}$	-0.013	0.069	-0.19

Note: $\eta = \Delta_{12}/\overline{\xi}$

TABLE V (Cont'd)

SUMMARY OF "CRITICAL" FOURIER COEFFICIENTS

Shell A9	Δ_{12}	$\overline{\xi}$	η
$A_{2,\frac{1}{2}}$	0.015	-0.240	-0.06
$A_{12,\frac{1}{2}}$	-0.025	-0.034	0.73
$A_{14,\frac{1}{2}}$	-0.010	0.001	-10.00
$A_{1,1}$	0.017	0.007	2.43
$A_{9,1}$	0.027	0.022	1.23
$A_{10,1}$	0.015	0.015	1.00
$A_{11,1}$	0.023	0.015	1.53
$A_{13,1}$	0.013	0.004	3.25
$A_{14,1}$	0.014	0.005	2.80
$A_{12,\frac{3}{2}}$	0.016	0.005	3.20
$A_{14,\frac{3}{2}}$	0.010	0.005	2.00
$A_{15,\frac{3}{2}}$	0.013	0.002	6.50
$A_{17,\frac{3}{2}}$	0.010	0.001	10.00

TABLE V (Cont'd)

SUMMARY OF "CRITICAL" FOURIER COEFFICIENTS

Shell A9	Δ_{12}	$\overline{\xi}$	η
$B_{6,\frac{1}{2}}$	0.011	0.035	0.31
$B_{10,\frac{1}{2}}$	-0.011	-0.020	0.55
$B_{12,\frac{1}{2}}$	-0.023	0.022	-1.05
$B_{13,\frac{1}{2}}$	-0.014	-0.019	0.74
$B_{13,1}$	-0.019	-0.008	2.37
$B_{15,1}$	-0.011	0.002	-5.50
$B_{16,1}$	-0.012	-0.009	1.33
$B_{13,\frac{3}{2}}$	0.012	0.004	3.00
$B_{16,2}$	0.011	0.002	5.50
$B_{18,2}$	0.010	0.0003	33.33

TABLE V (Cont'd)

SUMMARY OF "CRITICAL" FOURIER COEFFICIENTS

Shell A9	Δ_{12}	$\bar{\xi}$	η
$C_{4,\frac{1}{2}}$	-0.011	0.014	-0.79
$C_{5,\frac{1}{2}}$	0.011	-0.052	-0.21
$C_{8,\frac{1}{2}}$	-0.029	-0.014	2.07
$C_{9,\frac{1}{2}}$	-0.061	-0.087	0.70
$C_{10,\frac{1}{2}}$	-0.039	-0.008	4.87
$C_{11,\frac{1}{2}}$	-0.039	-0.008	4.87
$C_{12,\frac{1}{2}}$	-0.011	-0.042	0.26
$C_{14,\frac{1}{2}}$	-0.011	-0.010	1.10
$C_{2,1}$	0.011	-0.183	-0.06
$C_{12,1}$	-0.030	-0.031	0.97
$C_{14,1}$	-0.014	-0.002	7.00
$C_{15,1}$	-0.011	-0.006	1.83
$C_{1,\frac{3}{2}}$	0.011	-0.001	-11.00
$C_{13,\frac{3}{2}}$	0.011	0.005	2.20
$C_{14,\frac{3}{2}}$	0.012	0.002	6.00

TABLE V (Cont'd)

SUMMARY OF "CRITICAL" FOURIER COEFFICIENTS

Shell A9	Δ_{12}	$\bar{\xi}$	η
$D_{6,\frac{1}{2}}$	-0.019	-0.013	1.46
$D_{8,\frac{1}{2}}$	0.015	0.054	0.28
$D_{10,\frac{1}{2}}$	0.022	-0.001	-22.00
$D_{12,\frac{1}{2}}$	-0.015	0.017	-0.88
$D_{13,\frac{1}{2}}$	0.013	-0.002	-6.50
$D_{10,1}$	-0.011	-0.021	0.52
$D_{12,1}$	-0.025	0.013	1.92
$D_{13,1}$	-0.018	-0.018	1.00
$D_{13,\frac{3}{2}}$	-0.016	-0.010	1.60
$D_{15,\frac{3}{2}}$	-0.014	-0.0004	35.00
$D_{16,\frac{3}{2}}$	-0.015	-0.009	1.67

TABLE V (Cont'd)

SUMMARY OF "CRITICAL" FOURIER COEFFICIENTS

Shell A10	Δ_4	$\bar{\xi}$	η
$A_{2,0}$	-0.008	-0.033	0.24
$A_{3,0}$	0.013	-0.046	-0.28
$A_{4,0}$	-0.007	0.244	-0.03
$A_{8,0}$	0.007	0.060	0.17
$A_{9,0}$	-0.008	-0.063	0.13
$A_{13,0}$	-0.006	-0.007	0.86

Note: $\eta = \Delta_4/\bar{\xi}$

TABLE V (Cont'd)

SUMMARY OF "CRITICAL" FOURIER COEFFICIENTS

Shell A10	A_4	$\underline{\xi}$	η
$B_{2,0}$	-0.011	-0.096	0.15
$B_{3,0}$	-0.011	-0.399	0.03
$B_{4,0}$	0.007	-0.102	-0.07
$B_{6,0}$	-0.006	-0.073	0.08
$B_{9,0}$	0.011	0.026	0.42
$B_{10,0}$	0.007	-0.057	-0.12
$B_{12,0}$	-0.010	0.015	-0.67
$B_{13,0}$	-0.008	0.003	-2.67
$A_{3,\frac{1}{2}}$	-0.008	0.167	-0.05
$A_{13,\frac{1}{2}}$	0.007	0.003	2.33
$B_{3,\frac{1}{2}}$	0.006	0.155	0.04
$B_{4,\frac{1}{2}}$	-0.006	-0.018	0.33
$B_{14,\frac{1}{2}}$	-0.013	0.008	-1.62
$B_{12,1}$	-0.010	0.013	-0.77

TABLE V (Cont'd)

SUMMARY OF "CRITICAL" FOURIER COEFFICIENTS

Shell A10	Δ_4	$\bar{\xi}$	η
$C_{2,\frac{1}{2}}$	-0.010	-0.043	0.23
$C_{3,\frac{1}{2}}$	0.018	-0.003	-6.00
$C_{4,\frac{1}{2}}$	-0.008	0.308	-0.03
$C_{6,\frac{1}{2}}$	-0.007	-0.215	0.03
$C_{8,\frac{1}{2}}$	0.011	0.078	0.14
$C_{9,\frac{1}{2}}$	-0.012	-0.081	0.15
$C_{10,\frac{1}{2}}$	0.009	-0.007	-1.29
$C_{11,\frac{1}{2}}$	0.008	-0.014	-0.57
$C_{13,\frac{1}{2}}$	-0.009	-0.015	0.60
$C_{3,1}$	-0.007	0.126	-0.06
$C_{13,1}$	0.007	0.006	1.17

TABLE V (Cont'd)

SUMMARY OF "CRITICAL" FOURIER COEFFICIENTS

Shell A10	Δ_4	$\bar{\xi}$	η
$D_{2,\frac{1}{2}}$	-0.014	-0.127	0.11
$D_{3,\frac{1}{2}}$	-0.014	-0.509	0.03
$D_{4,\frac{1}{2}}$	0.009	-0.129	-0.07
$D_{6,\frac{1}{2}}$	-0.009	-0.093	0.09
$D_{8,\frac{1}{2}}$	-0.007	0.001	-7.00
$D_{9,\frac{1}{2}}$	0.016	0.036	0.45
$D_{10,\frac{1}{2}}$	0.010	-0.065	-0.15
$D_{12,\frac{1}{2}}$	-0.016	0.013	-1.23
$D_{13,\frac{1}{2}}$	-0.012	-0.001	12.00

TABLE V (Cont'd)

SUMMARY OF "CRITICAL" FOURIER COEFFICIENTS

Shell A12	Δ_5	$\bar{\xi}$	η
$A_{2,0}$	0.022	0.076	0.29
$A_{4,0}$	-0.014	0.190	-0.07
$A_{5,0}$	0.011	0.011	1.00
$A_{6,0}$	0.014	-0.053	-0.26
$A_{8,0}$	-0.012	0.102	-0.12
$A_{9,0}$	-0.069	-0.011	6.28
$A_{10,0}$	-0.041	-0.022	1.86
$A_{11,0}$	0.030	0.014	2.14
$A_{12,0}$	0.016	-0.027	-0.59

Note: $\eta = \Delta_5 / \bar{\xi}$

TABLE V (Cont'd)

SUMMARY OF "CRITICAL" FOURIER COEFFICIENTS

Shell A12	Δ_5	$\bar{\xi}$	η
$B_{6,0}$	-0.014	0.070	-0.20
$B_{10,0}$	0.070	-0.046	-1.52
$B_{11,0}$	0.063	-0.024	-2.63
$B_{13,0}$	-0.025	0.007	-3.57
$A_{15,\frac{1}{2}}$	0.018	0.004	4.50
$A_{9,1}$	0.044	0.052	0.85
$A_{10,1}$	0.023	0.026	0.88
$A_{11,1}$	-0.017	-0.012	1.42
$A_{16,1}$	0.024	-0.016	-1.50
$A_{17,1}$	-0.012	-0.007	1.72
$A_{18,1}$	-0.017	0.004	-4.25
$A_{15,\frac{3}{2}}$	-0.012	-0.005	2.40
$A_{17,\frac{3}{2}}$	0.011	0.004	2.75

TABLE V (Cont'd)

SUMMARY OF "CRITICAL" FOURIER COEFFICIENTS

Shell A12	Δ_5	$\bar{\xi}$	η
$B_{10,\frac{1}{2}}$	-0.017	-0.012	1.42
$B_{11,\frac{1}{2}}$	-0.012	0.060	-0.20
$B_{12,\frac{1}{2}}$	0.010	0.018	0.56
$B_{14,\frac{1}{2}}$	-0.029	0.015	-1.94
$B_{10,1}$	-0.041	-0.039	1.05
$B_{11,1}$	-0.041	-0.042	0.98
$B_{15,1}$	-0.015	-0.015	1.00
$B_{16,1}$	-0.010	0.008	-1.25
$B_{14,\frac{3}{2}}$	0.016	0.008	2.00
$B_{13,1}$	0.018	0.028	0.64

TABLE V (Cont'd)

SUMMARY OF "CRITICAL" FOURIER COEFFICIENTS

Shell A12	Δ_5	$\bar{\xi}$	η
$C_{2,\frac{1}{2}}$	0.029	0.102	0.28
$C_{4,\frac{1}{2}}$	-0.020	0.242	-0.08
$C_{5,\frac{1}{2}}$	0.016	-0.004	-4.00
$C_{6,\frac{1}{2}}$	0.022	-0.065	-0.34
$C_{7,\frac{1}{2}}$	0.012	-0.154	-0.08
$C_{8,\frac{1}{2}}$	-0.018	0.131	-0.14
$C_{10,\frac{1}{2}}$	-0.063	-0.040	1.58
$C11,\frac{1}{2}$	0.045	0.023	1.96
$C_{12,\frac{1}{2}}$	0.023	-0.027	0.85
$C_{15,\frac{1}{2}}$	0.011	-0.001	-11.00

TABLE V (Cont'd)

SUMMARY OF "CRITICAL" FOURIER COEFFICIENTS

Shell A12	Δ_5	$\bar{\xi}$	η
$C_{11,1}$	-0.011	-0.005	2.20
$C_{13,1}$	-0.011	0.008	-1.38
$C_{14,1}$	-0.013	-0.004	3.25
$C_{15,1}$	0.022	0.006	3.67
$C_{16,\frac{3}{2}}$	0.025	0.00004	625.0
$C_{17,\frac{3}{2}}$	-0.011	0.001	-11.0
$C_{18,\frac{3}{2}}$	-0.019	-0.0003	64.40

TABLE V (Cont'd)

SUMMARY OF "CRITICAL" FOURIER COEFFICIENTS

Shell A12	Δ_5	$\bar{\xi}$	η
$D_{4,\frac{1}{2}}$	0.013	0.276	0.05
$D_{5,\frac{1}{2}}$	-0.014	-0.386	0.04
$D_{6,\frac{1}{2}}$	-0.022	0.087	-0.25
$D_{9,\frac{1}{2}}$	0.014	0.058	0.24
$D_{11,\frac{1}{2}}$	0.098	-0.011	-8.90
$D_{13,\frac{1}{2}}$	-0.039	-0.004	9.75
$D_{15,\frac{1}{2}}$	0.012	-0.002	6.00
$D_{10,1}$	-0.017	-0.011	1.55
$D_{11,1}$	-0.012	0.045	-0.27
$D_{12,1}$	0.014	0.012	1.17
$D_{14,1}$	-0.033	0.008	-4.12
$D_{16,1}$	0.011	-0.001	-11.00
$D_{16,\frac{3}{2}}$	-0.013	0.002	-6.50

TABLE VI

SUMMARY OF WAVENUMBERS

i	Shell k	A7 ℓ	A8 ℓ	A9 ℓ	A10 ℓ	A12 ℓ
1	$\frac{1}{2}$	9.70	9.62	9.68	9.74	9.41
2	1	13.48	13.37	13.45	13.52	13.08
3	$\frac{3}{2}$	16.22	16.08	16.17	16.24	15.73
4	2	18.38	18.21	18.33	18.38	17.83
5	$\frac{5}{2}$	20.16	19.96	20.09	20.12	19.56
6	3	21.64	21.42	21.57	21.57	21.00
7	$\frac{7}{2}$	22.88	22.65	22.81	22.77	22.22

TABLE VII

NUMBERICAL RESULTS (Shell A7)

	$\overline{\xi}_1$		$\overline{\xi}_2$	λ_M
		$A_{9,\frac{1}{2}}$	-0.0050	0.998
$A_{0,1}$	-0.0214	$A_{10,\frac{1}{2}}$	0.0402	0.840
		$A_{11,\frac{1}{2}}$	0.0292	0.956
		$A_{12,1}$	-0.0135	0.992
$A_{0,2}$	-0.0421	$A_{13,1}$	0.0066	0.931
		$A_{14,1}$	0.0064	0.929
		$A_{15,\frac{3}{2}}$	-0.0122	0.936
$A_{0,3}$	-0.0314	$A_{16,\frac{3}{2}}$	-0.0017	0.944
		$A_{17,\frac{3}{2}}$	0.0122	0.902
		$A_{17,2}$	0.0040	0.949
$A_{0,4}$	-0.0326	$A_{18,2}$	-0.0061	0.905
		$A_{19,2}$	0.0039	0.917
		$A_{19,\frac{5}{2}}$	0.0032	0.920
$A_{0,5}$	-0.0329	$A_{20,\frac{5}{2}}$	-0.0003	0.923
		$A_{21,\frac{5}{2}}$	-0.0003	0.931

TABLE VII (Cont'd)

NUMERICAL RESULTS (Shell A7)

	$\overline{\xi}_1$			$\overline{\xi}_2$	λ_M
$A_{0,6}$	-0.0308		$A_{21,3}$	-0.0003	0.913
			$A_{22,3}$	-0.0017	0.986
			$A_{23,3}$	0.0003	0.925
$A_{0,7}$	-0.0423		$A_{22,\frac{7}{2}}$	-0.0003	0.862
			$A_{23,\frac{7}{2}}$	0.0015	0.842
			$A_{24,\frac{7}{2}}$	0.0002	0.862

TABLE VII (Cont'd)

NUMERICAL RESULTS (Shell A7)

$\overline{\xi}_1$			$\overline{\xi}_2$	λ_M
$A_{0,1}$	-0.0214	$B_{9,\frac{1}{2}}$	0.0322	0.914
		$B_{10,\frac{1}{2}}$	-0.0243	0.885
		$B_{11,\frac{1}{2}}$	0.0359	0.933
$A_{0,2}$	-0.0421	$B_{12,1}$	-0.0036	1.031
		$B_{13,1}$	0.0347	0.845
		$B_{14,1}$	-0.0091	0.916
$A_{0,3}$	-0.0314	$B_{15,\frac{3}{2}}$	0.0088	0.948
		$B_{16,\frac{3}{2}}$	0.0079	0.912
		$B_{17,\frac{3}{2}}$	-0.0053	0.933
$A_{0,4}$	-0.0326	$B_{17,2}$	0.0013	0.966
		$B_{18,2}$	0.0035	0.918
		$B_{19,2}$	0.0016	0.932
$A_{0,5}$	-0.0329	$B_{19,\frac{5}{2}}$	-0.0012	0.924
		$B_{20,\frac{5}{2}}$	0.0005	0.920
		$B_{21,\frac{5}{2}}$	-0.0012	0.921

TABLE VII (Cont'd)

NUMERICAL RESULTS (Shell A7)

	$\bar{\xi}_1$			$\bar{\xi}_2$	λ_M
$A_{0,6}$	-0.0308		$B_{21,3}$	0.0008	0.908
			$B_{22,3}$	-0.0003	0.910
			$B_{23,3}$	-0.00005	0.929
$A_{0,7}$	-0.0423		$B_{22,\frac{7}{2}}$	-0.0010	0.854
			$B_{23,\frac{7}{2}}$	0.0018	0.840
			$B_{24,\frac{7}{2}}$	$-0.8 \cdot 10^{-7}$	0.867

TABLE VII (Cont'd)

NUMERICAL RESULTS (Shell A7)

	$\overline{\xi}_1$			$\overline{\xi}_2$ or $\overline{\xi}_3$	λ_M
$C_{0,1}$	0.0683	{	$C_{9,\frac{1}{2}}$	0.0512	0.902
			$C_{10,\frac{1}{2}}$	-0.0734	0.794
			$C_{11,\frac{1}{2}}$	0.0399	0.957
$C_{0,2}$	0.0131	{	$A_{12,1}$	-0.0135	1.016
			$A_{13,1}$	0.0066	0.955
			$A_{14,1}$	0.0064	0.952
$C_{0,3}$	0.0101	{	$A_{15,\frac{3}{2}}$	-0.0122	0.961
			$A_{16,\frac{3}{2}}$	-0.0017	0.970
			$A_{17,\frac{3}{2}}$	0.0122	0.927
$C_{0,4}$	0.0051	{	$A_{17,2}$	0.0040	0.995
			$A_{18,2}$	-0.0061	0.950
			$A_{19,2}$	0.0039	0.962
$C_{0,5}$	0.0038	{	$A_{19,\frac{5}{2}}$	0.0032	0.981
			$A_{20,\frac{5}{2}}$	-0.0003	0.986
			$A_{21,\frac{5}{2}}$	-0.0003	0.995

TABLE VII (Cont'd)

NUMERICAL RESULTS (Shell A7)

	$\overline{\xi}_1$		$\overline{\xi}_2$ or $\overline{\xi}_3$	λ_M
$C_{0,6}$	0.0013	$A_{21,3}$	-0.0003	0.994
		$A_{22,3}$	-0.0017	0.976
		$A_{23,3}$	0.0003	1.009
$C_{0,7}$	$0.14 \cdot 10^{-6}$	$A_{22,\frac{7}{2}}$	-0.0003	1.001
		$A_{23,\frac{7}{2}}$	0.0015	0.978
		$A_{24,\frac{7}{2}}$	0.0002	1.005

TABLE VII (Cont'd)

NUMERICAL RESULTS (Shell A7)

	$\overline{\xi}_1$			$\overline{\xi}_3$	λ_M
$C_{0,1}$	0.0683	{	$B_{9,\frac{1}{2}}$	0.0322	0.893
			$B_{10,\frac{1}{2}}$	-0.0243	0.823
			$B_{11,\frac{1}{2}}$	0.0359	0.914
$C_{0,2}$	0.0131	{	$B_{12,1}$	-0.0036	1.055
			$B_{13,1}$	0.0347	0.955
			$B_{14,1}$	-0.0091	0.939
$C_{0,3}$	0.0101	{	$B_{15,\frac{3}{2}}$	0.0088	0.974
			$B_{16,\frac{3}{2}}$	0.0079	0.970
			$B_{17,\frac{3}{2}}$	-0.0053	0.959
$C_{0,4}$	0.0051	{	$B_{17,2}$	0.0013	1.012
			$B_{18,2}$	0.0035	0.950
			$B_{19,2}$	0.	0.979
$C_{0,5}$	0.0038	{	$B_{19,\frac{5}{2}}$	-0.00	0.986
			$B_{20,\frac{5}{2}}$	0.0005	0.986
			$B_{21,\frac{5}{2}}$	-0.0012	0.984

TABLE VII (Cont'd)

NUMERICAL RESULTS (Shell A7)

	$\overline{\xi}_1$			$\overline{\xi}_3$	λ_M
$C_{0,6}$	0.0013	{	$B_{21,3}$	0.0008	0.988
			$B_{22,3}$	-0.0003	0.976
			$B_{23,3}$	-0.00005	1.013
$C_{0,7}$	$0.14 \cdot 10^{-6}$	{	$B_{22,\frac{7}{2}}$	-0.0010	0.991
			$B_{23,\frac{7}{2}}$	0.0018	0.978
			$B_{24,\frac{7}{2}}$	$-0.8 \cdot 10^{-7}$	1.011

TABLE VII (Cont'd)

NUMBERICAL RESULTS (Shell A8)

$\overline{\xi}_1$			$\overline{\xi}_2$ or $\overline{\xi}_3$	λ_M
$A_{0,1}$	0.1027	$C_{9,\frac{1}{2}}$	-0.0248	0.889
		$C_{10,\frac{1}{2}}$	-0.0145	0.888
		$C_{11,\frac{1}{2}}$	-0.0009	1.117
$A_{0,2}$	-0.1992	$A_{12,1}$	-0.0070	0.877
		$A_{13,1}$	-0.0230	0.759
		$A_{14,1}$	0.0024	0.835
$A_{0,3}$	-0.0796	$A_{15,\frac{3}{2}}$	-0.0025	0.910
		$A_{16,\frac{3}{2}}$	-0.0010	0.890
		$A_{17,\frac{3}{2}}$	-0.0002	0.915
$A_{0,4}$	-0.0813	$A_{17,2}$	-0.0026	0.872
		$A_{18,2}$	0.0006	0.859
		$A_{19,2}$	$-0.8 \cdot 10^{-5}$	0.875
$A_{0,5}$	-0.0625	$A_{19,\frac{5}{2}}$	-0.0029	0.856
		$A_{20,\frac{5}{2}}$	0.0011	0.854
		$A_{21,\frac{5}{2}}$	0.0009	0.867

TABLE VII (Cont'd)

NUMERICAL RESULTS (Shell A8)

$\overline{\xi}_1$			$\overline{\xi}_2$ or $\overline{\xi}_3$	λ_M
$A_{0,6}$	-0.0637	$A_{21,3}$	-0.0015	0.819
		$A_{22,3}$	-0.0026	0.812
		$A_{23,3}$	0.0003	0.846
$A_{0,7}$	-0.0716	$A_{22,\frac{7}{2}}$	0.0011	0.771
		$A_{23,\frac{7}{2}}$	0.0005	0.771
		$A_{24,\frac{7}{2}}$	-0.0027	0.765

TABLE VII (Cont'd)

NUMERICAL RESULTS (Shell A8)

	$\overline{\xi}_1$		$\overline{\xi}_2$ or $\overline{\xi}_3$	λ_M
$A_{0,1}$	0.1027	$D_{9,\frac{1}{2}}$	-0.0026	0.967
		$D_{10,\frac{1}{2}}$	-0.0681	0.748
		$D_{11,\frac{1}{2}}$	0.0062	1.034
$A_{0,2}$	-0.1992	$B_{12,1}$	0.0132	0.857
		$B_{13,1}$	-0.0155	0.780
		$B_{14,1}$	0.0128	0.790
$A_{0,3}$	-0.0796	$B_{15,\frac{3}{2}}$	0.0003	0.926
		$B_{16,\frac{3}{2}}$	0.0027	0.879
		$B_{17,\frac{3}{2}}$	-0.0047	0.884
$A_{0,4}$	-0.0813	$B_{17,2}$	0.0017	0.877
		$B_{18,2}$	-0.0013	0.854
		$B_{19,2}$	-0.0018	0.857
$A_{0,5}$	-0.0625	$B_{19,\frac{5}{2}}$	0.0002	0.876
		$B_{20,\frac{5}{2}}$	0.0007	0.857
		$B_{21,\frac{5}{2}}$	-0.0034	0.849

TABLE VII (Cont'd)

NUMERICAL RESULTS (Shell A8)

	$\overline{\xi}_1$		$\overline{\xi}_2$ or $\overline{\xi}_3$	λ_M
$A_{0,6}$	-0.0637	$B_{21,3}$	0.0012	0.821
		$B_{22,3}$	0.0010	0.823
		$B_{23,3}$	0.0005	0.844
$A_{0,7}$	-0.0716	$B_{22,\frac{7}{2}}$	0.0004	0.776
		$B_{23,\frac{7}{2}}$	-0.0019	0.761
		$B_{24,\frac{7}{2}}$	$0.3 \cdot 10^{-6}$	0.788

TABLE VII (Cont'd)

NUMERICAL RESULTS (Shell A8)

	$\overline{\xi}_1$		$\overline{\xi}_2$ or $\overline{\xi}_3$	λ_M
$C_{0,1}$	0.6106	$A_{9,\frac{1}{2}}$	0.0096	0.748
		$A_{10,\frac{1}{2}}$	0.0141	0.713
		$A_{11,\frac{1}{2}}$	-0.0157	0.798
$C_{0,2}$	0.2661	$A_{12,1}$	-0.0070	0.828
		$A_{13,1}$	-0.0230	0.716
		$A_{14,1}$	0.0024	0.789
$C_{0,3}$	0.0209	$A_{15,\frac{3}{2}}$	-0.0025	0.981
		$A_{16,\frac{3}{2}}$	-0.0010	0.961
		$A_{17,\frac{3}{2}}$	-0.0002	0.988
$C_{0,4}$	0.0752	$A_{17,2}$	-0.0026	0.881
		$A_{18,2}$	0.0006	0.868
		$A_{19,2}$	$-0.8 \cdot 10^{-5}$	0.885
$C_{0,5}$	0.0216	$A_{19,\frac{5}{2}}$	-0.0029	0.937
		$A_{20,\frac{5}{2}}$	0.0011	0.937
		$A_{21,\frac{5}{2}}$	0.0009	0.951

TABLE VII (Cont'd)

NUMERICAL RESULTS (Shell A8)

	$\overline{\xi}_1$			$\overline{\xi}_2$ or $\overline{\xi}_3$	λ_M
$C_{0,6}$	0.0075	$\Big\{$	$A_{21,3}$	-0.0015	0.960
			$A_{22,3}$	-0.0026	0.952
			$A_{23,3}$	0.0003	0.995
$C_{0,7}$	-0.00001	$\Big\{$	$C_{22,\frac{7}{2}}$	-0.0013	0.984
			$C_{23,\frac{7}{2}}$	0.0003	0.993
			$C_{24,\frac{7}{2}}$	0.0003	1.009

TABLE VII (Cont'd)

NUMERICAL RESULTS (Shell A8)

	$\overline{\xi}_1$			$\overline{\xi}_2$ or $\overline{\xi}_3$	λ_M
$C_{0,1}$	0.6106	$\Big\{$	$B_{9,\frac{1}{2}}$	-0.0551	0.651
			$B_{10,\frac{1}{2}}$	-0.0254	0.682
			$B_{11,\frac{1}{2}}$	0.0098	0.821
$C_{0,2}$	0.2661	$\Big\{$	$B_{12,1}$	0.0132	0.809
			$B_{13,1}$	-0.0155	0.736
			$B_{14,1}$	0.0128	0.747
$C_{0,3}$	0.0209	$\Big\{$	$B_{15,\frac{3}{2}}$	0.0003	0.998
			$B_{16,\frac{3}{2}}$	0.0027	0.948
			$B_{17,\frac{3}{2}}$	-0.0047	0.954
$C_{0,4}$	0.0752	$\Big\{$	$B_{17,2}$	0.0017	0.886
			$B_{18,2}$	-0.0013	0.863
			$B_{19,2}$	-0.0018	0.866
$C_{0,5}$	0.0216	$\Big\{$	$B_{19,\frac{5}{2}}$	0.0002	0.960
			$B_{20,\frac{5}{2}}$	0.0007	0.940
			$B_{21,\frac{5}{2}}$	-0.0034	0.931

TABLE VII (Cont'd)

NUMERICAL RESULTS (Shell A8)

$\overline{\xi}_1$		$\overline{\xi}_2$ or $\overline{\xi}_3$		λ_M
$C_{0,6}$	0.0075	$B_{21,3}$	0.0012	0.963
		$B_{22,3}$	0.0010	0.966
		$B_{23,3}$	0.0005	0.993
$C_{0,7}$	-0.00001	$D_{22,\frac{7}{2}}$	0.0003	0.996
		$D_{23,\frac{7}{2}}$	-0.0005	0.991
		$D_{24,\frac{7}{2}}$	$-0.4 \cdot 10^{-6}$	1.016

TABLE VII (Cont'd)

NUMERICAL RESULTS (Shell A9)

$\bar{\xi}_1$			$\bar{\xi}_2$ or $\bar{\xi}_3$	λ_M
$A_{0,1}$ $\quad$ -0.0466		$A_{9,\frac{1}{2}}$	0.0149	0.947
		$A_{10,\frac{1}{2}}$	-0.0216	0.884
		$A_{11,\frac{1}{2}}$	0.0108	1.024
$A_{0,2}$ $\quad$ -0.0509		$A_{12,1}$	0.0055	1.010
		$A_{13,1}$	0.0044	0.933
		$A_{14,1}$	0.0046	0.932
$A_{0,3}$ $\quad$ -0.0340		$A_{15,\frac{3}{2}}$	0.0020	0.974
		$A_{16,\frac{3}{2}}$	-0.0005	0.951
		$A_{17,\frac{3}{2}}$	0.0009	0.960
$A_{0,4}$ $\quad$ -0.0365		$A_{17,2}$	0.0013	0.957
		$A_{18,2}$	0.0007	0.930
		$A_{19,2}$	0.0004	0.937
$A_{0,5}$ $\quad$ -0.0389		$A_{19,\frac{5}{2}}$	-0.0019	0.913
		$A_{20,\frac{5}{2}}$	-0.0006	0.906
		$A_{21,\frac{5}{2}}$	-0.0022	0.901

TABLE VII (Cont'd)

NUMERICAL RESULTS (Shell A9)

$\overline{\xi}_1$			$\overline{\xi}_2$	λ_M
$A_{0,6}$	-0.0357	$A_{21,3}$	-0.0002	0.902
		$A_{22,3}$	0.00004	0.901
		$A_{23,3}$	-0.0004	0.912
$A_{0,7}$	-0.0469	$A_{22,\frac{7}{2}}$	-0.0004	0.845
		$A_{23,\frac{7}{2}}$	-0.0006	0.837
		$A_{24,\frac{7}{2}}$	0.0004	0.846

TABLE VII (Cont'd)

NUMERICAL RESULTS (Shell A9)

	$\bar{\xi}_1$		$\bar{\xi}_2$	λ_M
		$B_{9,\frac{1}{2}}$	0.0026	0.996
$A_{0,1}$	-0.0466	$B_{10,\frac{1}{2}}$	-0.0199	0.889
		$B_{11,\frac{1}{2}}$	0.0317	0.941
		$B_{12,1}$	-0.0012	1.033
$A_{0,2}$	-0.0509	$B_{13,1}$	-0.0081	0.916
		$B_{14,1}$	-0.0040	0.935
		$B_{15,\frac{3}{2}}$	0.0009	0.982
$A_{0,3}$	-0.0340	$B_{16,\frac{3}{2}}$	0.0052	0.920
		$B_{17,\frac{3}{2}}$	-0.0037	0.940
		$B_{17,2}$	0.0030	0.945
$A_{0,4}$	-0.0365	$B_{18,2}$	0.0019	0.921
		$B_{19,2}$	0.0039	0.912
		$B_{19,\frac{5}{2}}$	-0.0005	0.925
$A_{0,5}$	-0.389	$B_{20,\frac{5}{2}}$	-0.00005	0.914
		$B_{21,\frac{5}{2}}$	-0.0017	0.905

TABLE VII (Cont'd)

NUMERICAL RESULTS (Shell A9)

	$\overline{\xi}_1$		$\overline{\xi}_2$	λ_M
$A_{0,6}$	-0.0357	$B_{21,3}$	0.0005	0.897
		$B_{22,3}$	-0.0008	0.892
		$B_{23,3}$	0.0007	0.908
$A_{0,7}$	-0.0469	$B_{22,\frac{7}{2}}$	-0.0008	0.841
		$B_{23,\frac{7}{2}}$	-0.0003	0.840
		$B_{24,\frac{7}{2}}$	$-0.15 \cdot 10^{-7}$	0.854

TABLE VII (Cont'd)

NUMERICAL RESULTS (Shell A9)

	$\overline{\xi}_1$			$\overline{\xi}_3$	λ_M
$C_{0,1}$	0.0695	$\Big\{$	$A_{9,\frac{1}{2}}$	0.0149	0.937
			$A_{10,\frac{1}{2}}$	-0.0216	0.875
			$A_{11,\frac{1}{2}}$	0.0108	1.014
$C_{0,2}$	0.0257	$\Big\{$	$A_{12,1}$	0.0055	1.031
			$A_{13,1}$	0.0044	0.953
			$A_{14,1}$	0.0046	0.952
$C_{0,3}$	0.0220	$\Big\{$	$A_{15,\frac{3}{2}}$	0.0020	0.989
			$A_{16,\frac{3}{2}}$	-0.0005	0.965
			$A_{17,\frac{3}{2}}$	0.0009	0.975
$C_{0,4}$	0.0086	$\Big\{$	$A_{17,2}$	0.0013	1.003
			$A_{18,2}$	0.0007	0.977
			$A_{19,2}$	0.0004	0.984
$C_{0,5}$	0.0067	$\Big\{$	$A_{19,\frac{5}{2}}$	-0.0019	0.981
			$A_{20,\frac{5}{2}}$	-0.0006	0.975
			$A_{21,\frac{5}{2}}$	-0.0022	0.970

TABLE VII (Cont'd)

NUMERICAL RESULTS (Shell A9)

	$\overline{\xi}_1$			$\overline{\xi}_3$	λ_M
$C_{0,6}$	0.0046		$A_{21,3}$	-0.0002	0.986
			$A_{22,3}$	0.00004	0.986
			$A_{23,3}$	-0.0004	0.999
$C_{0,7}$	$-0.20 \cdot 10^{-7}$		$A_{22,\frac{7}{2}}$	-0.0004	0.997
			$A_{23,\frac{7}{2}}$	-0.0006	0.998
			$A_{24,\frac{7}{2}}$	0.0004	1.003

TABLE VII (Cont'd)

NUMERICAL RESULTS (Shell A9)

	$\overline{\xi}_1$		$\overline{\xi}_2$ or $\overline{\xi}_3$	λ_M
$C_{0,1}$	0.0695	$C_{9,\frac{1}{2}}$	-0.0873	0.827
		$C_{10,\frac{1}{2}}$	-0.0082	0.981
		$C_{11,\frac{1}{2}}$	-0.0082	1.091
$C_{0,2}$	0.0257	$B_{12,1}$	-0.0012	1.054
		$B_{13,1}$	-0.0081	0.936
		$B_{14,1}$	-0.0040	0.956
$C_{0,3}$	0.0220	$B_{15,\frac{3}{2}}$	0.0009	0.997
		$B_{16,\frac{3}{2}}$	0.0052	0.934
		$B_{17,\frac{3}{2}}$	-0.0037	0.955
$C_{0,4}$	0.0086	$B_{17,2}$	0.0030	0.991
		$B_{18,2}$	0.0019	0.966
		$B_{19,2}$	0.0039	0.958
$C_{0,5}$	0.0067	$B_{19,\frac{5}{2}}$	-0.0005	0.994
		$B_{20,\frac{5}{2}}$	-0.00005	0.983
		$B_{21,\frac{5}{2}}$	-0.0017	0.974

TABLE VII (Cont'd)

NUMERICAL RESULTS (Shell A9)

$\bar{\xi}_1$			$\bar{\xi}_2$ or $\bar{\xi}_3$	λ_M
$C_{0,6}$	0.0046	$B_{21,3}$	0.0005	0.980
		$B_{22,3}$	-0.0008	0.976
		$B_{23,3}$	0.0007	0.995
$C_{0,7}$	$-0.20 \cdot 10^{-7}$	$B_{22,\frac{7}{2}}$	-0.0008	0.992
		$B_{23,\frac{7}{2}}$	-0.0003	0.993
		$B_{24,\frac{7}{2}}$	$-0.15 \cdot 10^{-7}$	1.013

TABLE VII (Cont'd)

NUMERICAL RESULTS (Shell A10)

	$\overline{\xi}_1$		$\overline{\xi}_2$	λ_M
$A_{0,1}$	-0.0263	$A_{9,\frac{1}{2}}$	-0.0035	1.007
		$A_{10,\frac{1}{2}}$	-0.0134	0.918
		$A_{11,\frac{1}{2}}$	0.0316	0.939
$A_{0,2}$	-0.0231	$A_{12,1}$	-0.0018	1.059
		$A_{13,1}$	0.0119	0.926
		$A_{14,1}$	0.0066	0.941
$A_{0,3}$	-0.0185	$A_{15,\frac{3}{2}}$	-0.0022	0.994
		$A_{16,\frac{3}{2}}$	0.0026	0.952
		$A_{17,\frac{3}{2}}$	0.0020	0.966
$A_{0,4}$	-0.0156	$A_{17,2}$	-0.0004	0.999
		$A_{18,2}$	-0.0003	0.968
		$A_{19,2}$	0.0015	0.959
$A_{0,5}$	-0.0156	$A_{19,\frac{5}{2}}$	-0.0004	0.972
		$A_{20,\frac{5}{2}}$	-0.0002	0.957
		$A_{21,\frac{5}{2}}$	0.00007	0.969

TABLE VII (Cont'd)

NUMERICAL RESULTS (Shell A10)

	$\overline{\xi}_1$			$\overline{\xi}_2$	λ_M
			$A_{21,3}$	0.0009	0.936
$A_{0,6}$	-0.0176	$\Big\{$	$A_{22,3}$	0.0018	0.925
			$A_{23,3}$	0.00008	0.961
			$A_{22,\frac{7}{2}}$	-0.0005	0.916
$A_{0,7}$	-0.0204	$\Big\{$	$A_{23,\frac{7}{2}}$	0.0001	0.915
			$A_{24,\frac{7}{2}}$	-0.0009	0.914

TABLE VII (Cont'd)

NUMERICAL RESULTS (Shell A10)

$\overline{\xi}_1$			$\overline{\xi}_2$	λ_M
$A_{0,1}$	-0.0263	$B_{9,\frac{1}{2}}$	0.0026	1.012
		$B_{10,\frac{1}{2}}$	0.0616	0.786
		$B_{11,\frac{1}{2}}$	0.0158	0.998
$A_{0,2}$	-0.0231	$B_{12,1}$	0.0131	1.011
		$B_{13,1}$	0.0106	0.930
		$B_{14,1}$	0.0001	0.985
$A_{0,3}$	-0.0185	$B_{15,\frac{3}{2}}$	0.0031	0.988
		$B_{16,\frac{3}{2}}$	0.0018	0.958
		$B_{17,\frac{3}{2}}$	0.0029	0.960
$A_{0,4}$	-0.0156	$B_{17,2}$	0.0027	0.981
		$B_{18,2}$	0.0010	0.960
		$B_{19,2}$	-0.0008	0.965
$A_{0,5}$	-0.0156	$B_{19,\frac{5}{2}}$	0.0011	0.965
		$B_{20,\frac{5}{2}}$	0.0004	0.955
		$B_{21,\frac{5}{2}}$	$0.8 \cdot 10^{-5}$	0.971

TABLE VII (Cont'd)

NUMERICAL RESULTS (Shell A10)

	$\bar{\xi}_1$		$\bar{\xi}_2$	λ_M
$A_{0,6}$	-0.0176	$B_{21,3}$	0.0003	0.943
		$B_{22,3}$	0.0002	0.941
		$B_{23,3}$	-0.0013	0.945
$A_{0,7}$	-0.0204	$B_{22,\frac{7}{2}}$	-0.0002	0.919
		$B_{23,\frac{7}{2}}$	0.0006	0.908
		$B_{24,\frac{7}{2}}$	$0.3 \cdot 10^{-8}$	0.929

TABLE VII (Cont'd)

NUMERICAL RESULTS   (Shell A10)

	$\overline{\xi}_1$			$\overline{\xi}_2$	λ_M
$C_{0,1}$	-0.0209		$C_{9,\frac{1}{2}}$	-0.0813	0.813
			$C_{10,\frac{1}{2}}$	-0.0072	0.946
			$C_{11,\frac{1}{2}}$	-0.0139	1.009
$C_{0,2}$	0.0040		$A_{12,1}$	-0.0018	1.077
			$A_{13,1}$	0.0119	0.942
			$A_{14,1}$	0.0066	0.957
$C_{0,3}$	0.0051		$A_{15,\frac{3}{2}}$	-0.0022	1.012
			$A_{16,\frac{3}{2}}$	0.0026	0.970
			$A_{17,\frac{3}{2}}$	0.0020	0.984
$C_{0,4}$	0.0029		$A_{17,2}$	-0.0004	1.023
			$A_{18,2}$	-0.0003	0.991
			$A_{19,2}$	0.0015	0.983
$C_{0,5}$	0.0014		$A_{19,\frac{5}{2}}$	-0.0004	1.007
			$A_{20,\frac{5}{2}}$	-0.0002	0.991
			$A_{21,\frac{5}{2}}$	0.00007	1.004

TABLE VII (Cont'd)

NUMERICAL RESULTS (Shell A10)

	$\overline{\xi}_1$		$\overline{\xi}_2$ or $\overline{\xi}_3$	λ_M
$C_{0,6}$	0.0005	$A_{21,3}$	0.0009	0.988
		$A_{22,3}$	0.0018	0.977
		$A_{23,3}$	0.00008	1.017
$C_{0,7}$	$0.4 \cdot 10^{-7}$	$A_{22,\frac{7}{2}}$	-0.0005	0.995
		$A_{23,\frac{7}{2}}$	0.0001	0.996
		$A_{24,\frac{7}{2}}$	-0.0009	0.996

TABLE VII (Cont'd)

NUMERICAL RESULTS (Shell A10)

	$\overline{\xi}_1$		$\overline{\xi}_2$ or $\overline{\xi}_3$	λ_M
$C_{0,1}$	-0.0209	$D_{9,\frac{1}{2}}$	0.0358	0.907
		$D_{10,\frac{1}{2}}$	-0.0654	0.780
		$D_{11,\frac{1}{2}}$	-0.0003	1.096
$C_{0,2}$	0.0040	$B_{12,1}$	0.0131	1.027
		$B_{13,1}$	0.0106	0.947
		$B_{14,1}$	0.0001	1.002
$C_{0,3}$	0.0051	$B_{15,\frac{3}{2}}$	0.0031	1.006
		$B_{16,\frac{3}{2}}$	0.0018	0.975
		$B_{17,\frac{3}{2}}$	0.0029	0.978
$C_{0,4}$	0.0029	$B_{17,2}$	0.0027	1.005
		$B_{18,2}$	0.0010	0.983
		$B_{19,2}$	-0.0008	0.988
$C_{0,5}$	0.0014	$B_{19,\frac{5}{2}}$	-0.0011	0.999
		$B_{20,\frac{5}{2}}$	0.0004	0.989
		$B_{21,\frac{5}{2}}$	$0.8 \cdot 10^{-4}$	1.006

TABLE VII (Cont'd)

NUMERICAL RESULTS (Shell A10)

	$\overline{\xi}_1$		$\overline{\xi}_2$ or $\overline{\xi}_3$	λ_M
$C_{0,6}$	0.0005	$B_{21,3}$	0.0003	0.996
		$B_{22,3}$	0.0002	0.995
		$B_{23,3}$	-0.0013	0.999
$C_{0,7}$	$0.4 \ 10^{-7}$	$B_{22,\frac{7}{2}}$	-0.0002	0.999
		$B_{23,\frac{7}{2}}$	0.0006	0.988
		$B_{24,\frac{7}{2}}$	$0.3 \cdot 10^{-8}$	1.013

TABLE VII (Cont'd)

NUMERICAL RESULTS (Shell A12)

$\overline{\xi}_1$			$\overline{\xi}_2$ or $\overline{\xi}_3$	λ_M
$A_{0,1}$	-0.0178	$A_{9,\frac{1}{2}}$	-0.0164	0.928
		$A_{10,\frac{1}{2}}$	-0.0511	0.825
		$A_{11,\frac{1}{2}}$	-0.0096	1.001
$A_{0,2}$	0.0087	$C_{12,1}$	0.0201	0.955
		$C_{13,1}$	0.0076	0.973
		$C_{14,1}$	-0.0039	0.989
$A_{0,3}$	0.0059	$C_{15,\frac{3}{2}}$	-0.0129	0.938
		$C_{16,\frac{3}{2}}$	0.00004	0.987
		$C_{17,\frac{3}{2}}$	0.0007	1.021
$A_{0,4}$	-0.0115	$A_{17,2}$	0.0022	0.972
		$A_{18,2}$	0.0051	0.940
		$A_{19,2}$	-0.0006	0.994
$A_{0,5}$	0.0099	$C_{19,\frac{5}{2}}$	0.0004	0.975
		$C_{20,\frac{5}{2}}$	0.0041	0.976
		$C_{21,\frac{5}{2}}$	-0.0020	0.982

TABLE VII (Cont'd)

NUMERICAL RESULTS (Shell A12)

$\overline{\xi}_1$			$\overline{\xi}_2$ or $\overline{\xi}_3$	λ_M
$A_{0,6}$	-0.0075	$A_{21,3}$	-0.0012	0.962
		$A_{22,3}$	-0.0011	0.972
		$A_{23,3}$	0.0007	1.008
$A_{0,7}$	-0.0024	$A_{22,\frac{7}{2}}$	0.0010	0.975
		$A_{23,\frac{7}{2}}$	-0.0001	0.992
		$A_{24,\frac{7}{2}}$	0.0010	1.002

TABLE VII (Cont'd)

NUMERICAL RESULTS (Shell A12)

$\bar{\xi}_1$			$\bar{\xi}_2$ or $\bar{\xi}_3$	λ_M
$A_{0,1}$	-0.0178	$B_{9,\frac{1}{2}}$	-0.0887	0.764
		$B_{10,\frac{1}{2}}$	-0.0117	0.947
		$B_{11,\frac{1}{2}}$	0.0601	0.910
$A_{0,2}$	0.0087	$D_{12,1}$	0.0118	0.981
		$D_{13,1}$	-0.0057	0.982
		$D_{14,1}$	0.0082	0.967
$A_{0,3}$	0.0059	$D_{15,\frac{3}{2}}$	-0.0120	0.941
		$D_{16,\frac{3}{2}}$	0.0019	0.968
		$D_{17,\frac{3}{2}}$	-0.0009	1.018
$A_{0,4}$	-0.0115	$B_{17,2}$	0.0038	0.963
		$B_{18,2}$	-0.0003	0.975
		$B_{19,2}$	-0.0028	0.975
$A_{0,5}$	0.0099	$D_{19,\frac{5}{2}}$	-0.0006	0.973
		$D_{20,\frac{5}{2}}$	-0.0005	1.006
		$D_{21,\frac{5}{2}}$	0.0037	0.969

TABLE VII (Cont'd)

NUMERICAL RESULTS (Shell A12)

	$\overline{\xi}_1$			$\overline{\xi}_2$ or $\overline{\xi}_3$	λ_M
$A_{0,6}$	-0.0075		$B_{21,3}$	0.0016	0.958
			$B_{22,3}$	0.0003	0.982
			$B_{23,3}$	-0.0006	1.010
$A_{0,7}$	-0.0024		$B_{22,\frac{7}{2}}$	0.0009	0.977
			$B_{23,\frac{7}{2}}$	0.0002	0.991
			$B_{24,\frac{7}{2}}$	$-0.14 \cdot 10^{-6}$	1.020

TABLE VII (Cont'd)

NUMERICAL RESULTS (Shell A12)

	$\overline{\xi}_1$		$\overline{\xi}_2$ or $\overline{\xi}_3$	λ_M
$C_{0,1}$	0.0092	$A_{9,\frac{1}{2}}$	-0.0164	0.931
		$A_{10,\frac{1}{2}}$	-0.0511	0.828
		$A_{11,\frac{1}{2}}$	-0.0096	1.105
$C_{0,2}$	0.0280	$A_{12,1}$	-0.0151	0.955
		$A_{13,1}$	-0.0057	0.937
		$A_{14,1}$	-0.0023	0.984
$C_{0,3}$	-0.0107	$C_{15,\frac{3}{2}}$	-0.0129	0.932
		$C_{16,\frac{3}{2}}$	0.00004	0.987
		$C_{17,\frac{3}{2}}$	0.0007	1.015
$C_{0,4}$	0.0092	$A_{17,2}$	0.0022	0.976
		$A_{18,2}$	0.0051	0.944
		$A_{19,2}$	-0.0006	0.998
$C_{0,5}$	0.0050	$A_{19,\frac{5}{2}}$	-0.0003	0.987
		$A_{20,\frac{5}{2}}$	0.0014	0.973
		$A_{21,\frac{5}{2}}$	0.0017	0.995

TABLE VII (Cont'd)

NUMERICAL RESULTS (Shell A12)

$\bar{\xi}_1$			$\bar{\xi}_2$ or $\bar{\xi}_3$	λ_M
$C_{0,6}$	-0.0041	$C_{21,3}$	-0.0006	0.977
		$C_{22,3}$	0.0012	0.981
		$C_{23,3}$	-0.0013	1.012
$C_{0,7}$	0.0104	$A_{22,\frac{7}{2}}$	0.0010	0.947
		$A_{23,\frac{7}{2}}$	-0.0001	0.963
		$A_{24,\frac{7}{2}}$	0.0010	0.972

TABLE VII (Cont'd)

NUMERICAL RESULTS (Shell A12)

$\bar{\xi}_1$			$\bar{\xi}_2$ or $\bar{\xi}_3$	λ_M
$C_{0,1}$	0.0092	$B_{9,\frac{1}{2}}$	-0.0887	0.767
		$B_{10,\frac{1}{2}}$	-0.0117	0.950
		$B_{11,\frac{1}{2}}$	0.0601	0.913
$C_{0,2}$	0.0280	$B_{12,1}$	-0.0076	0.982
		$B_{13,1}$	0.0280	0.861
		$B_{14,1}$	-0.0087	0.949
$C_{0,3}$	-0.0107	$D_{15,\frac{3}{2}}$	-0.0120	0.936
		$D_{16,\frac{3}{2}}$	0.0019	0.968
		$D_{17,\frac{3}{2}}$	-0.0009	1.012
$C_{0,4}$	0.0092	$B_{17,2}$	0.0038	0.966
		$B_{18,2}$	-0.0003	0.979
		$B_{19,2}$	-0.0028	0.979
$C_{0,5}$	0.0050	$B_{19,\frac{5}{2}}$	0.0018	0.973
		$B_{20,\frac{5}{2}}$	0.0015	0.972
		$B_{21,\frac{5}{2}}$	0.0034	0.982

TABLE VII (Cont'd)

NUMERICAL RESULTS (Shell A12)

$\overline{\xi}_1$			$\overline{\xi}_2$ or $\overline{\xi}_3$	λ_M
$C_{0,6}$	-0.0041	$D_{21,3}$	0.0013	0.970
		$D_{22,3}$	-0.0001	0.996
		$D_{23,3}$	-0.0010	1.014
$C_{0,7}$	0.0104	$B_{22,\frac{7}{2}}$	0.0009	0.949
		$B_{23,\frac{7}{2}}$	0.0002	0.961
		$B_{24,\frac{7}{2}}$	$-0.14 \ 10^{-6}$	0.989

TABLE VIII

COMPARISON OF THEORY AND EXPERIMENT

Shell	λ_{exp}	λ_{crit}	Pair of Critical Modal Components		$\Delta\lambda$	Remarks
A7	$0.553/0.597$	0.794	$C_{0,1}$	$C_{10,\frac{1}{2}}$	0.241	Local Buckling
A8	0.658	0.651	$C_{0,1}$	$B_{9,\frac{1}{2}}$	-0.007	
A9	0.736	0.827	$C_{0,1}$	$C_{9,\frac{1}{2}}$	0.091	
A10	$0.554/0.568$	0.780	$C_{0,1}$	$D_{10,\frac{1}{2}}$	0.226	Local Buckling
A12	0.673	0.764	$A_{0,1}$	$B_{9,\frac{1}{2}}$	0.091	
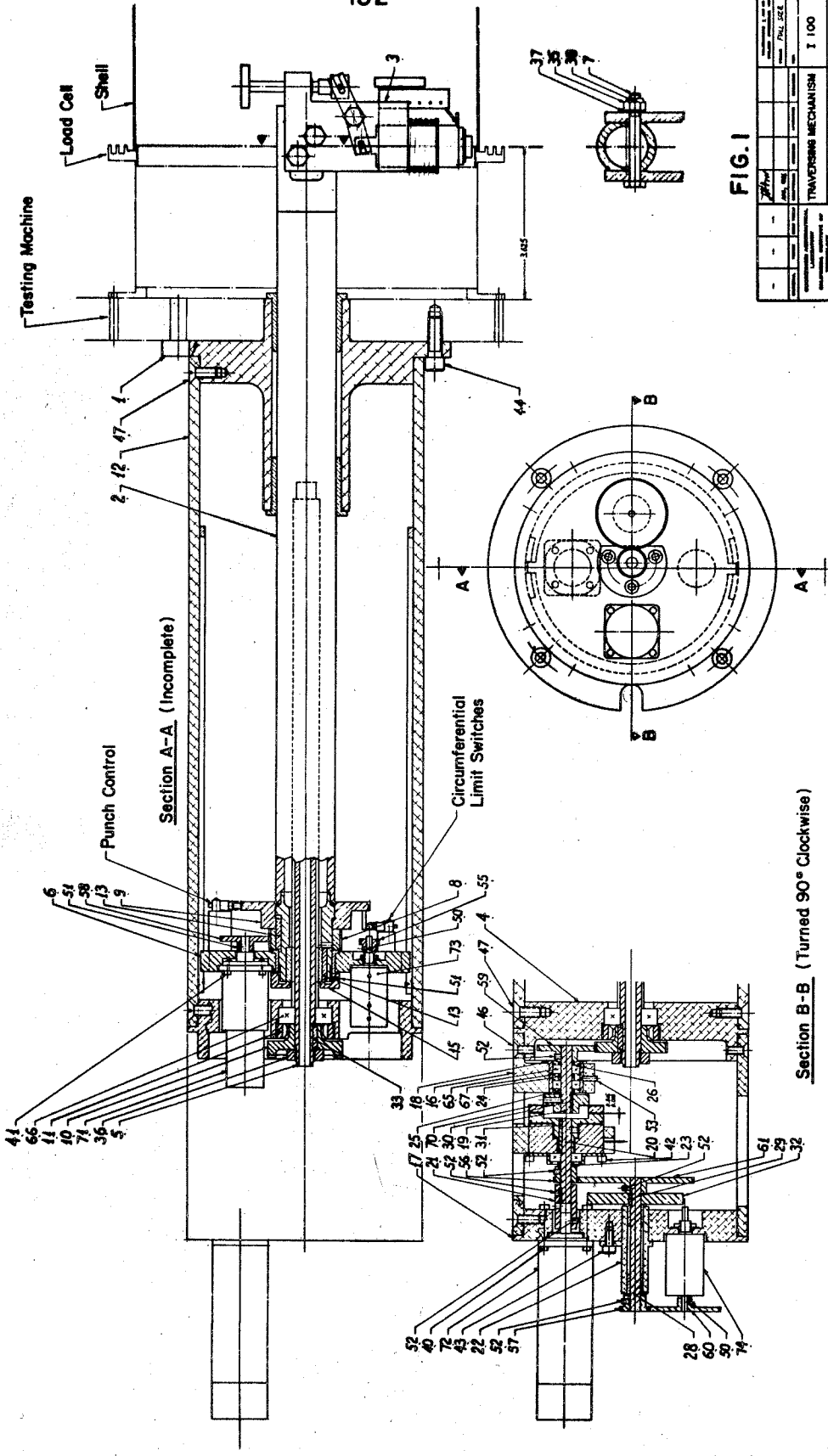
152

FIG. 1

Testing Machine

Load Cell
Shell

Section A-A (Incomplete)

Punch Control

Circumferential
Limit Switches

Section B-B (Turned 90° Clockwise)

TRAVERSING MECHANISM
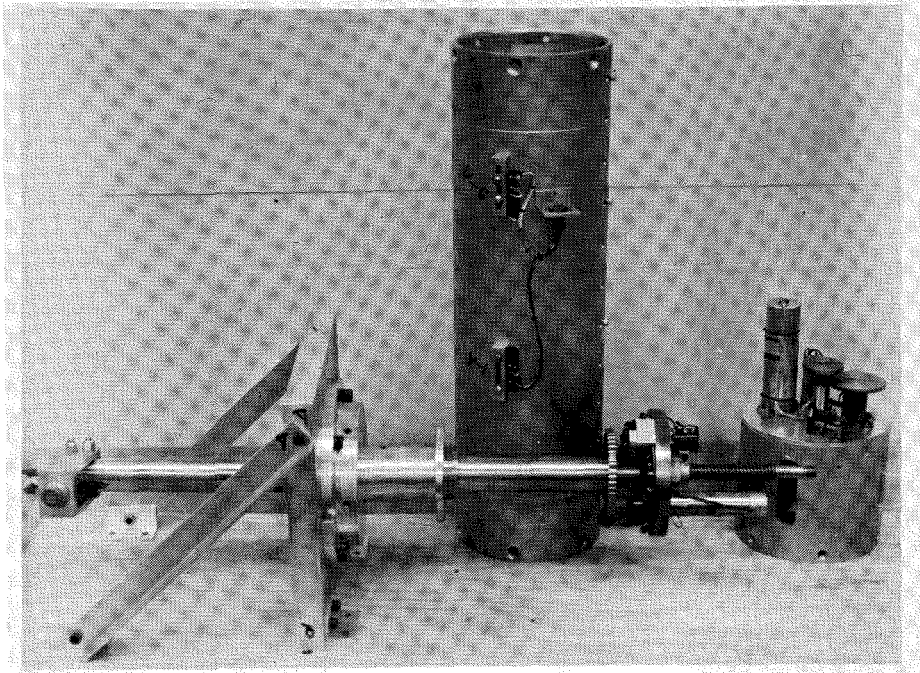
FIG. 2 PARTIALLY ASSEMBLED SCANNING MECHANISM

FIG. 3 SCHEMATIC LAYOUT OF THE SHELL BUCKLING EXPERIMENT MEASURING IMPERFECTIONS

Circumferential Limit Switches

Circumferential Motor

To The X-Axis Of The Plotter

Circumferential Position Indicator Helipot

Clutch

Automatic Starter

6

2

8

9

Clockwise

Counter Clockwise

1

3

Incremental Switch

Axial Motor

To Channel #26

Axial Position Indicator Helipot

Punch Trigger

10

11

4
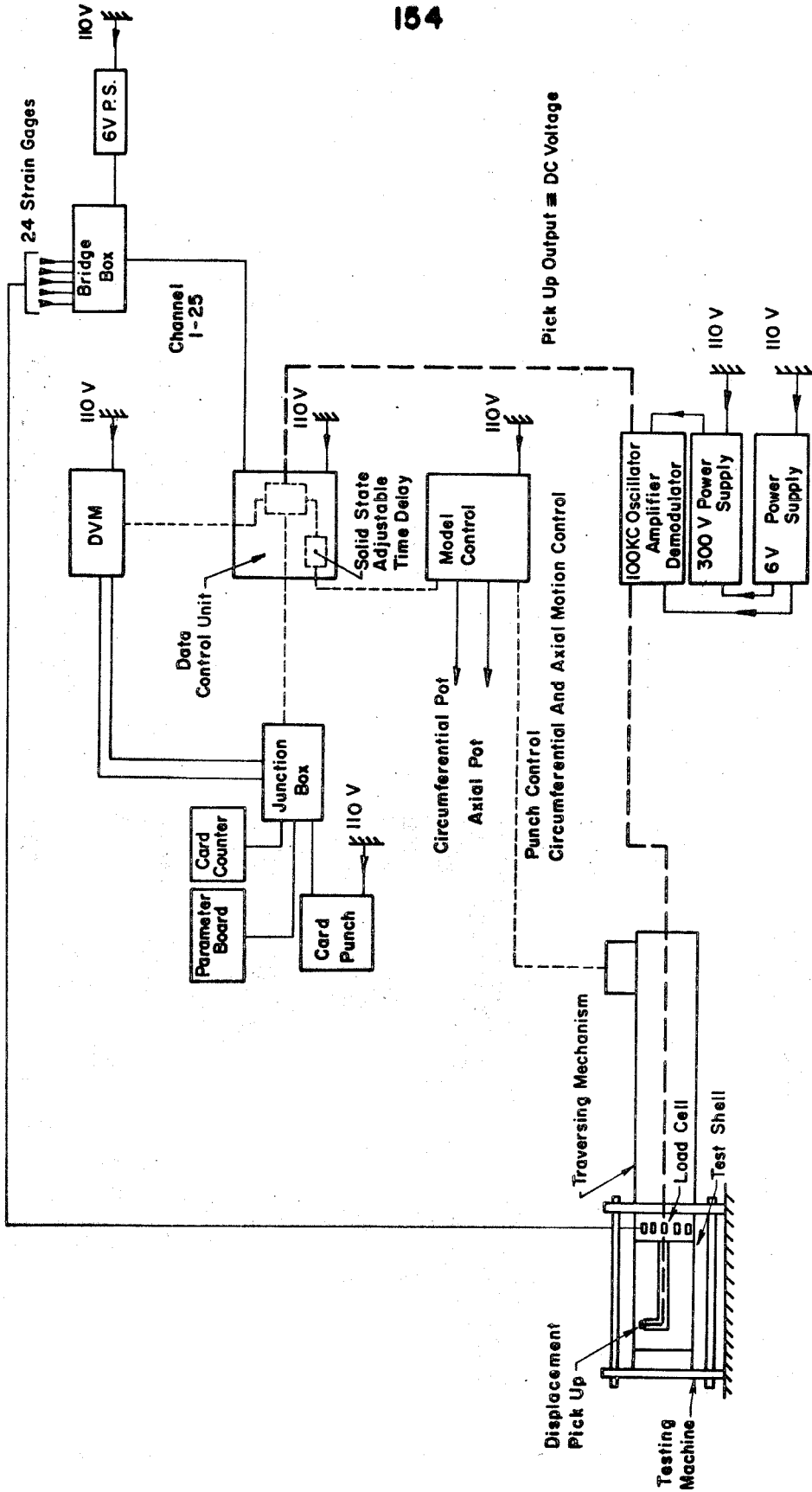
Axial Limit Switches
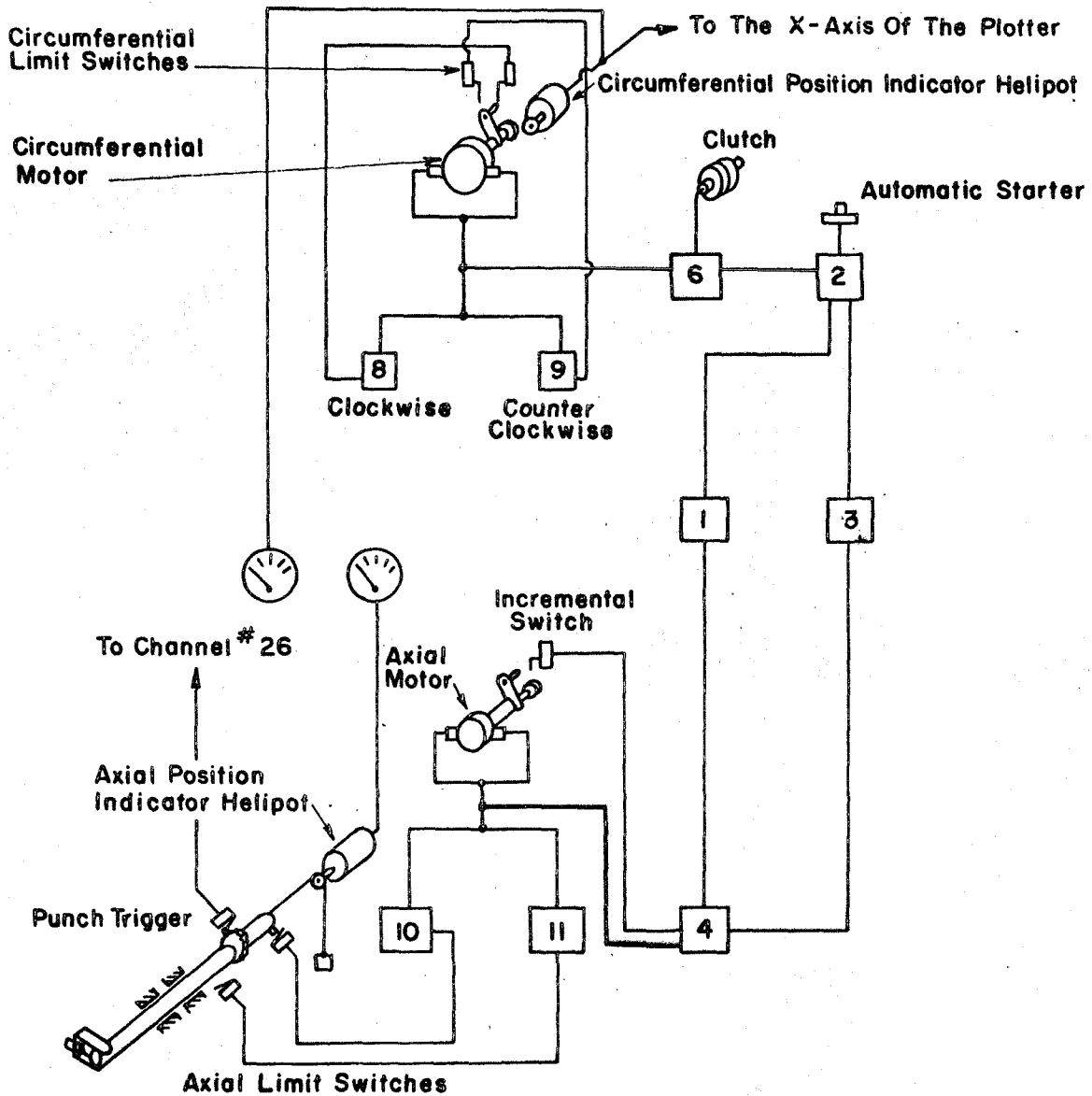
FIG. 4 MODEL CONTROL UNIT
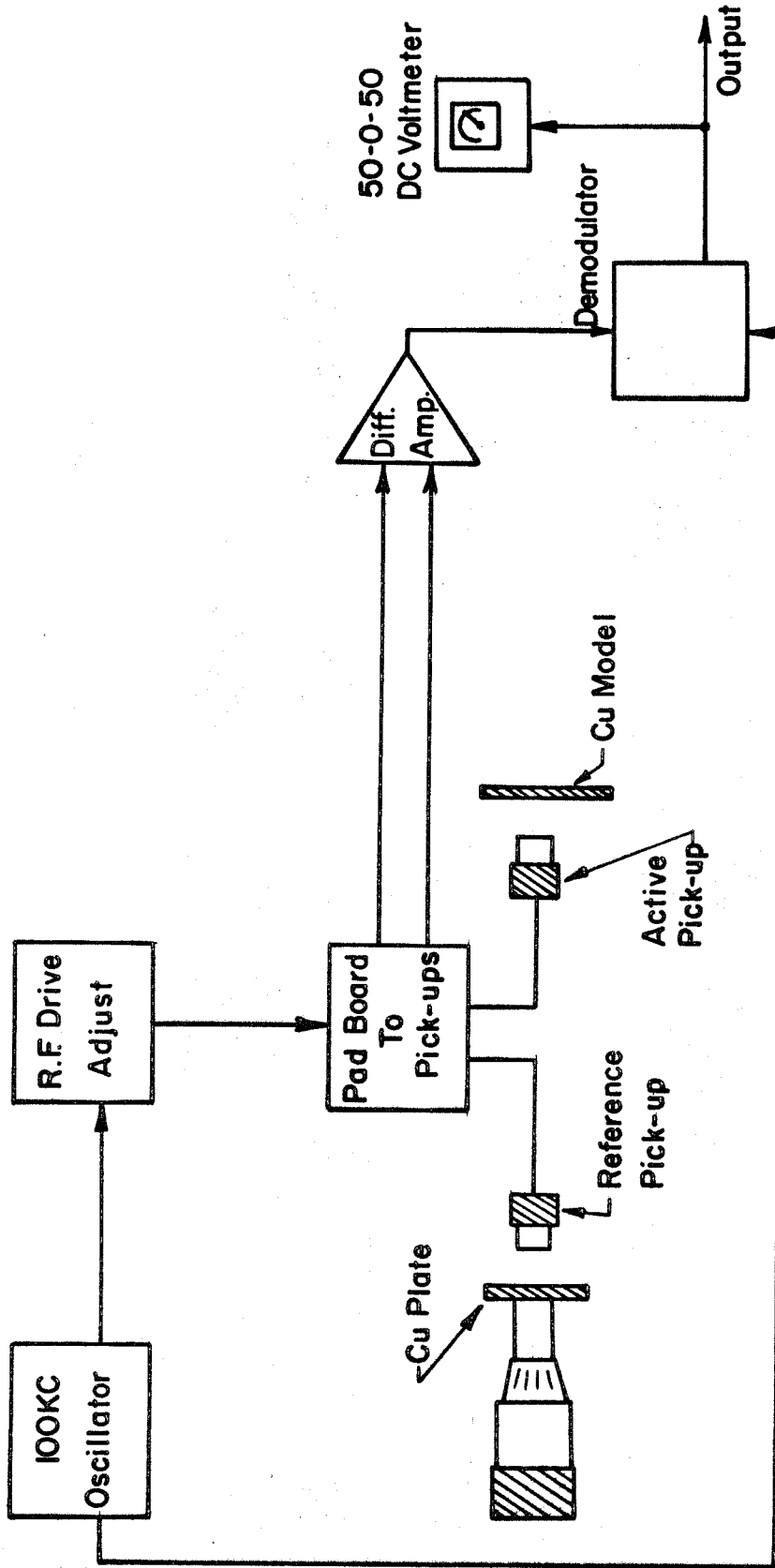
FIG. 5   PICK-UP CIRCUIT
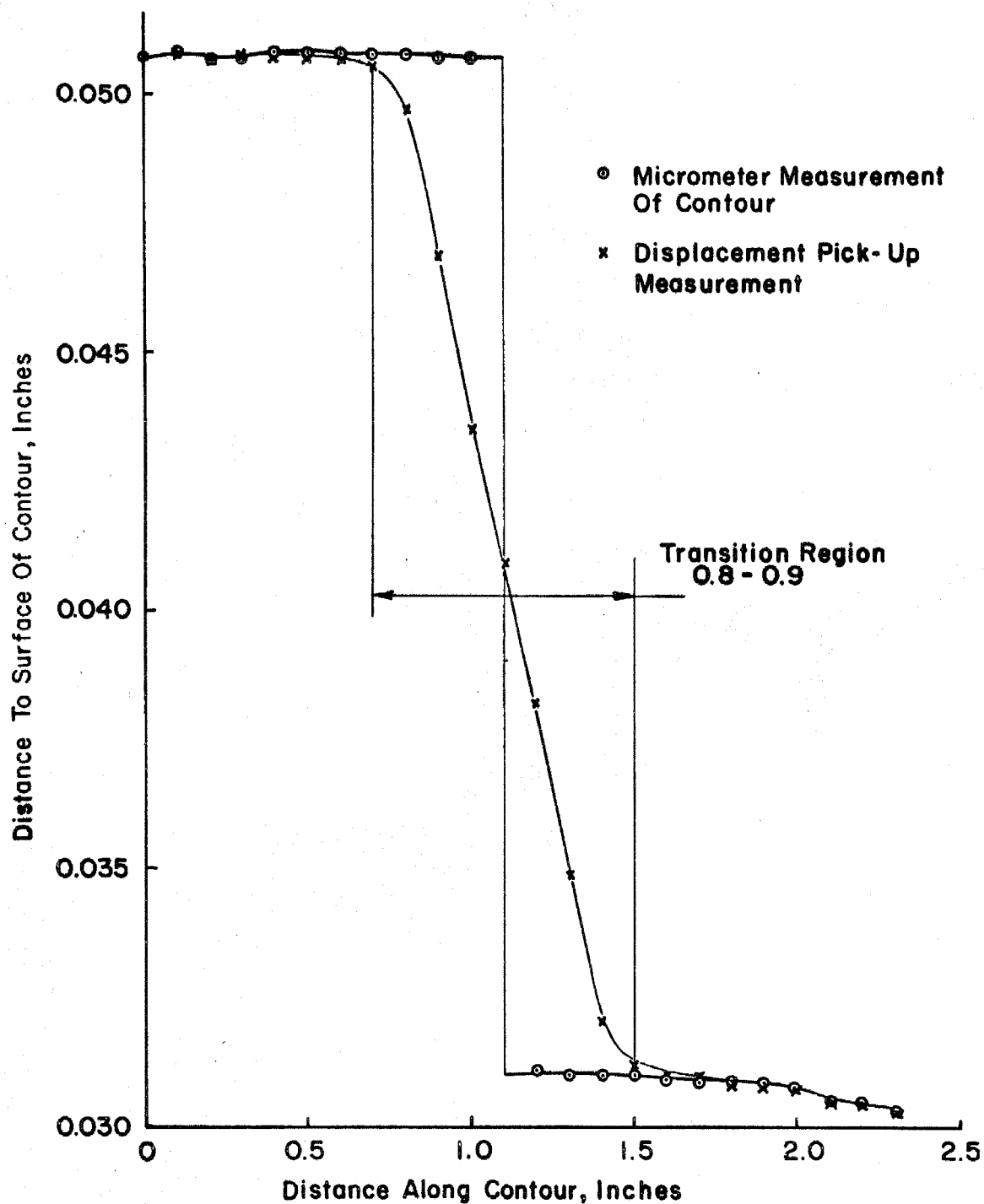
FIG. 6 MICROMETER MEASUREMENT OF KNOWN CONTOUR COMPARED TO PICK-UP MEASUREMENTS
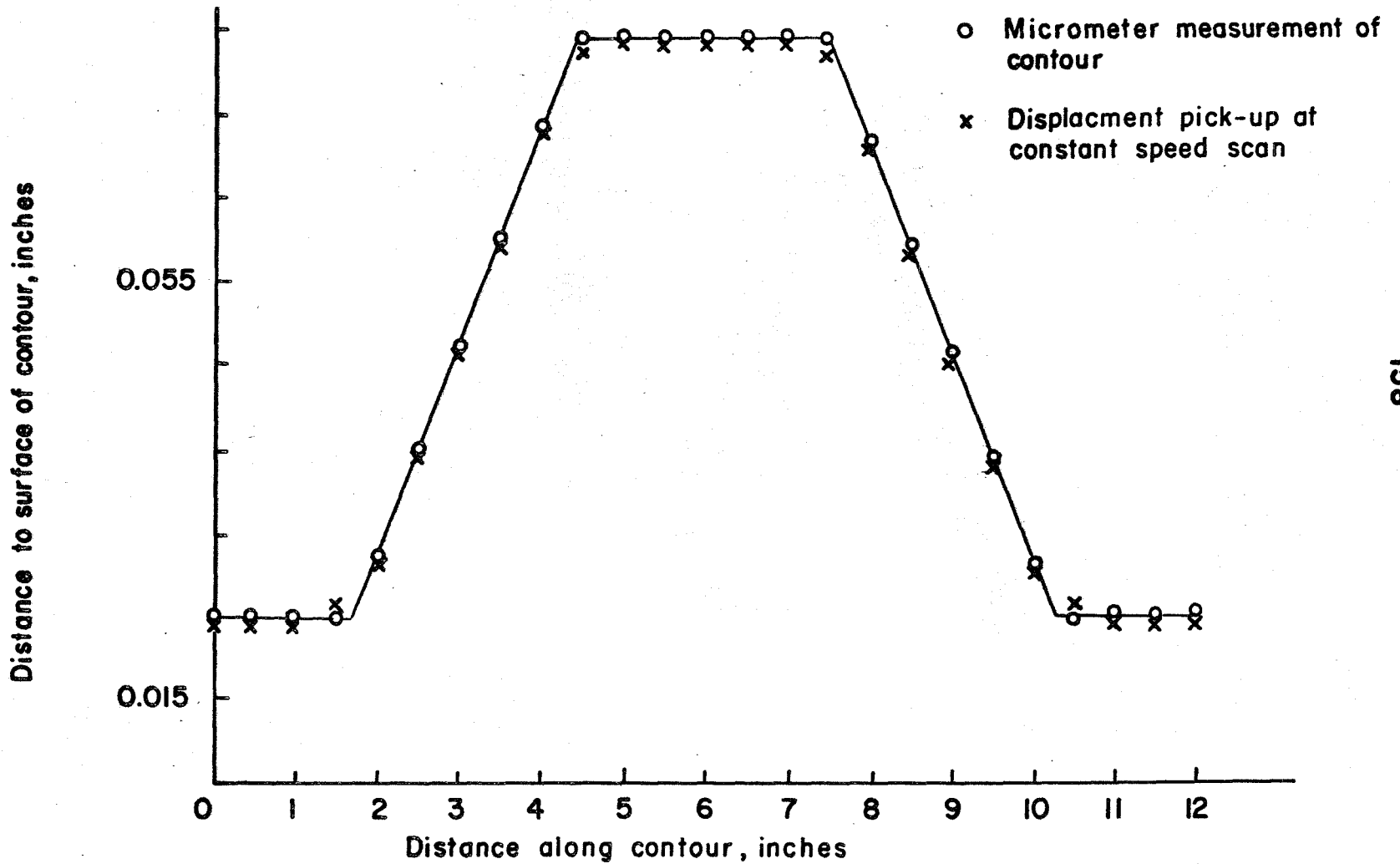
FIG. 7 CONSTANT SPEED TRAVERSE OF KNOWN CONTOUR COMPARED TO "STATIC" MICROMETER MEASUREMENT

159

Punching Actually Occurs Here

Time Delay In Punching When Rotating Clockwise

Time Delay In Punching When Rotating Counterclockwise

Punch Triggered When Rotating Clockwise

Punch Triggered When Rotating Counterclockwise
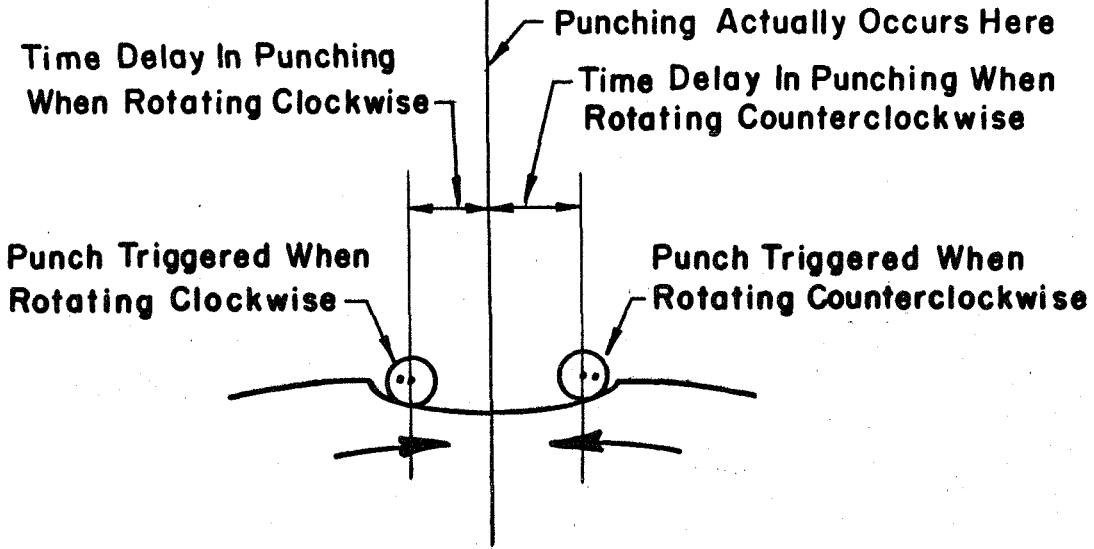
FIG. 8 TIME DELAY FOR PUNCH CONTROL

Punch Signal

Clockwise

Counterclockwise

7.5°
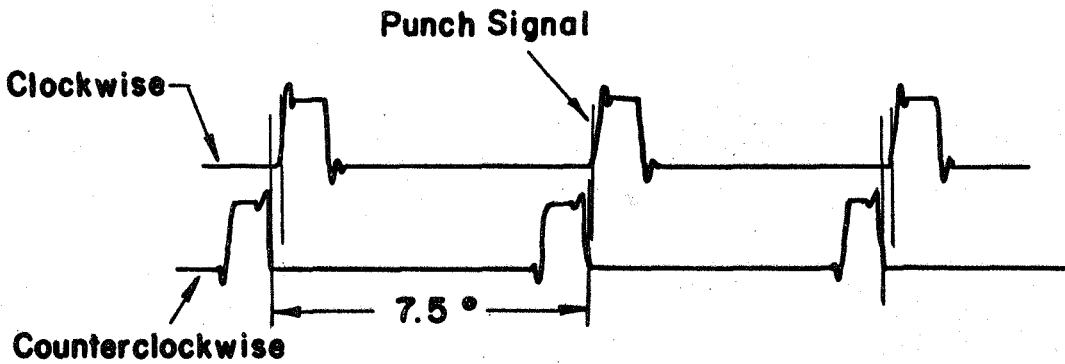
FIG. 9 ADJUSTMENT OF TIME DELAY

160
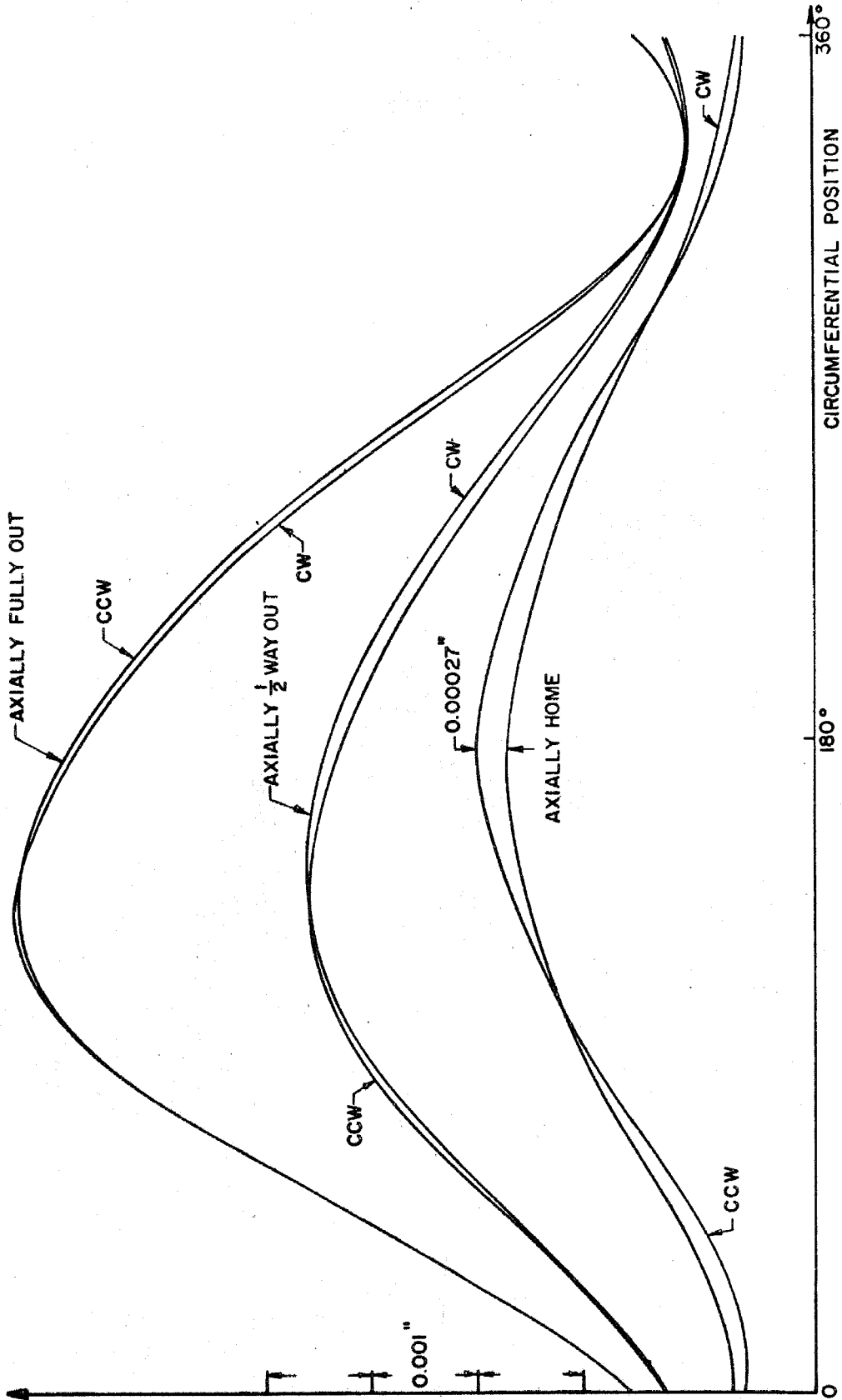
FIG. 10 HYSTERESIS CHECK
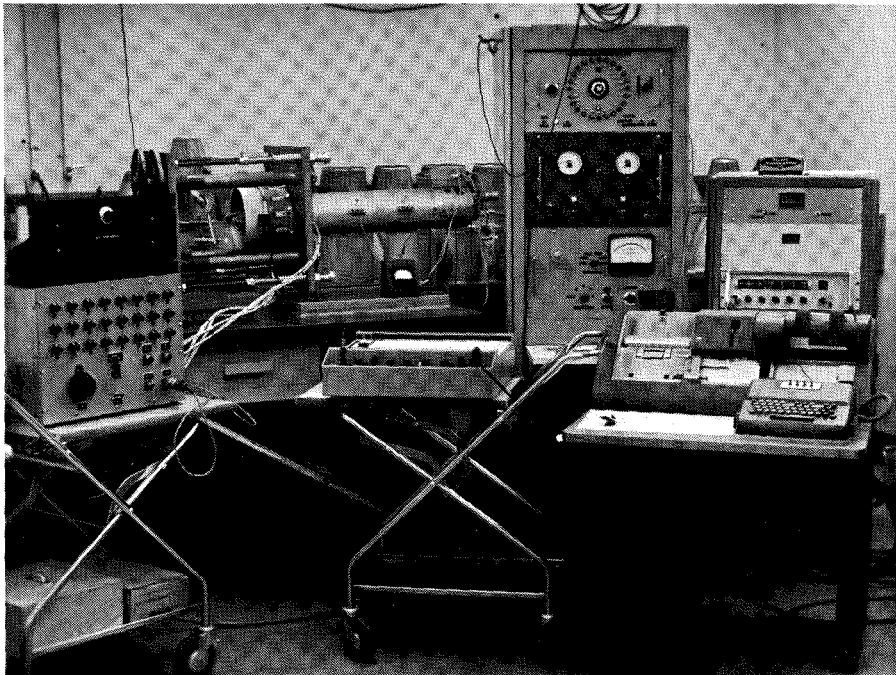
Fig. II   Testing Machine and Data Acquisition Equipment

40
Threads
Per
Inch

End Plates
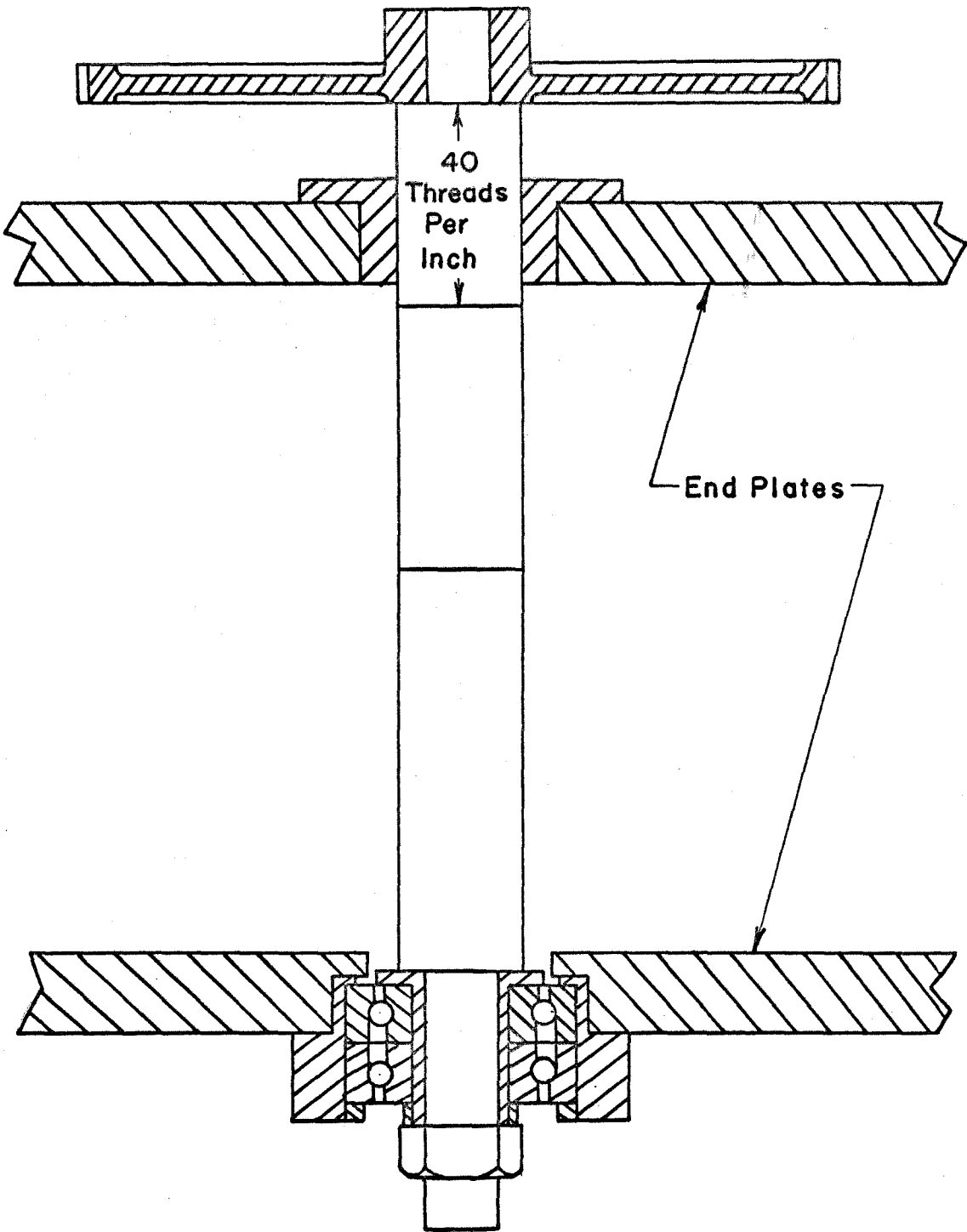
FIG.12 DETAILS OF TESTING MACHINE LOADING SCREW
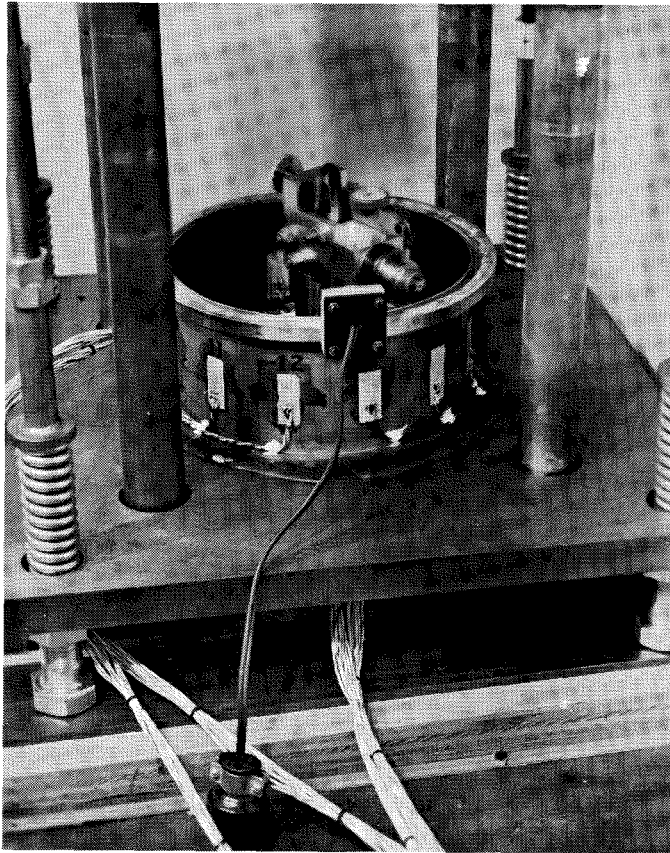
FIG. 13   Load Cell
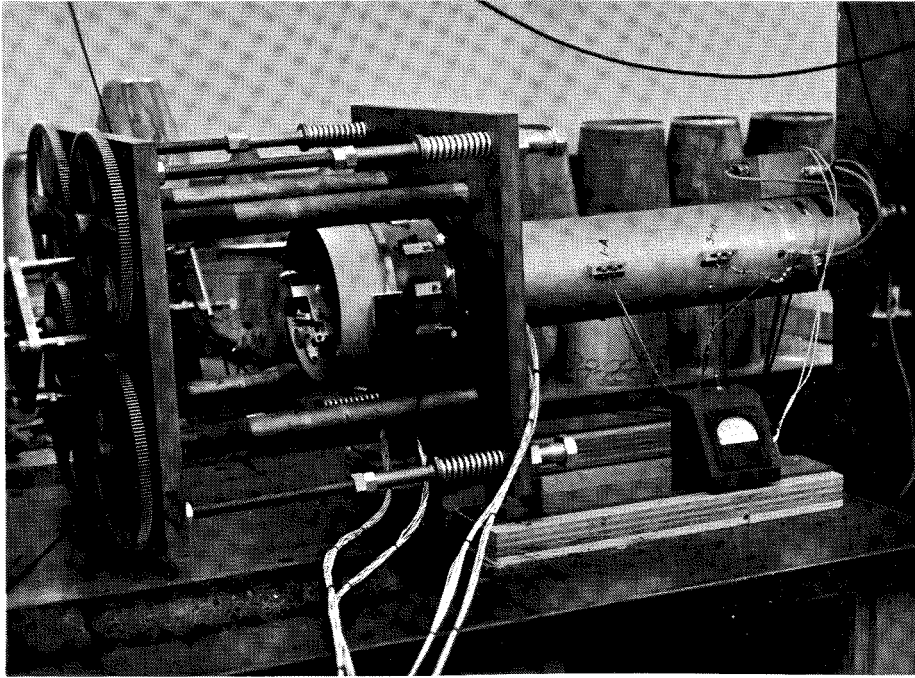
Fig. 14   Pick-up Calibration Set Up
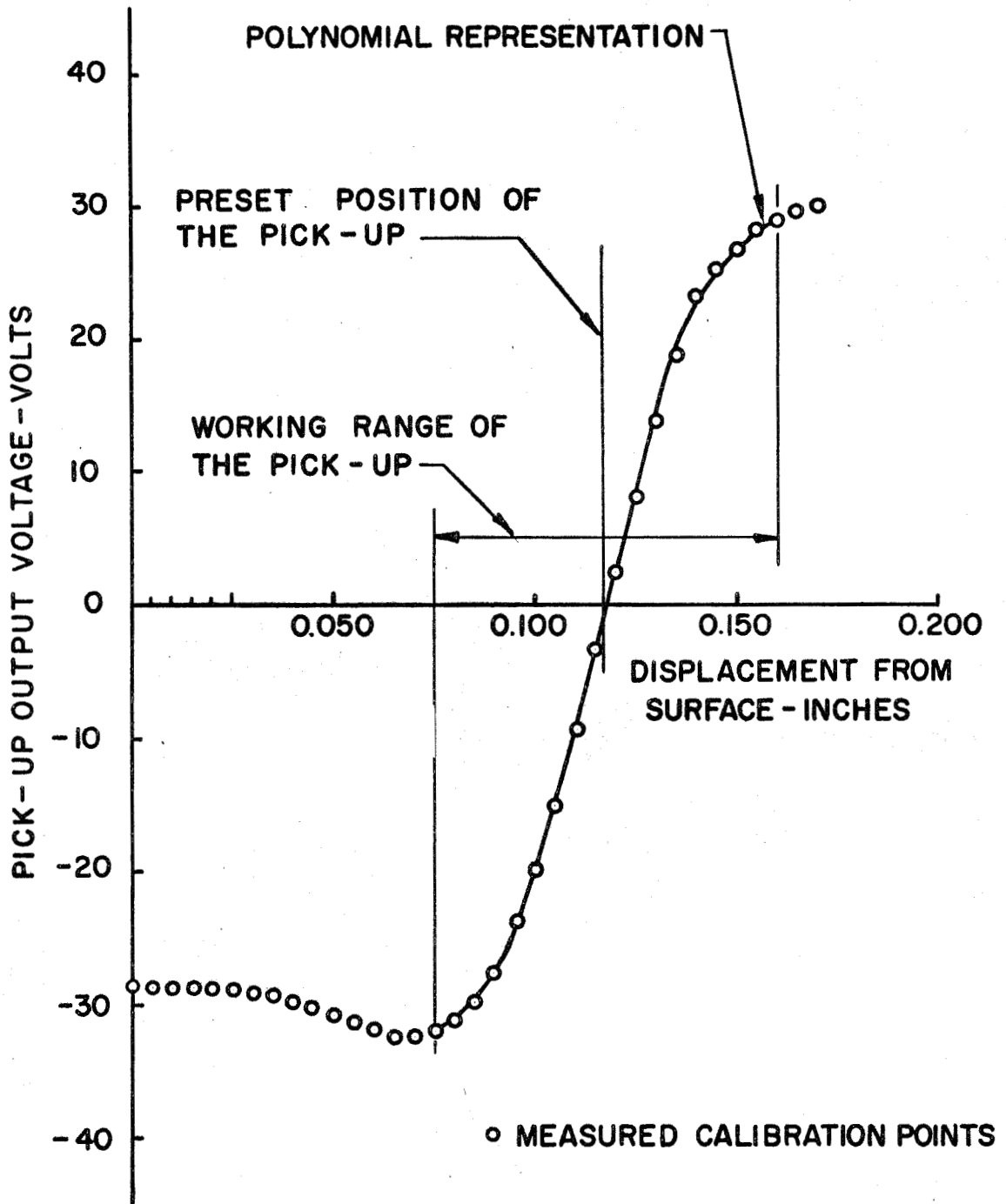
FIG. 15 TYPICAL PICK-UP CALIBRATION CURVE
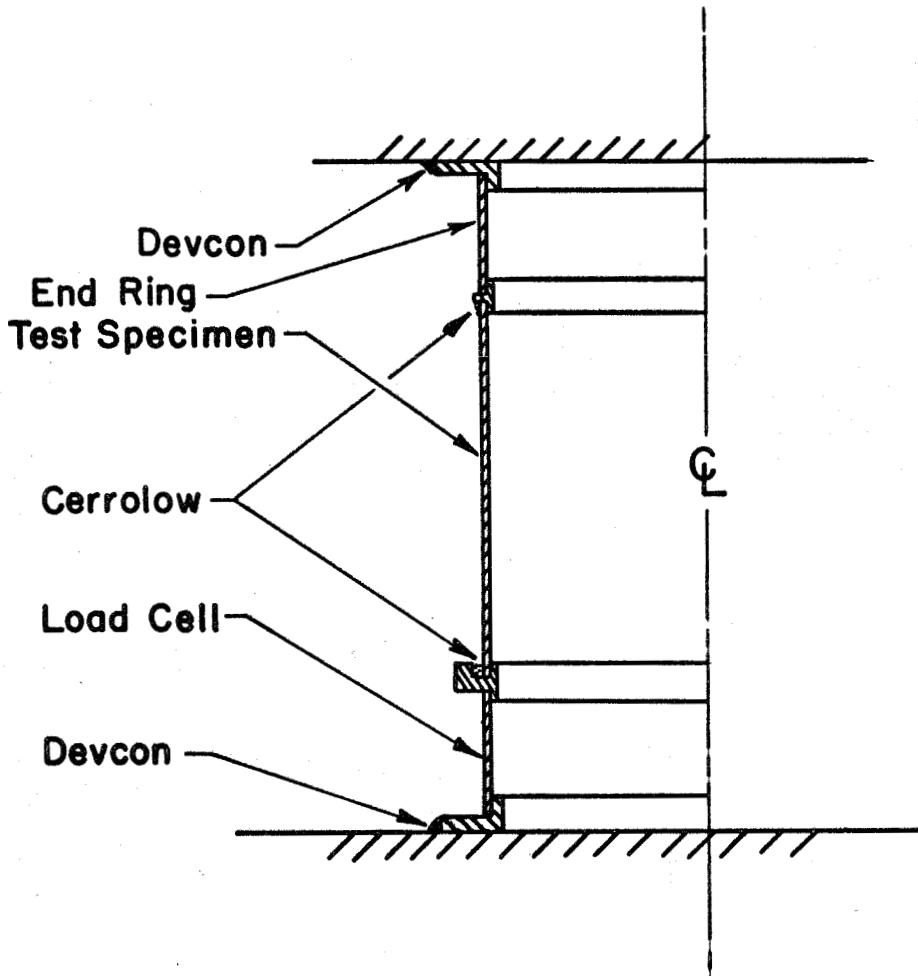
FIG. 16 CYLINDRICAL SHELL TESTING CONFIGURATION

FIG.17 LAYERED MAIN PROGRAM

MAIN CALLING PROGRAM

COMMON W,X

SUBROUTINE LSQ

$IBLDR*MLLLSQ

$IBLDR*MLLLSR

Link I

Polynomial Fit To Calibration Data

Reduction Of Measured Data To Displacements

SUBROUTINE BES

Link 2

Computation Of The Best Fit ("Perfect") Cylinder

SUBROUTINE HAR

Link 3

Harmonic Analysis Of The Measured Surface
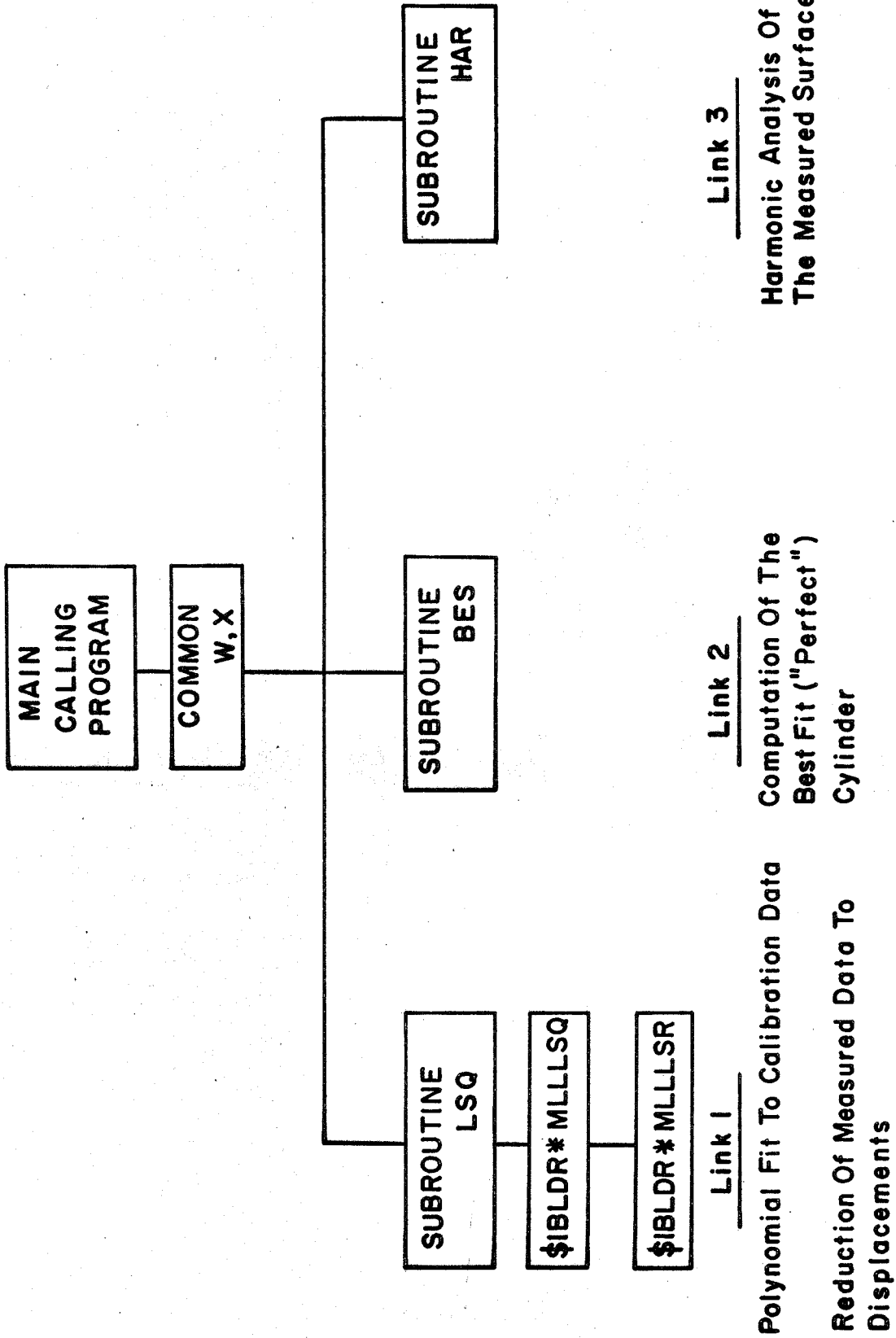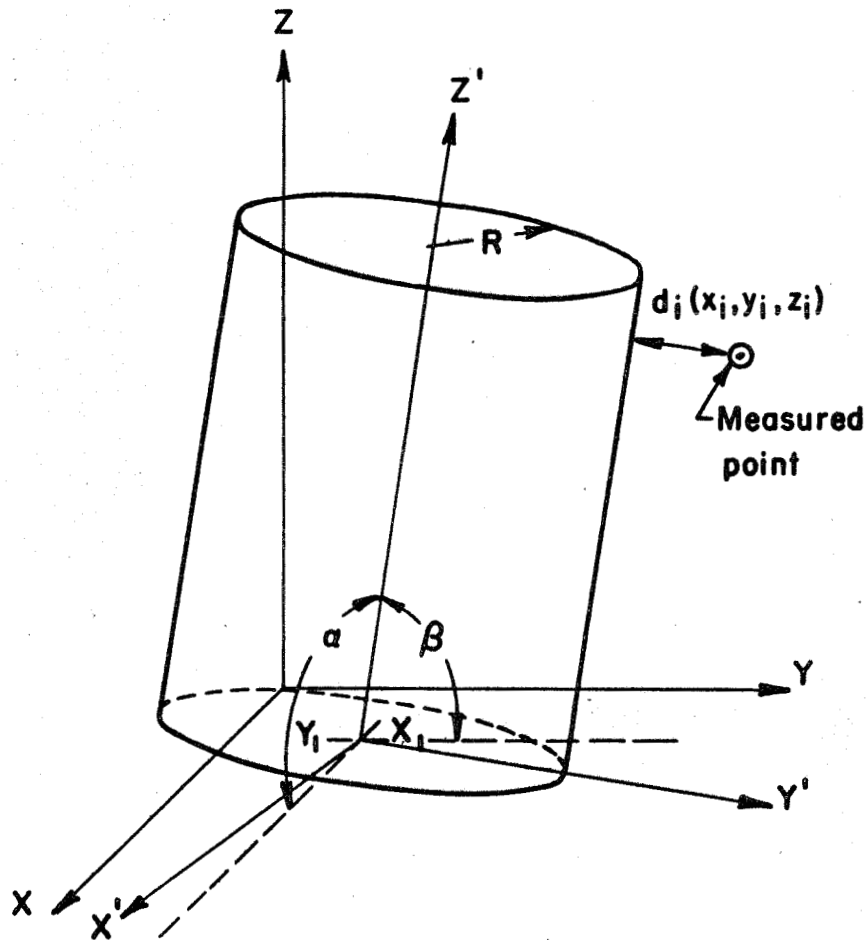
X,Y,Z   Reference axis of traversing pick-up

X',Y',Z'   Reference axis of best fit cylinder

d_i Normal distance from measured point
          to best fit cylinder

FIG. 18   BEST FIT CYLINDER REFERENCE AXIS
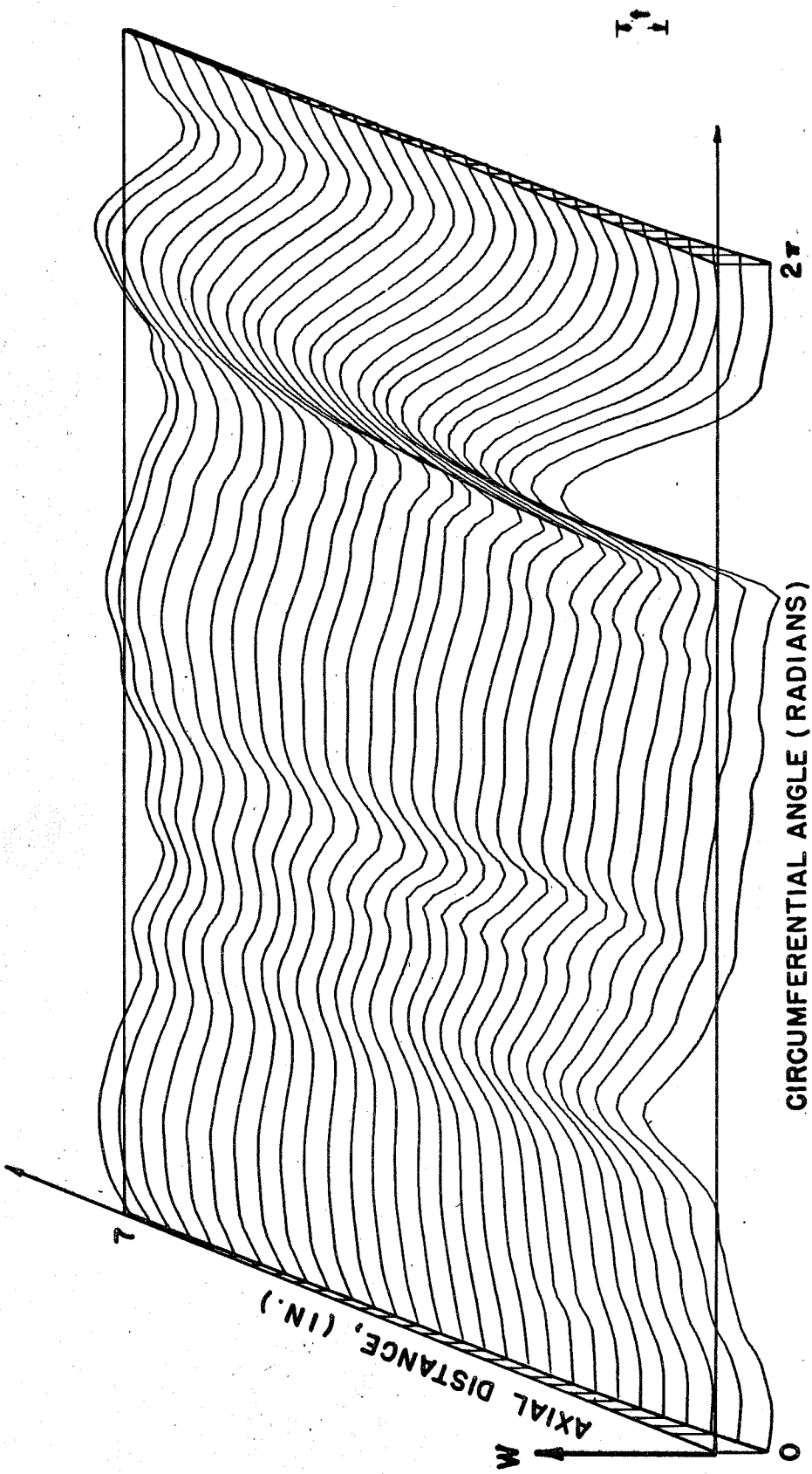
CIRCUMFERENTIAL ANGLE (RADIANS)

FIG. 19 INITIAL IMPERFECTION, SHELL A−7

CIRCUMFERENTIAL ANGLE (RADIANS)
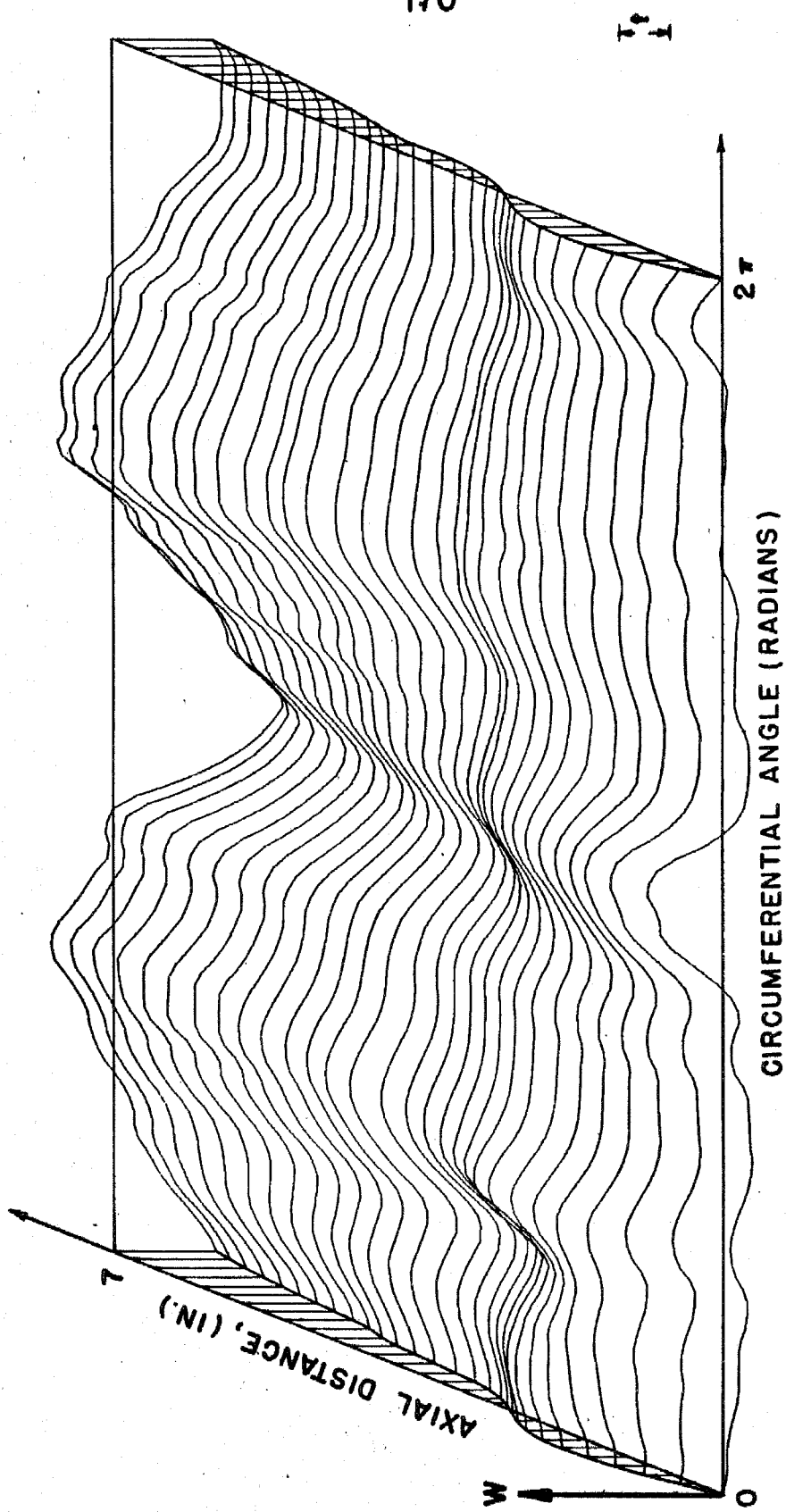
FIG. 20 INITIAL IMPERFECTION, SHELL A-8
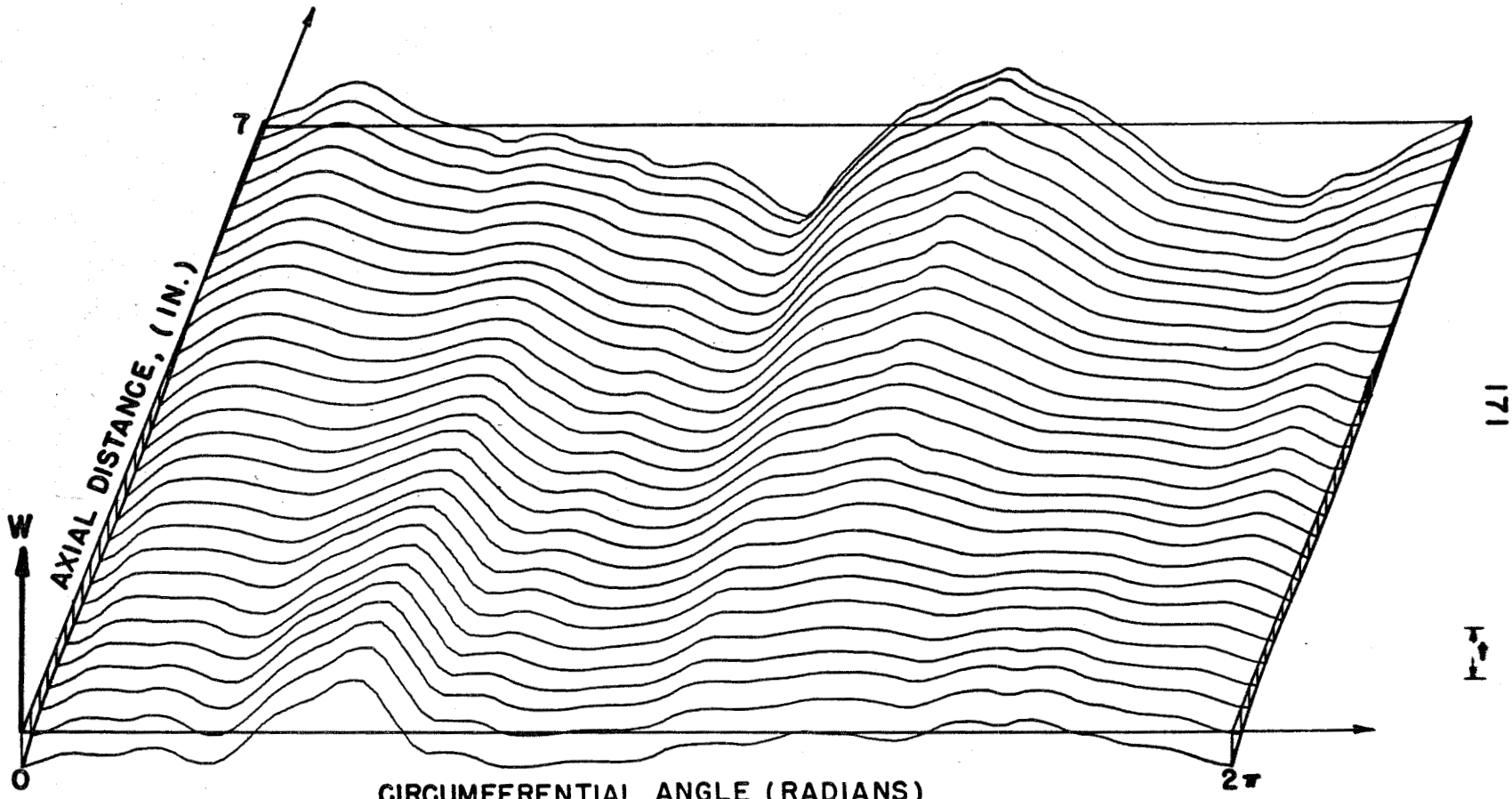
FIG. 21 INITIAL IMPERFECTION, SHELL A-9

AXIAL DISTANCE, (IN.)

CIRCUMFERENTIAL ANGLE (RADIANS)

W

O

7

2π

171

CIRCUMFERENTIAL ANGLE (RADIANS)
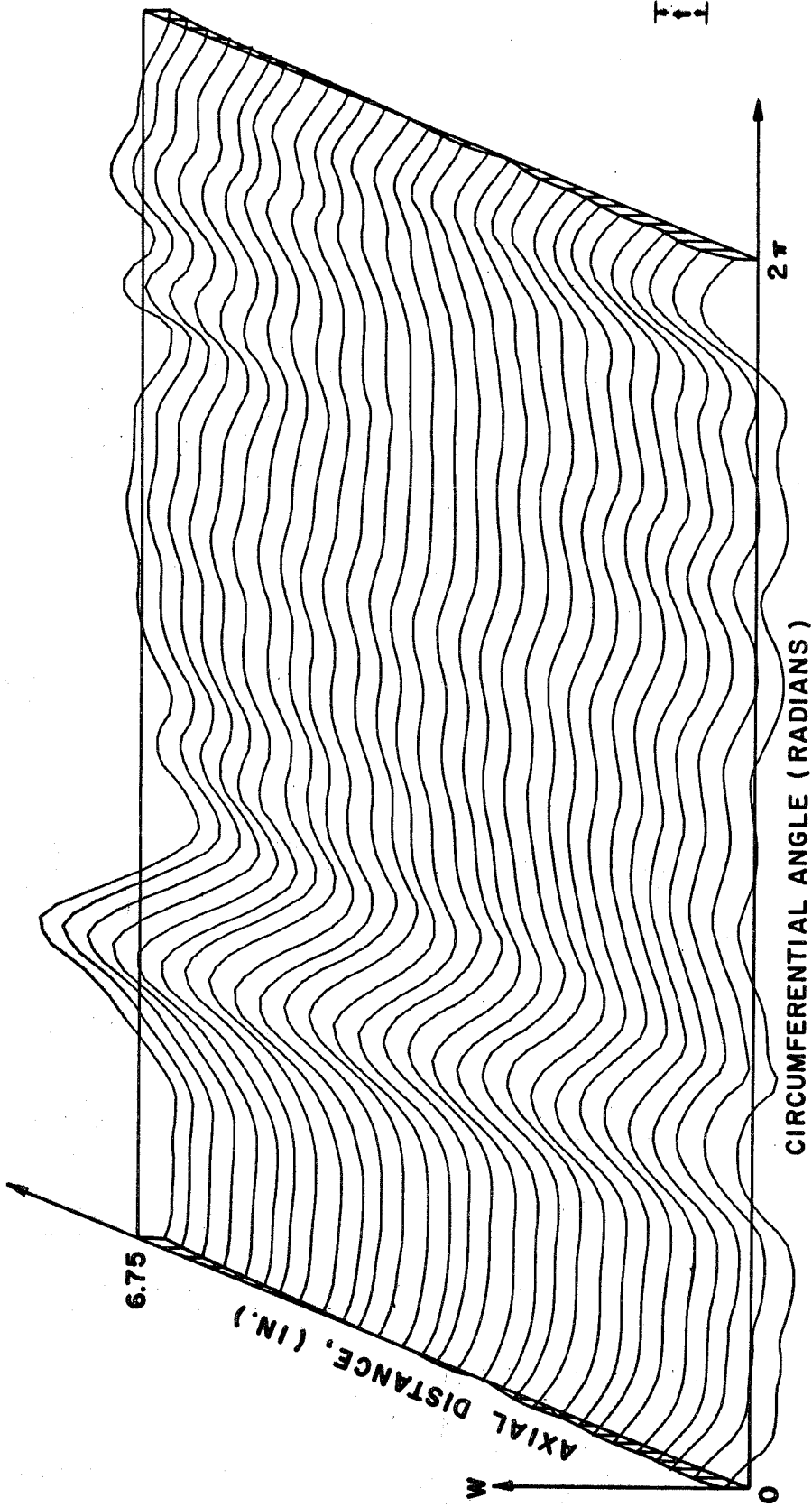
FIG.22 INITIAL IMPERFECTION, SHELL A-10
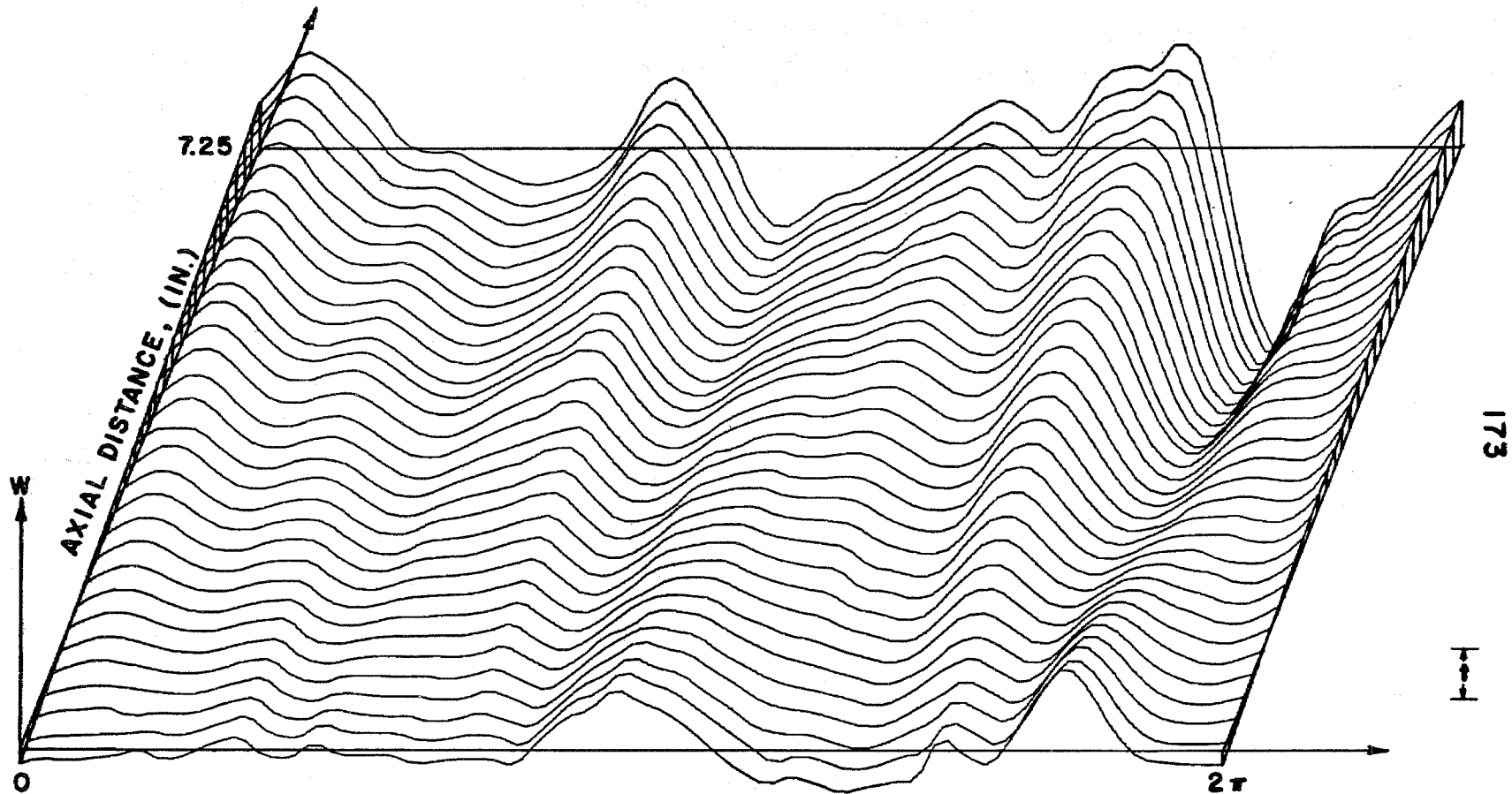
CIRCUMFERENTIAL ANGLE (RADIANS)

FIG.23 INITIAL IMPERFECTION, SHELL A - 12

173

174

2π

CIRCUMFERENTIAL ANGLE (RADIANS)

AXIAL DISTANCE, (IN.)

W

O
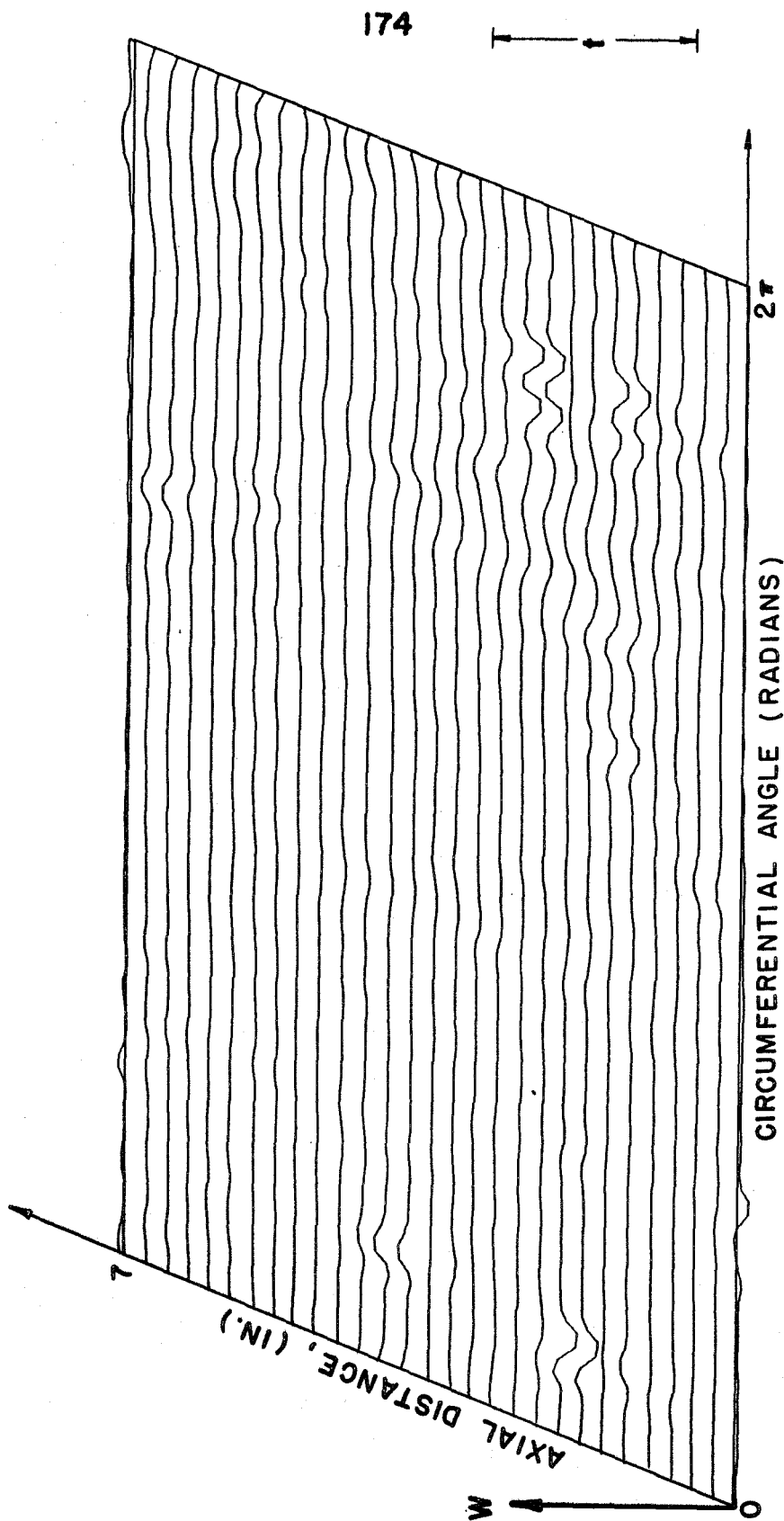
FIG. 24 PREBUCKLING DEFORMATION GROWTH AT $P/P_{CL} = 0.061$, SHELL A-7

175
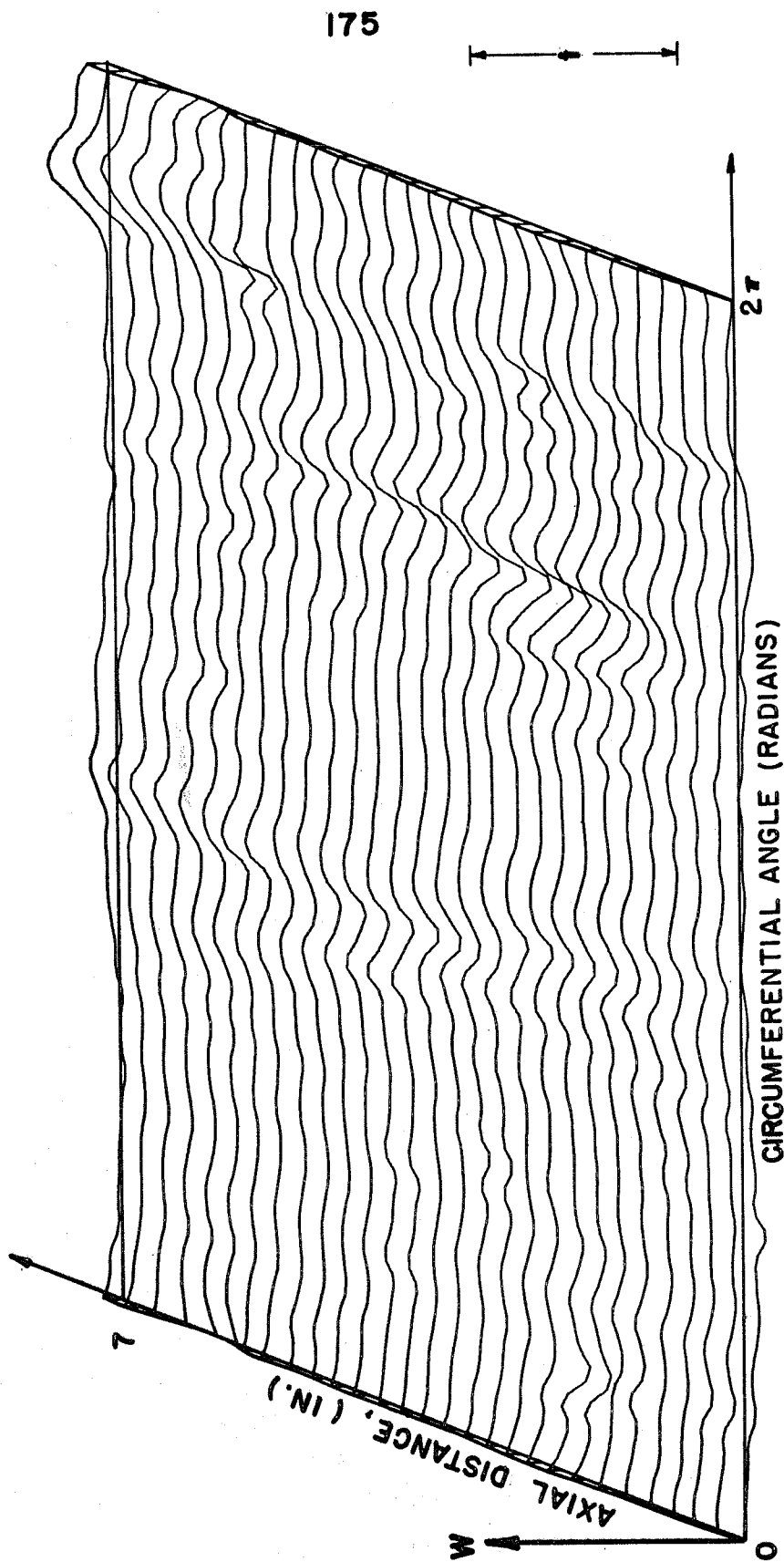
FIG. 25 PREBUCKLING DEFORMATION GROWTH AT $P/P_{CL} = 0.325$, SHELL A-7
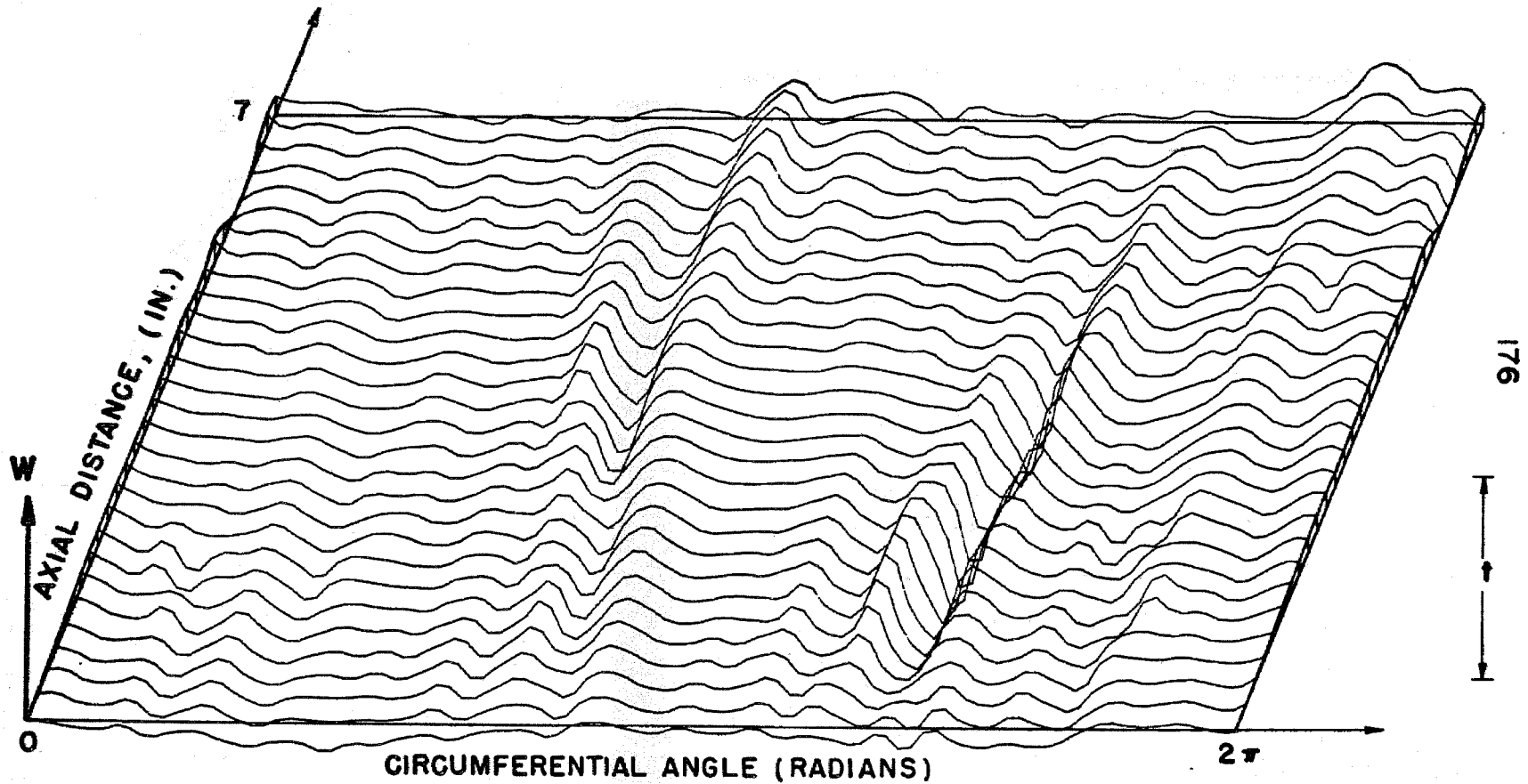
FIG. 26 PREBUCKLING DEFORMATION GROWTH AT $P/P_{CL} = 0.539$, SHELL A-7

176

CIRCUMFERENTIAL ANGLE (RADIANS)

FIG. 27 LOCAL BUCKLING DEFORMATION, SHELL A-7

·178

CIRCUMFERENTIAL ANGLE (RADIANS)
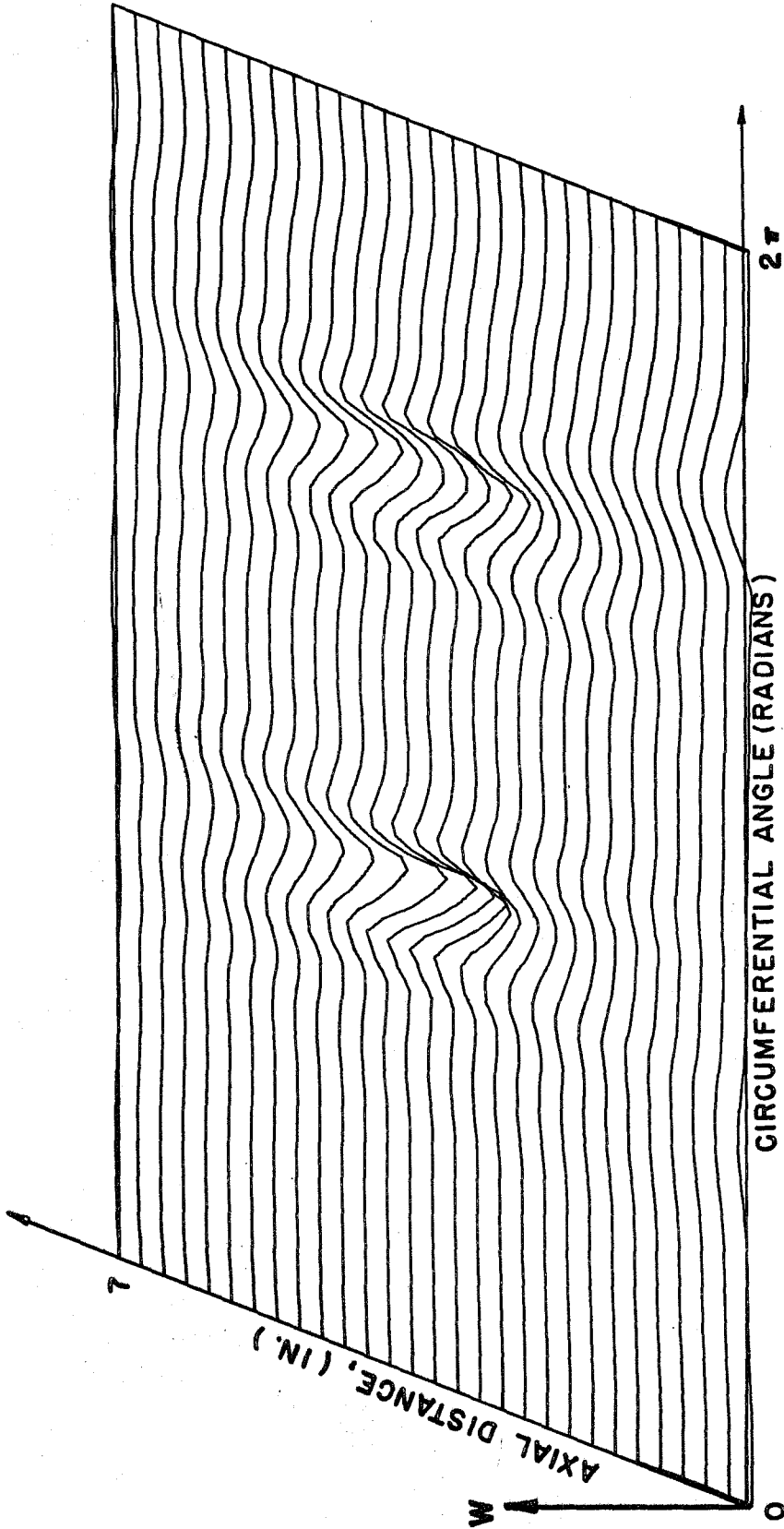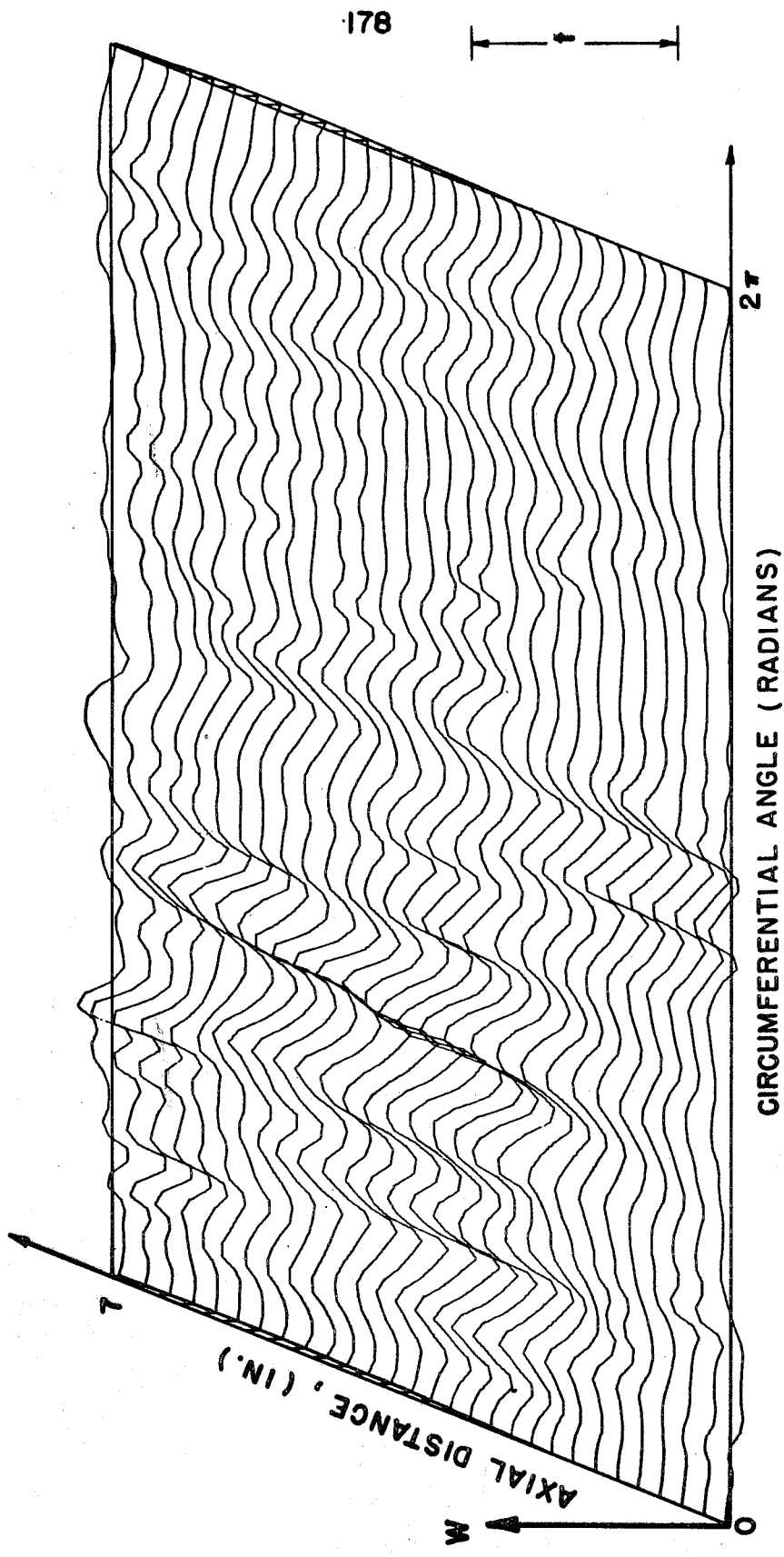
FIG. 28 PREBUCKLING DEFORMATION GROWTH AT $P/P_{CL} = 0.637$, SHELL A-8

CIRCUMFERENTIAL ANGLE (RADIANS)
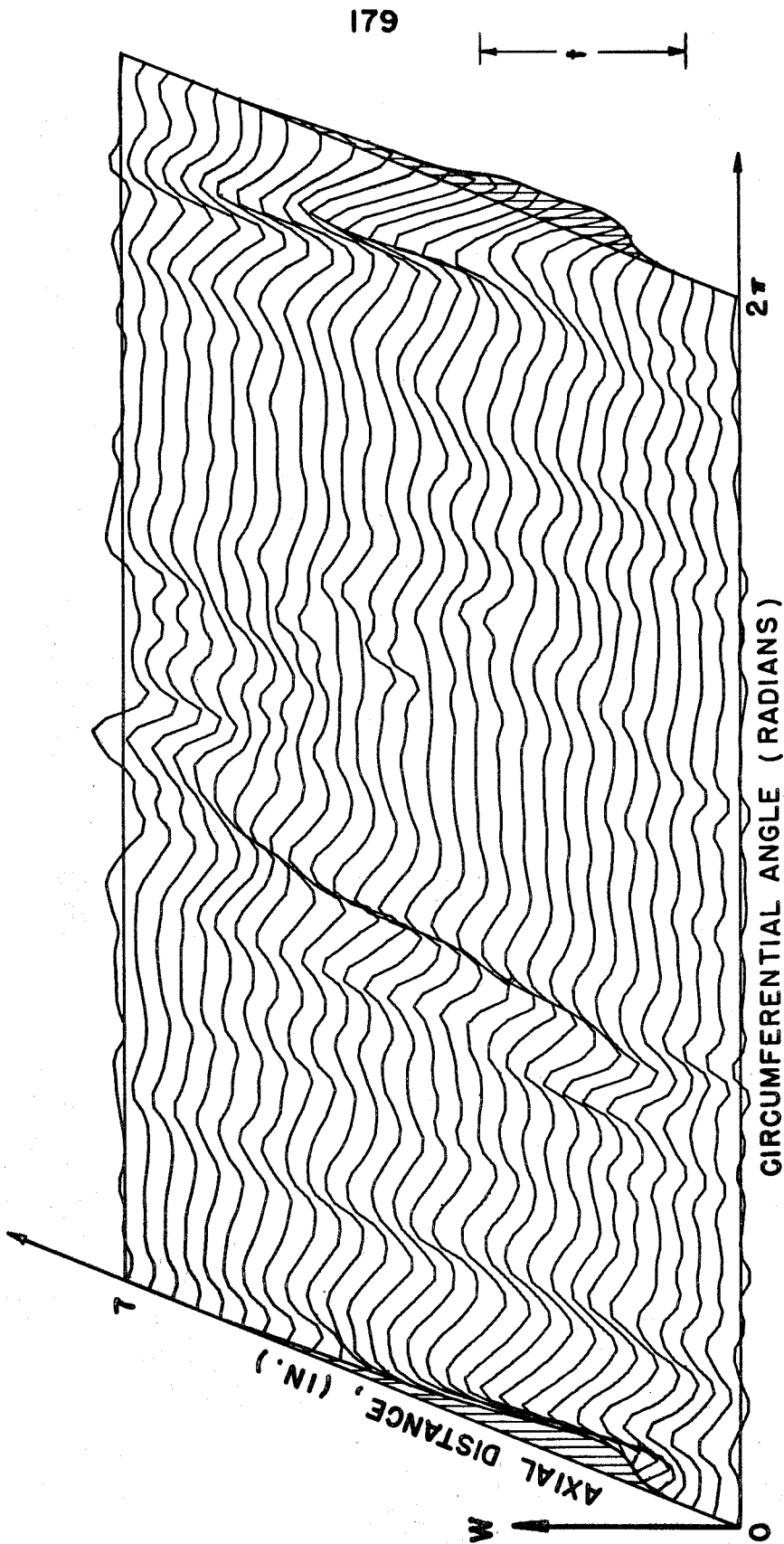
FIG.29 PREBUCKLING DEFORMATION GROWTH AT P/P_{CL} =0.722, SHELL A-9

180

CIRCUMFERENTIAL ANGLE (RADIANS)

2π

AXIAL DISTANCE, (IN.)

6.75

0

W
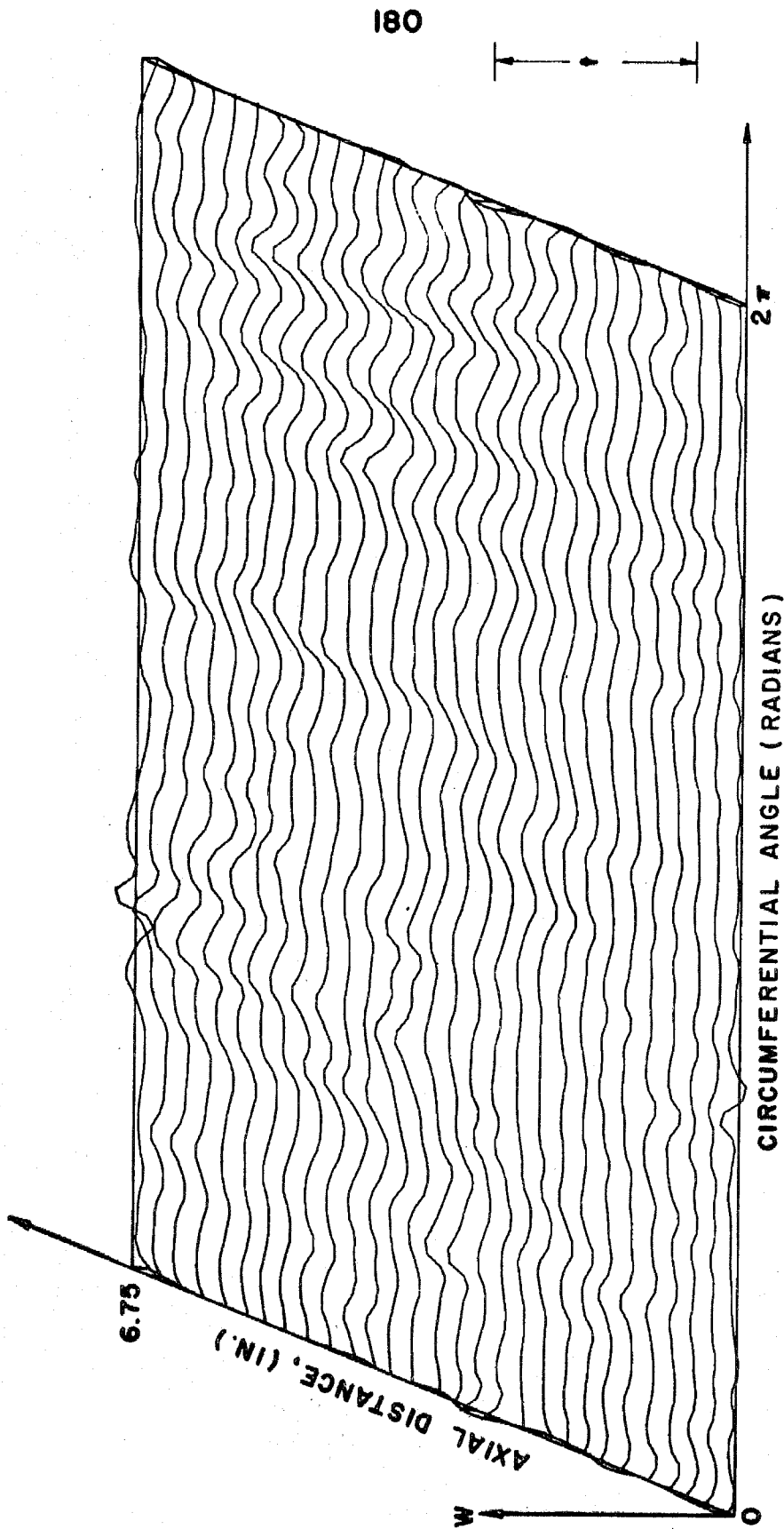
FIG. 30 PREBUCKLING DEFORMATION GROWTH AT $\frac{P}{P_{c\ell}}$ = 0.439, SHELL A-10
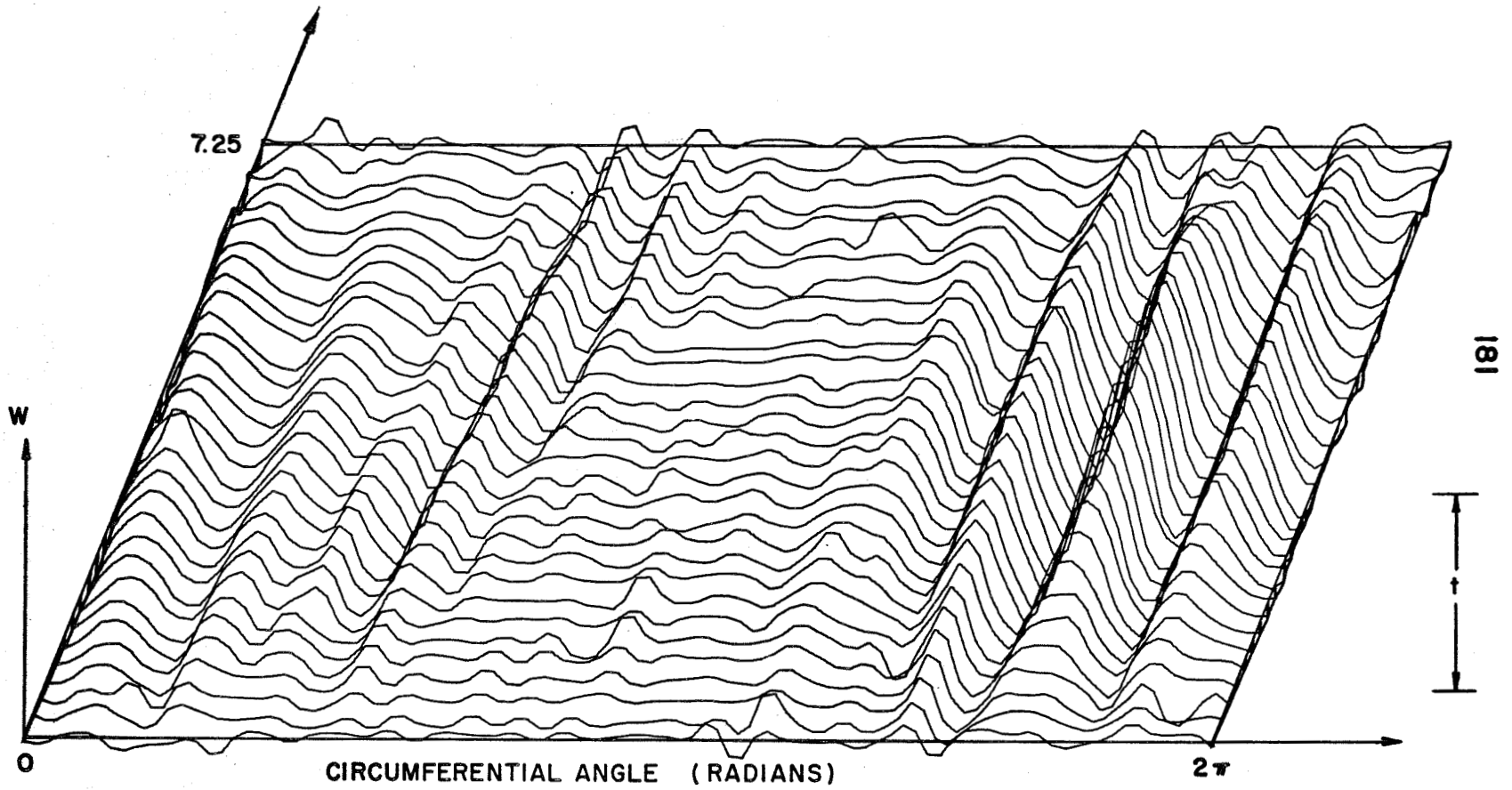
FIG. 31 PREBUCKLING DEFORMATION GROWTH AT $\dfrac{P}{P_{c\ell}} = 0.594$, SHELL A-12

181

CIRCUMFERENTIAL ANGLE (RADIANS)

FIG.33 POST BUCKLING DEFORMATION, SHELL A-7

CIRCUMFERENTIAL ANGLE (RADIANS)
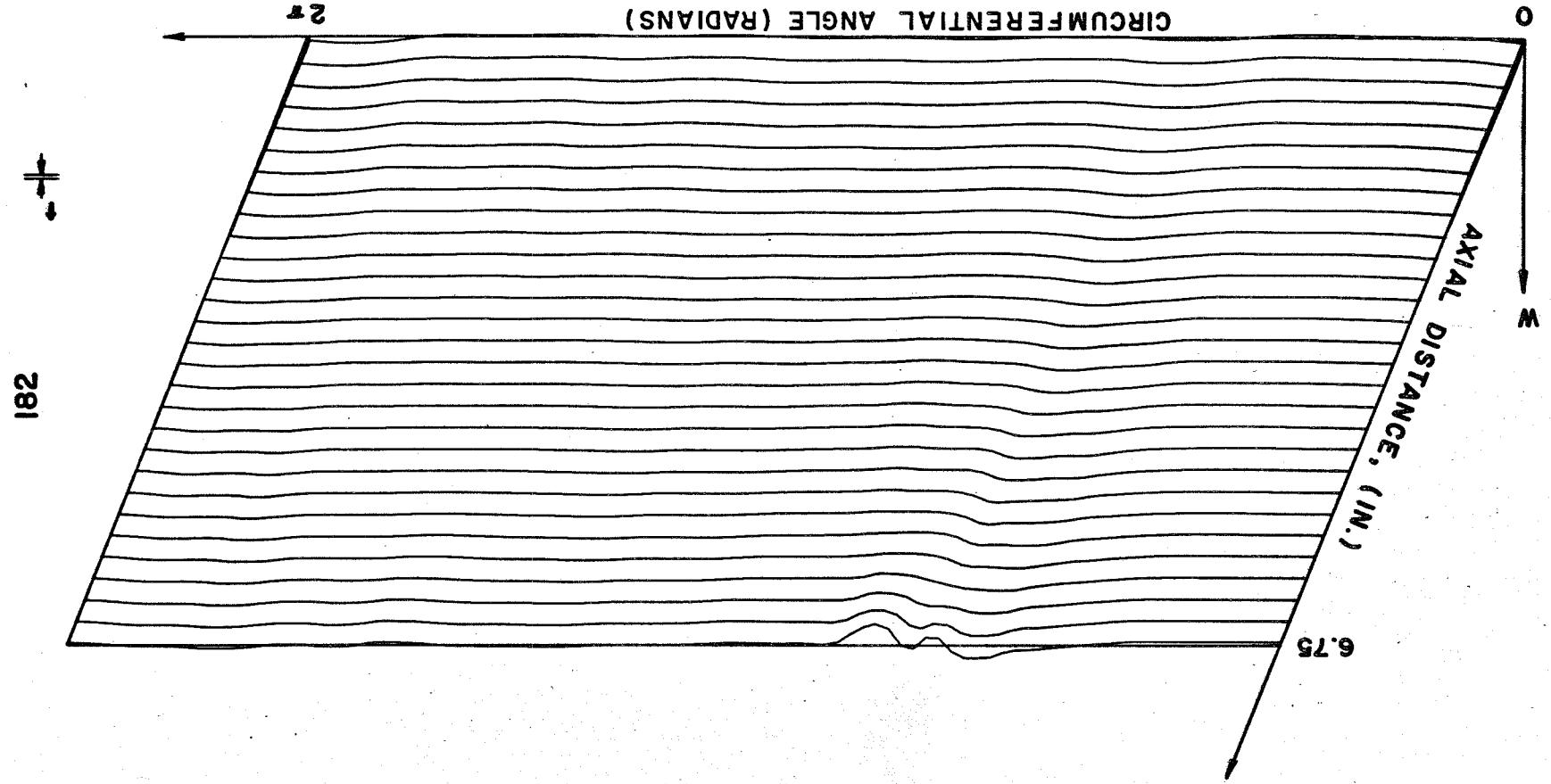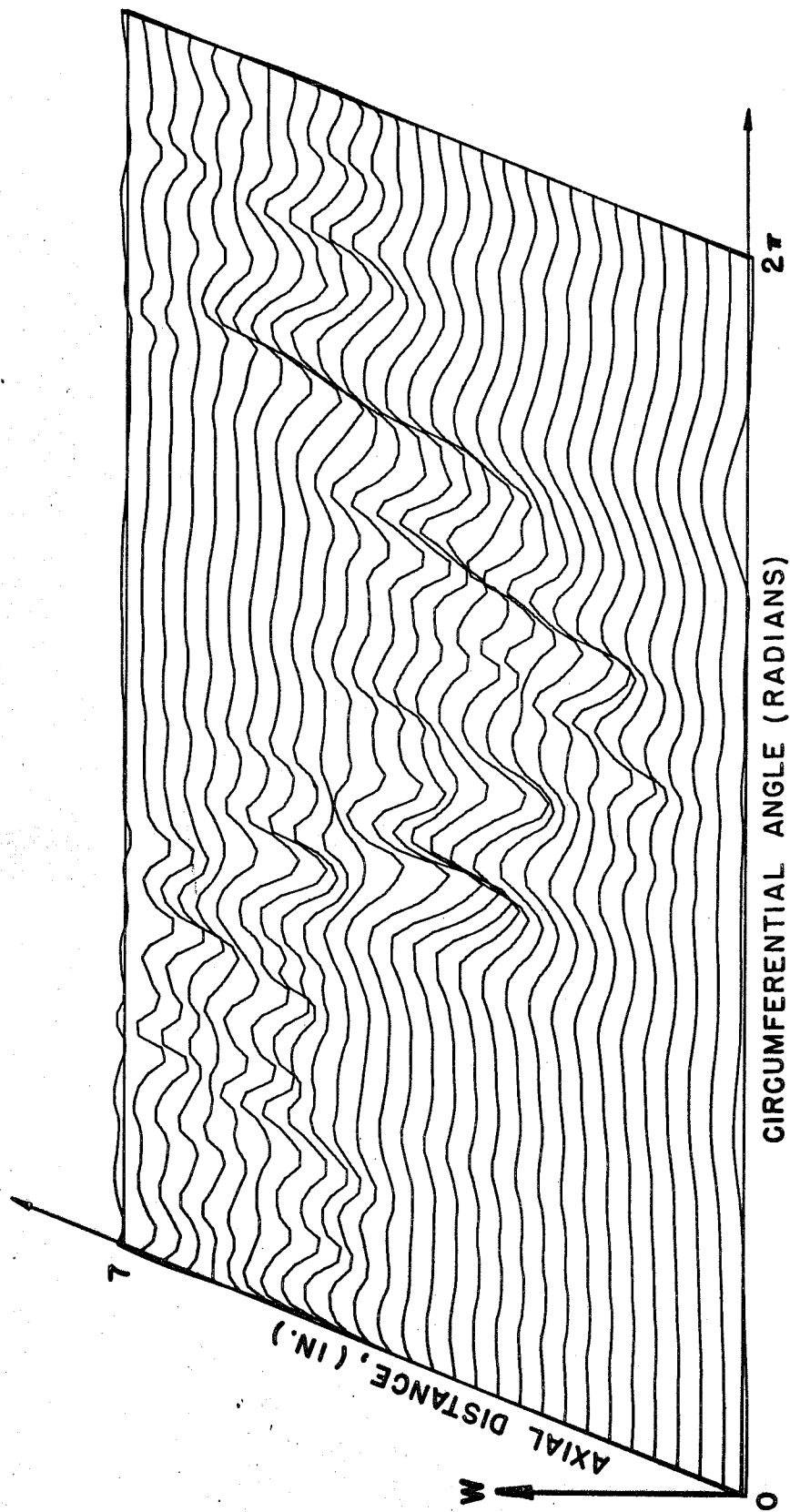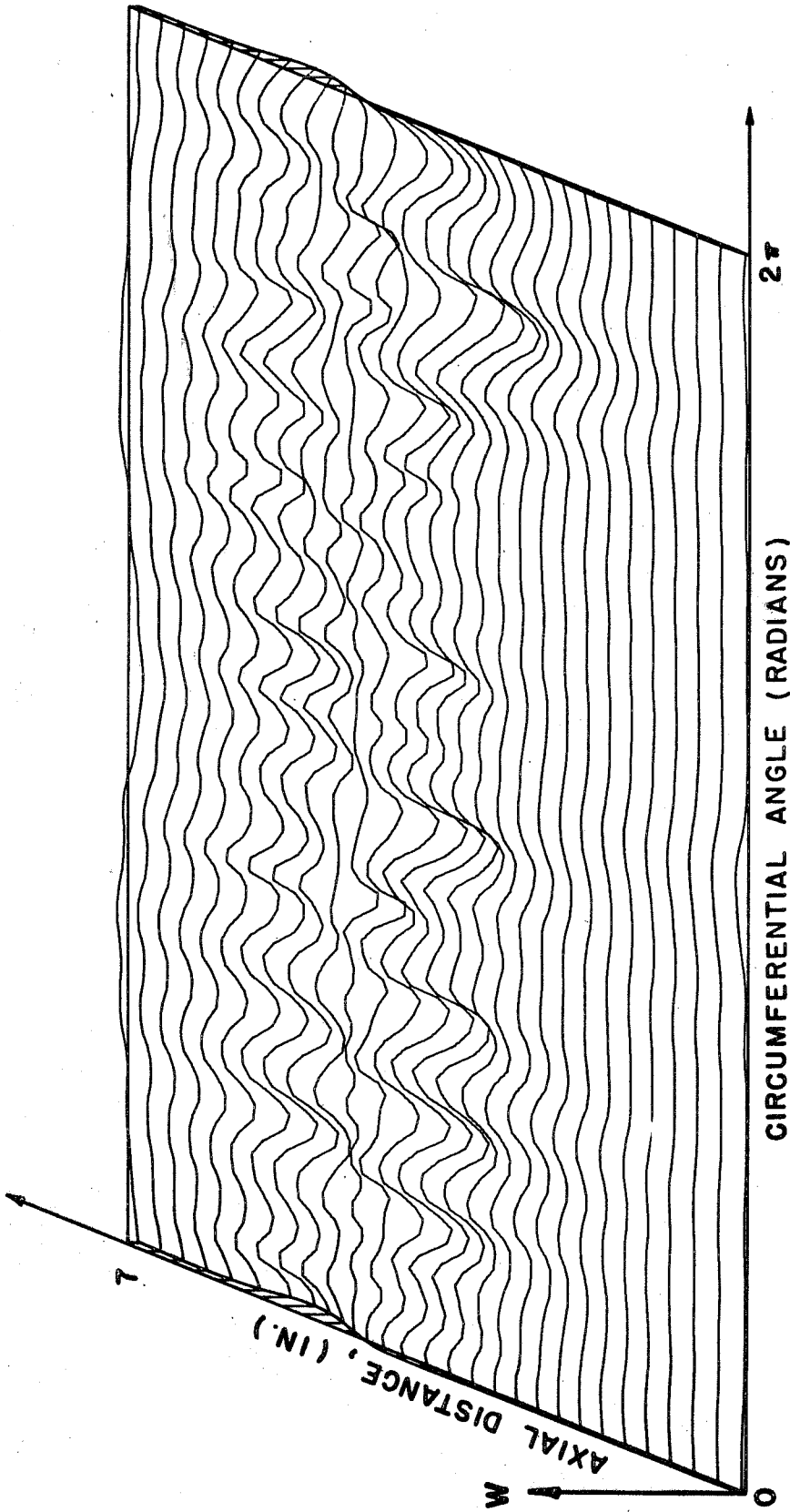
FIG.34 POSTBUCKLING DEFORMATION , SHELL A−8

CIRCUMFERENTIAL ANGLE (RADIANS)
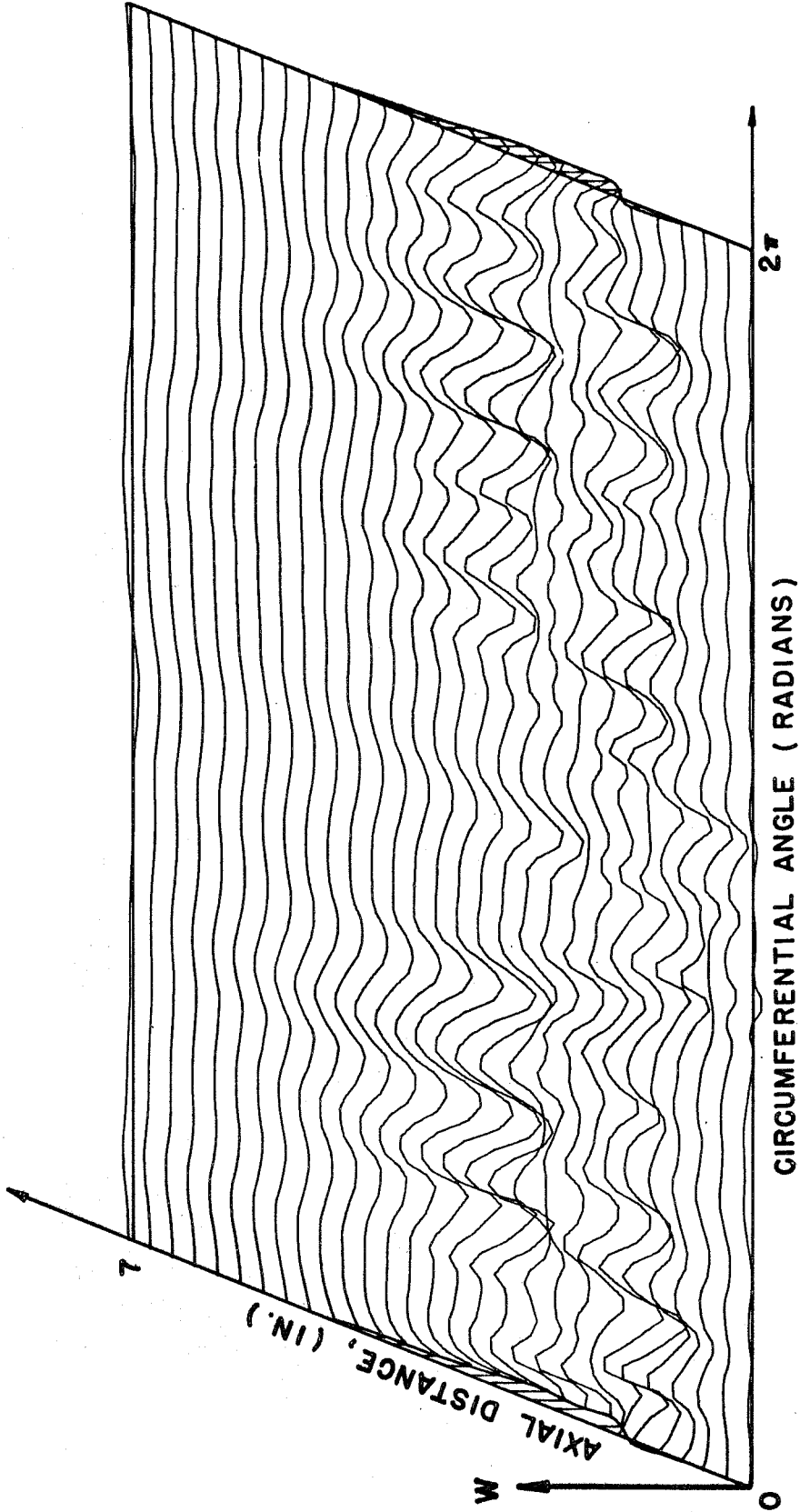
FIG. 35 POSTBUCKLING DEFORMATION , SHELL A - 9

CIRCUMFERENTIAL ANGLE (RADIANS)
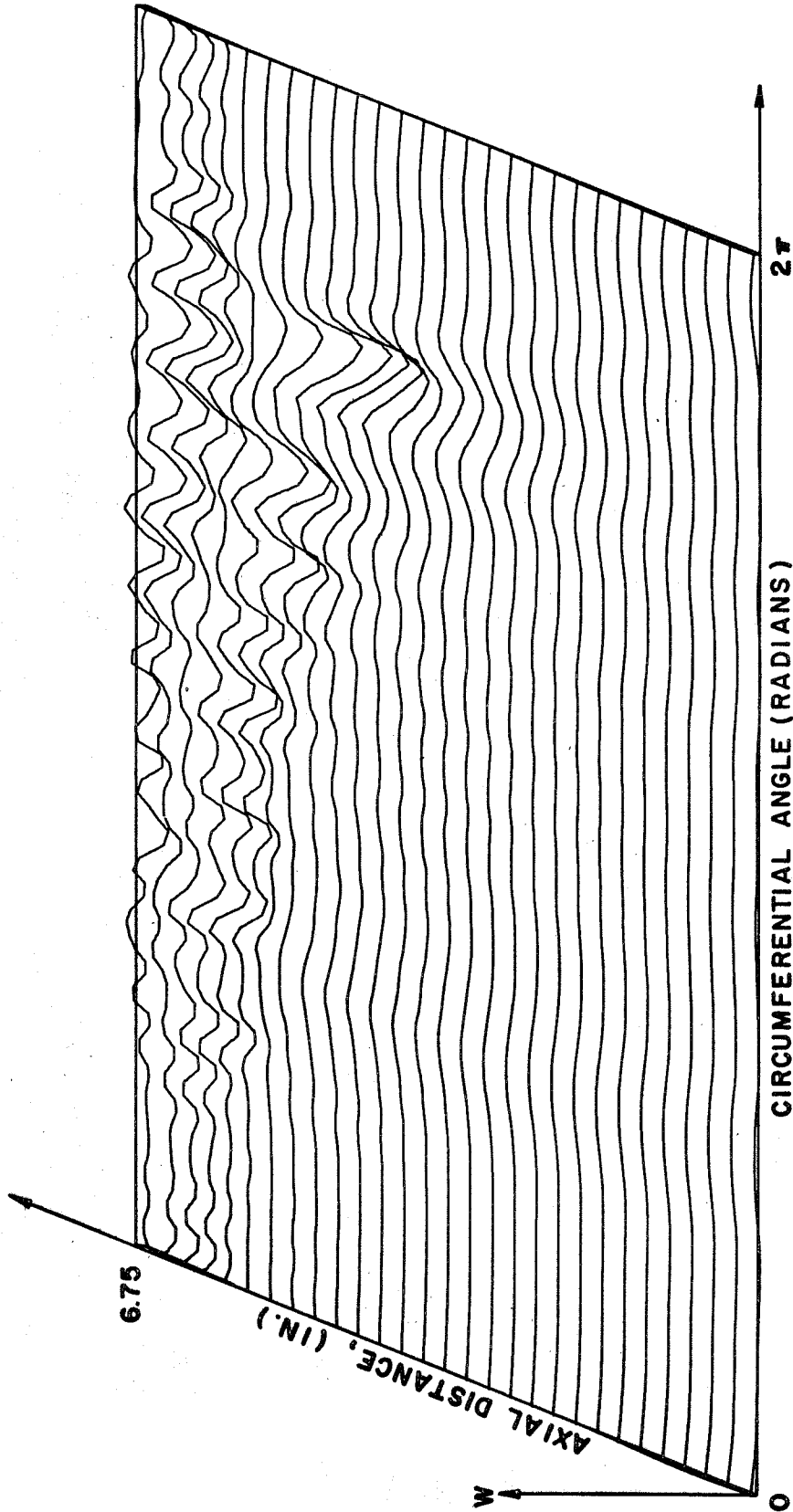
FIG.36 POST BUCKLING DEFORMATION, SHELL A - 10

CIRCUMFERENTIAL ANGLE (RADIANS)
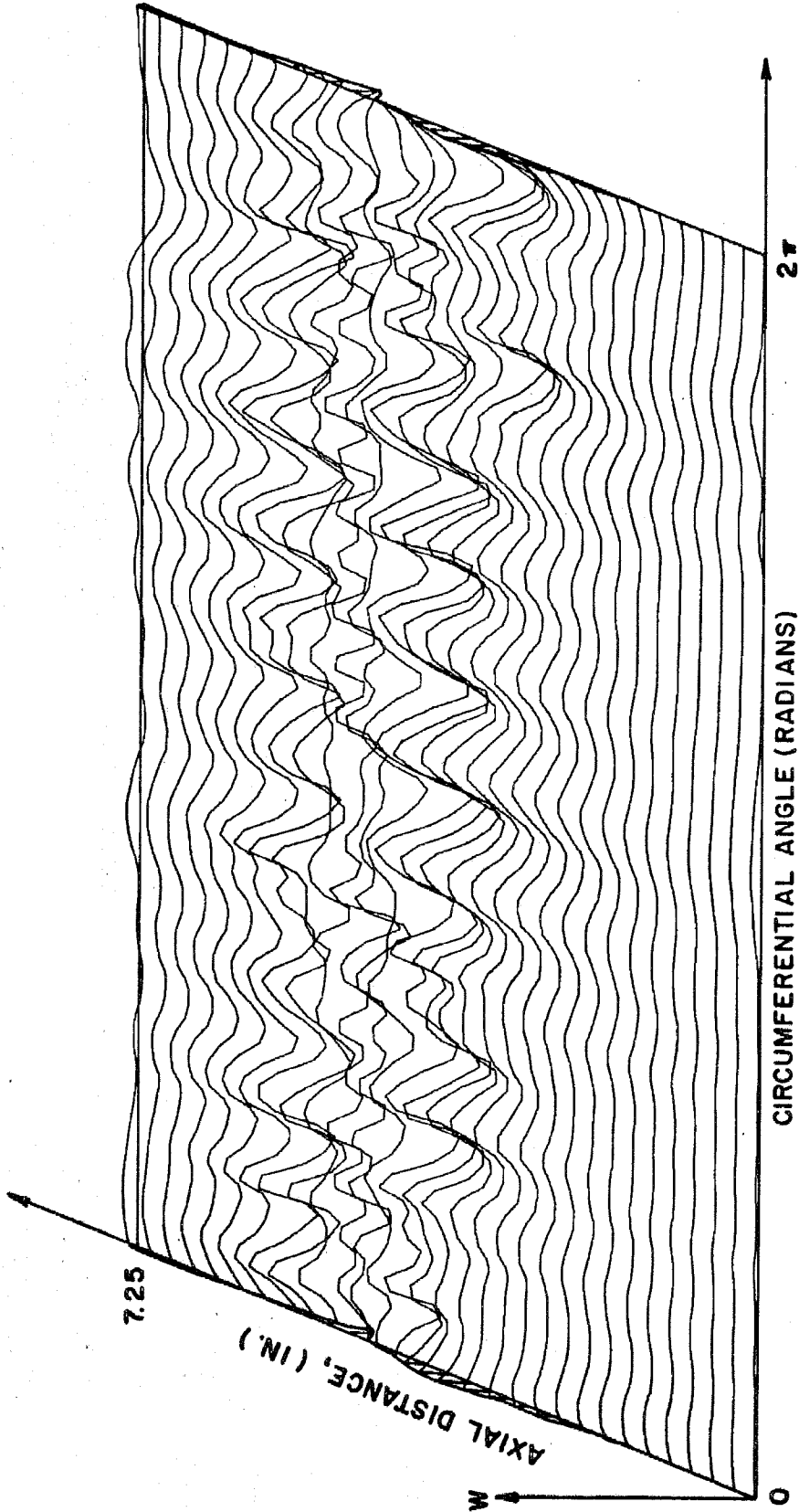
FIG.37 POST BUCKLING DEFORMATION, SHELL A – 12
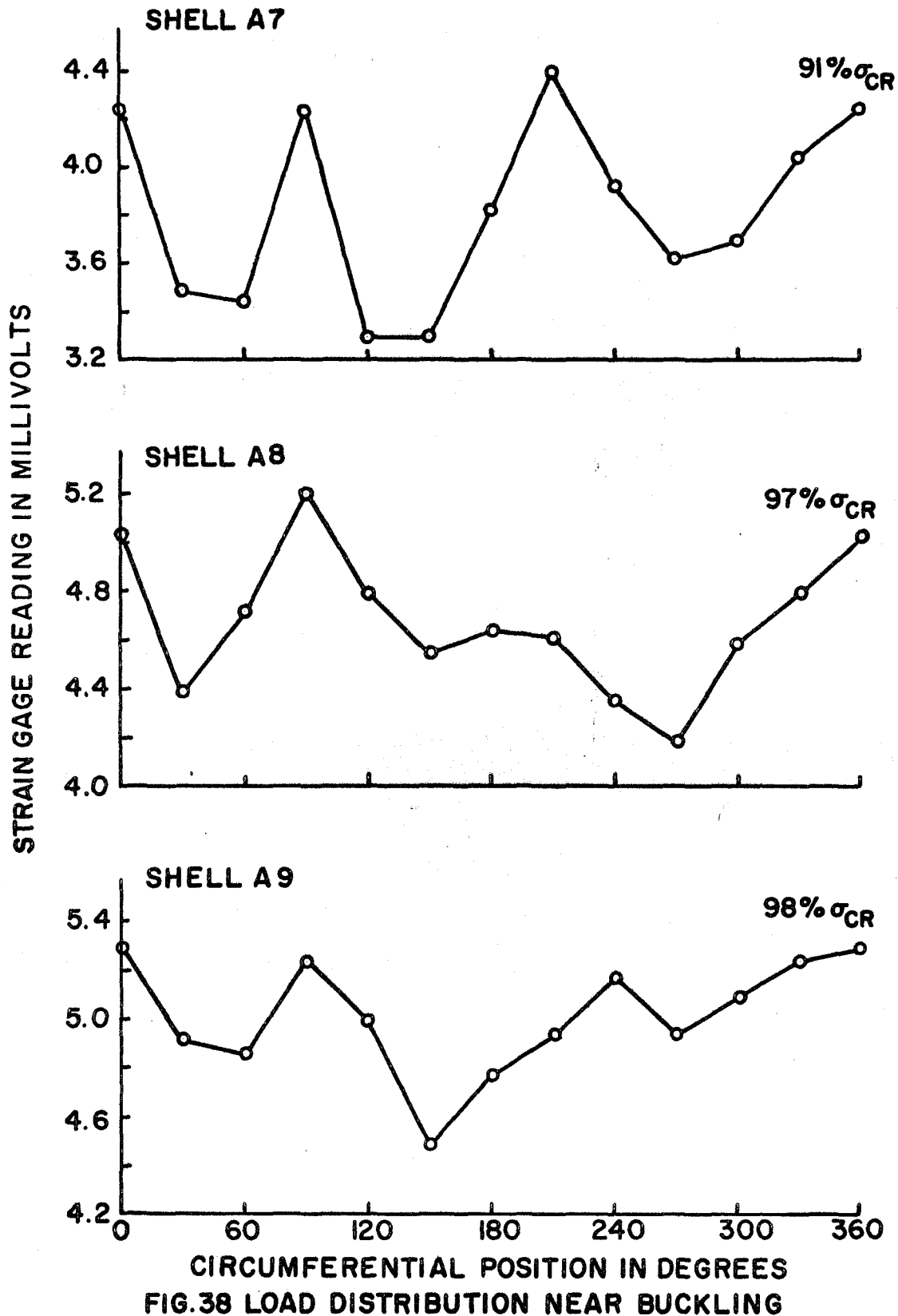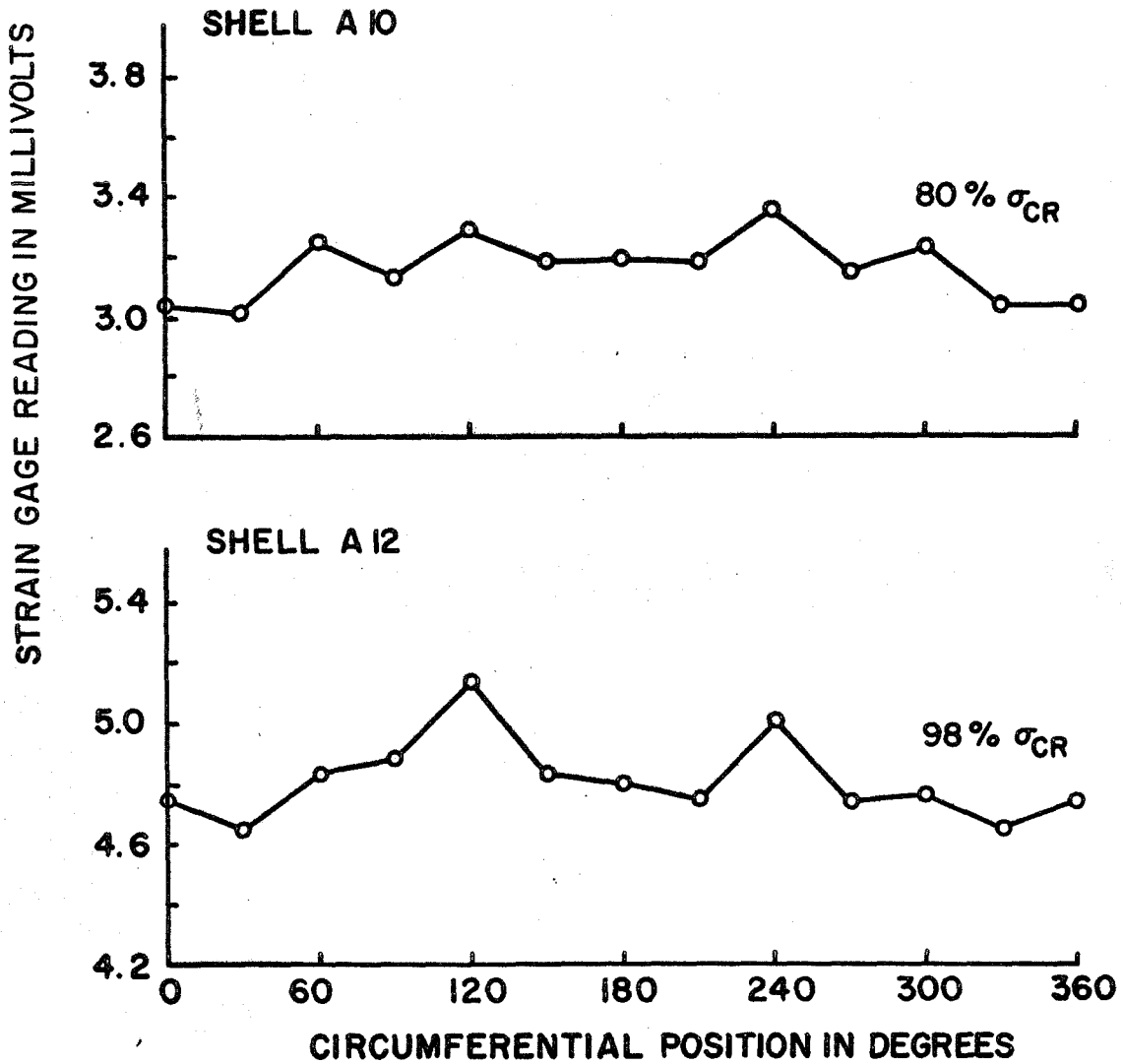
FIG.38 LOAD DISTRIBUTION NEAR BUCKLING

FIG.39 LOAD DISTRIBUTION NEAR BUCKLING
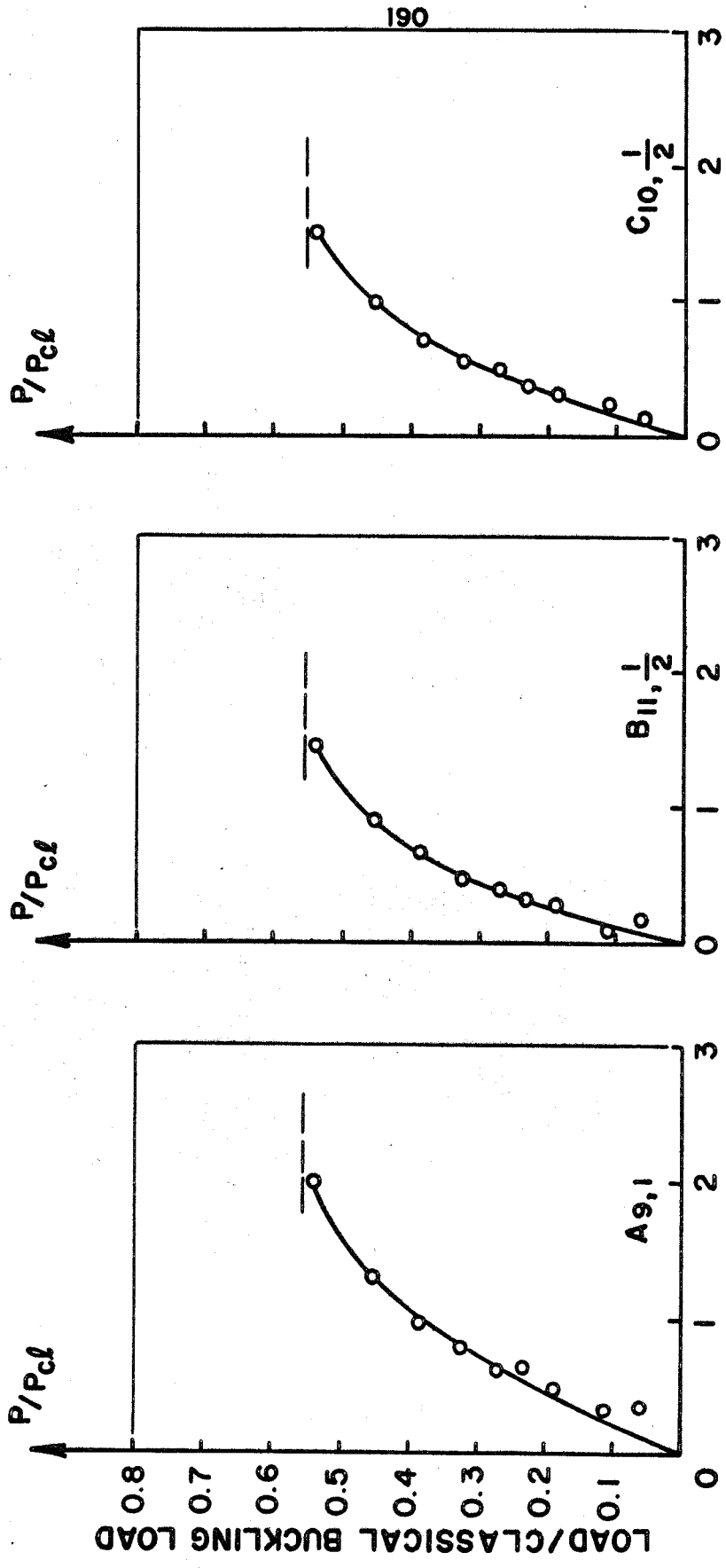
FIG. 40 GROWTH OF FOURIER COEFFICIENT FOR SHELL A7
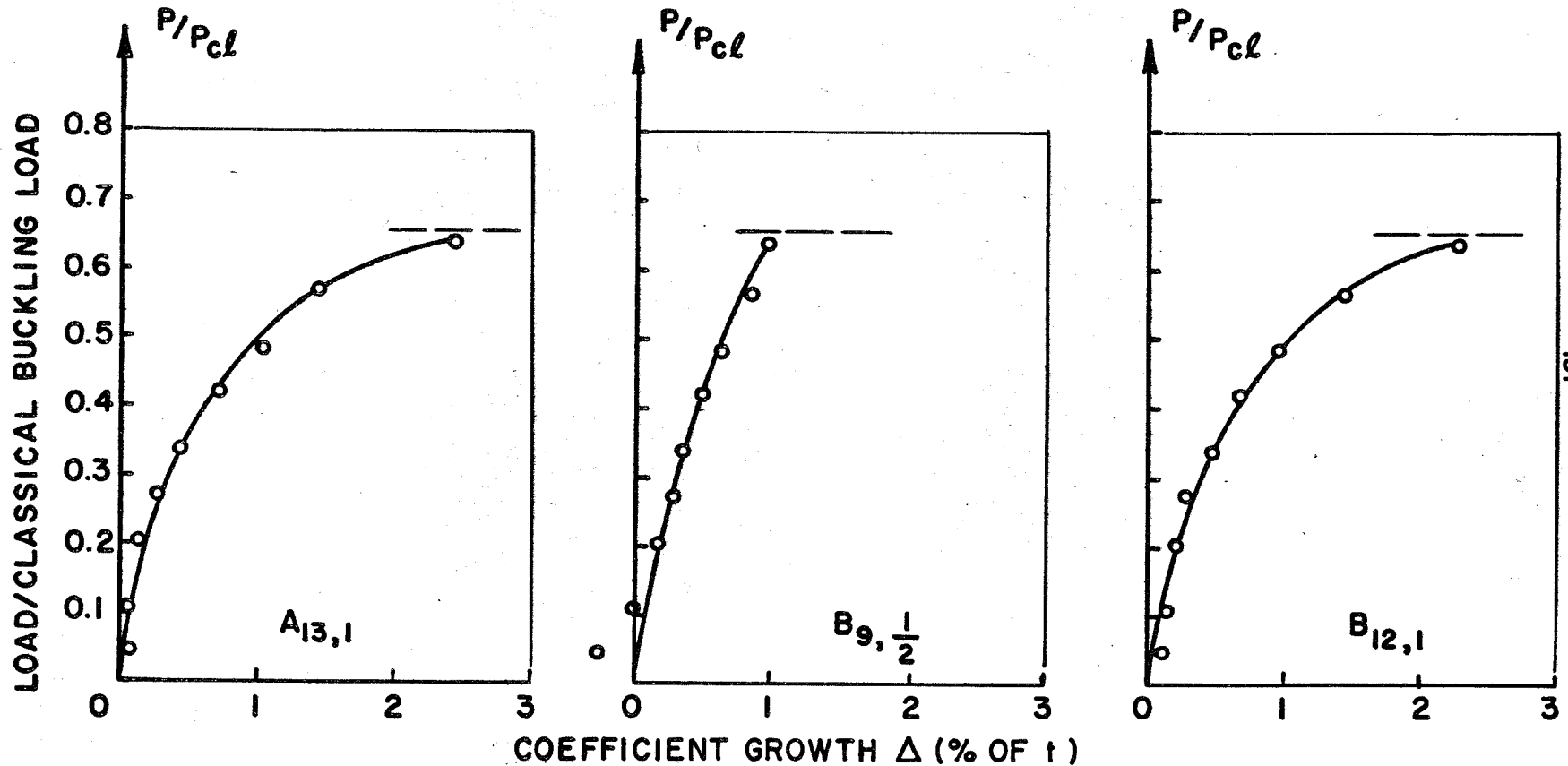
FIG. 41 GROWTH OF FOURIER COEFFICIENTS FOR SHELL A8

192
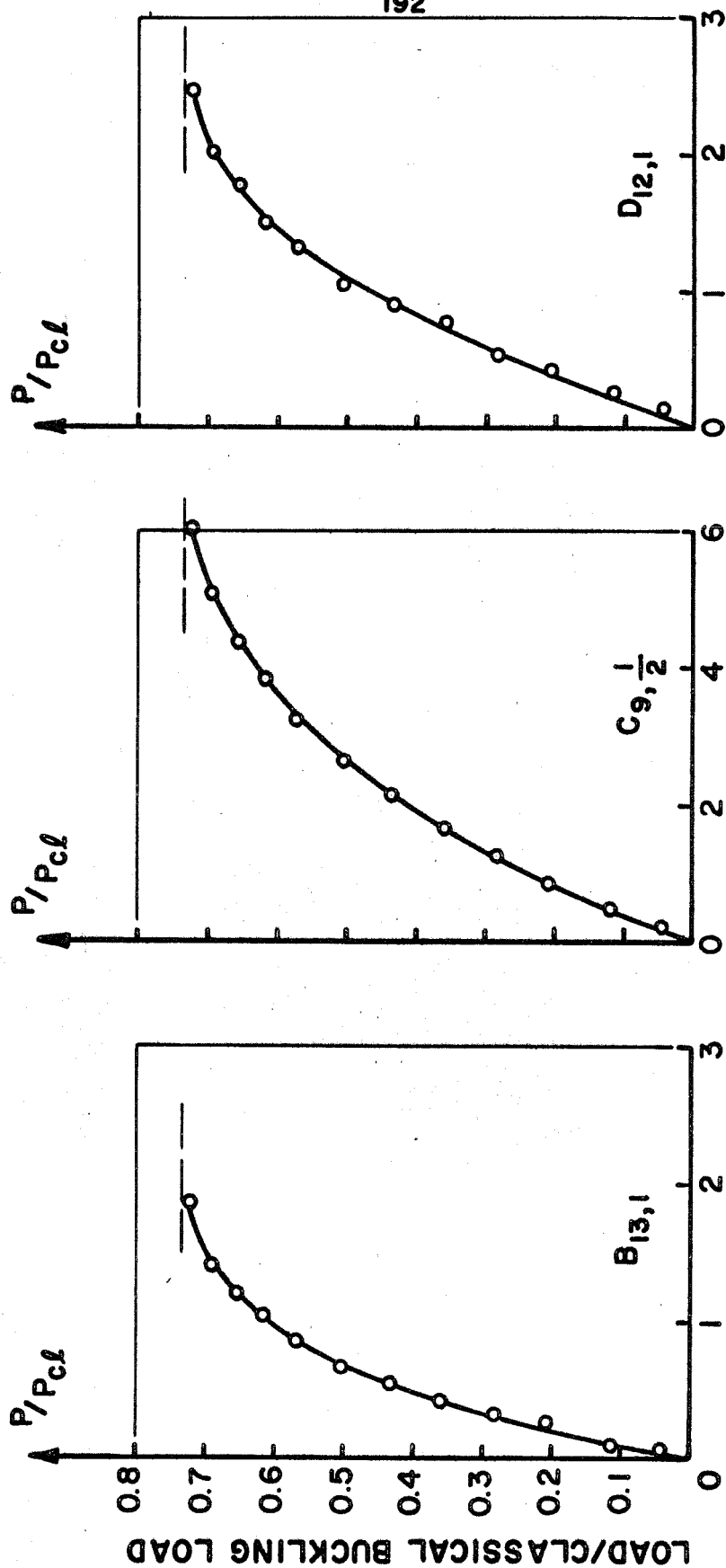
FIG. 42 GROWTH OF FOURIER COEFFICIENTS FOR SHELL A9
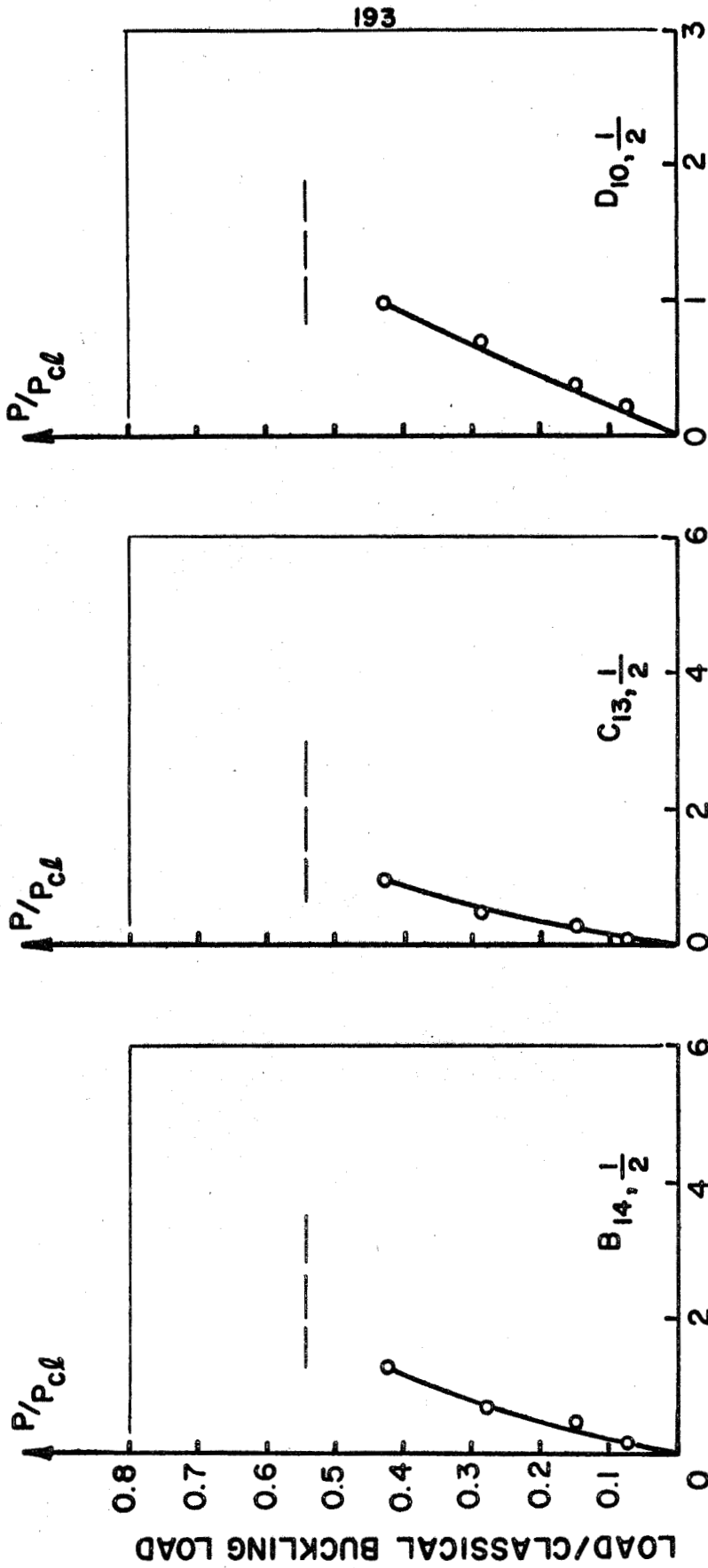
FIG. 43 GROWTH OF FOURIER COEFFICIENTS FOR SHELL A10
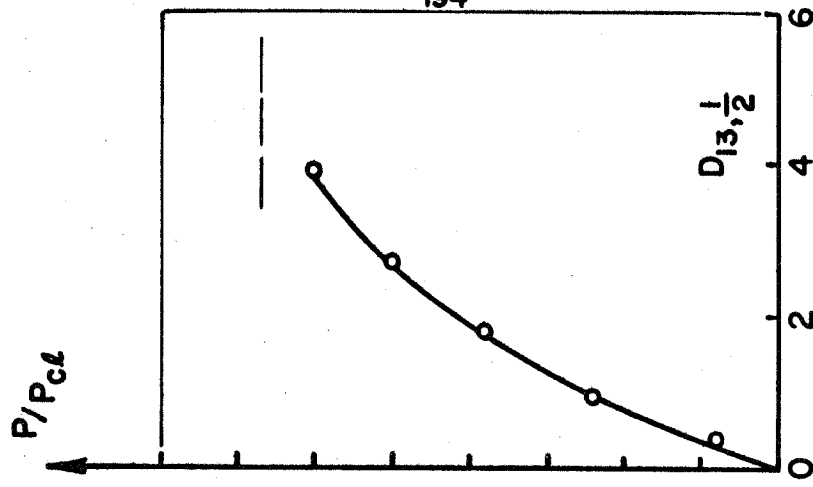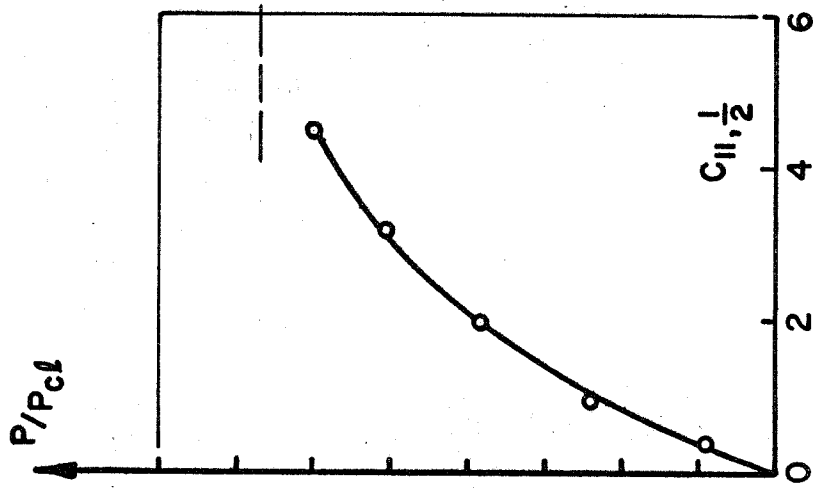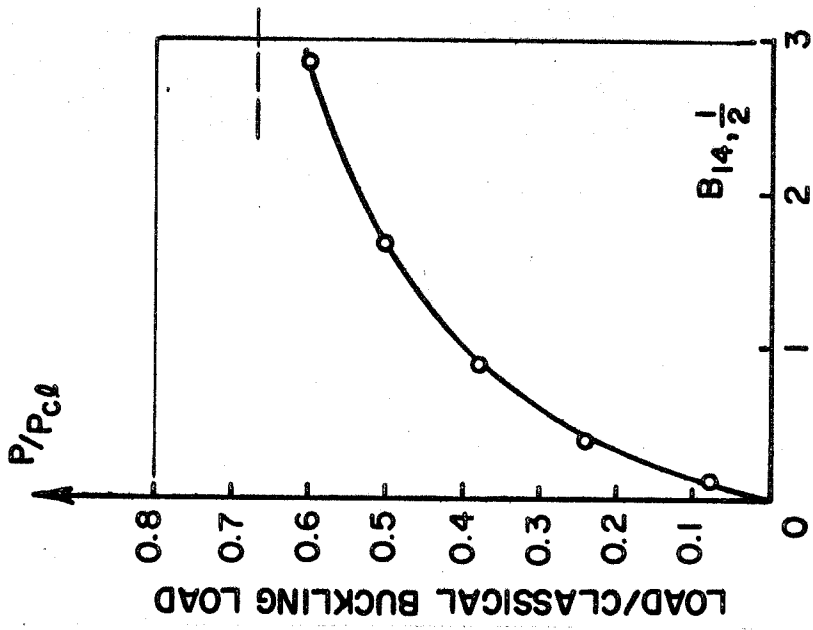
FIG. 44 GROWTH OF FOURIER COEFFICIENTS FOR SHELL A 12
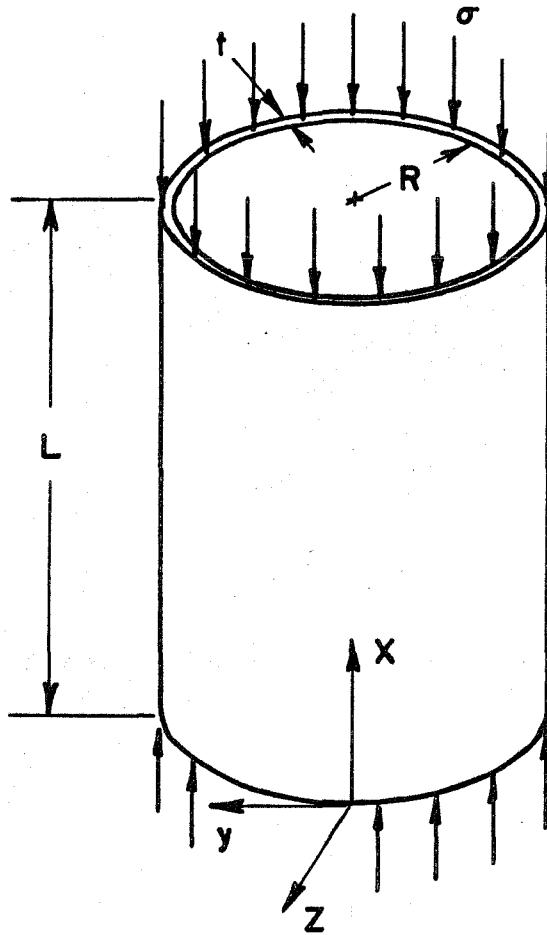
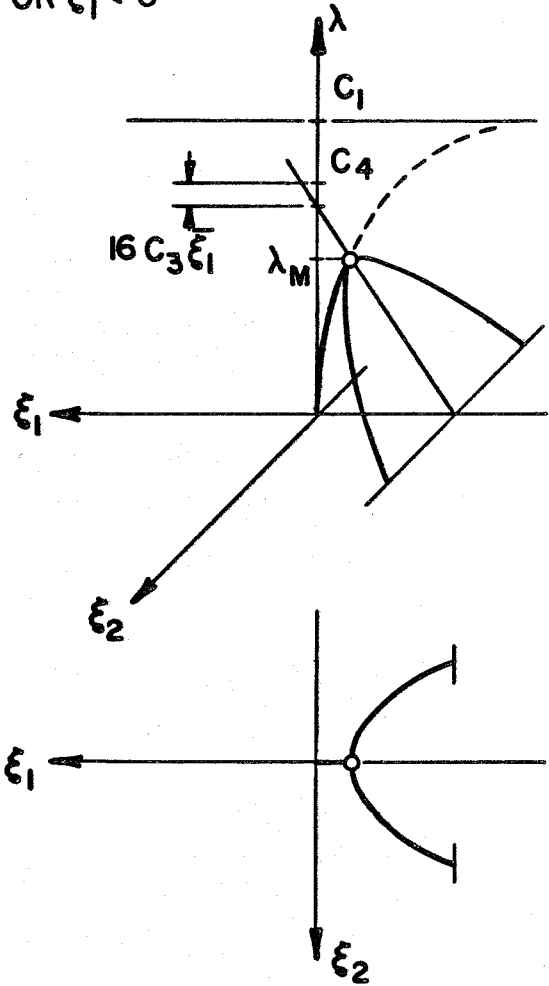FIG. 45 SHELL GEOMETRY AND COORDINATE SYSTEM

FOR $C_1 > C_4$

FOR $C_1 < C_4$
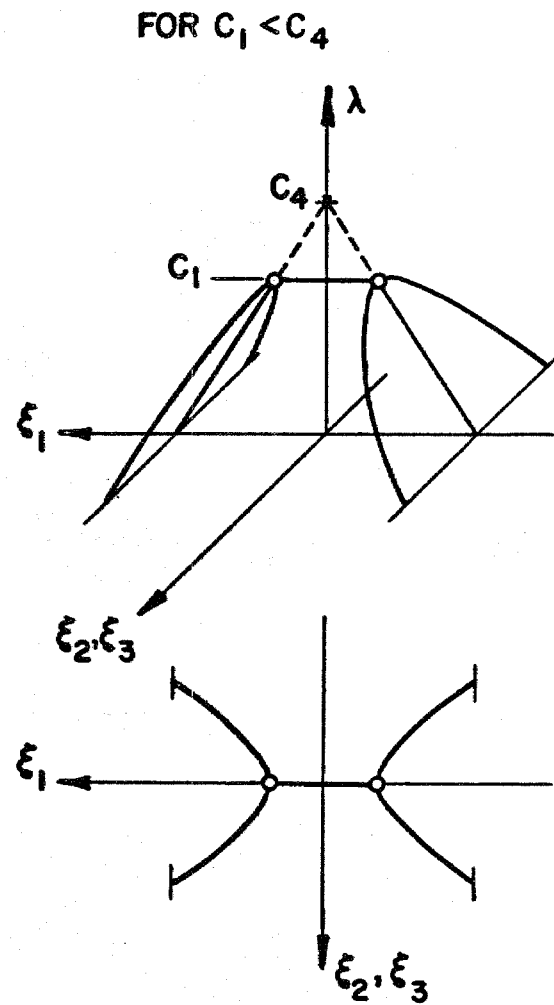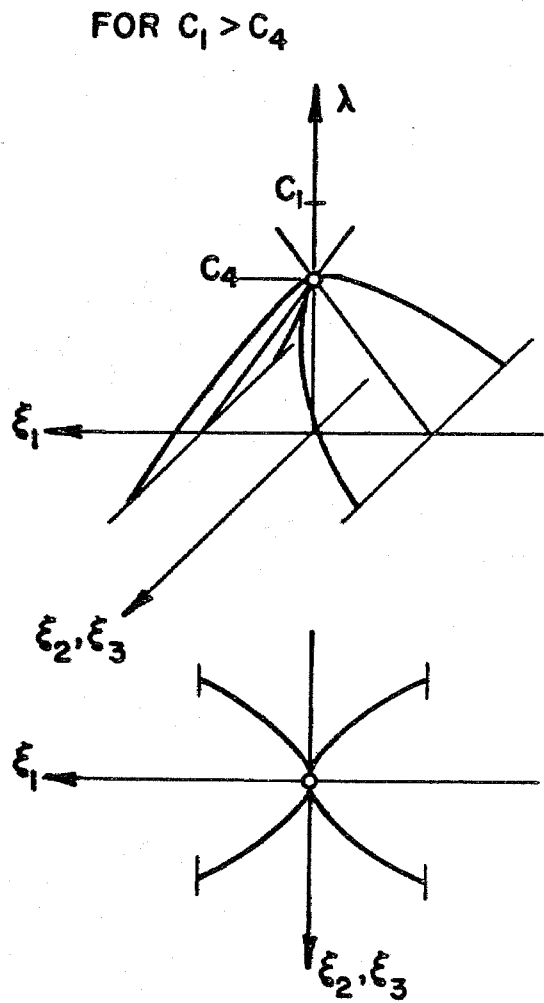
FIG. 46 POST-BUCKLING EQUILIBRIUM PATHS FOR PERFECT SHELLS

196
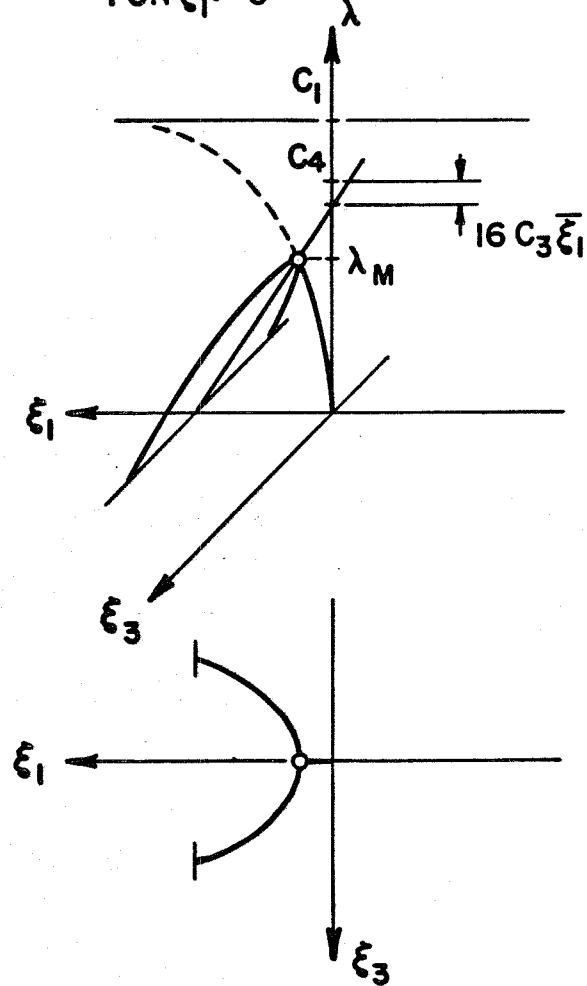
FIG. 47   POST BUCKLING EQUILIBRIUM PATHS FOR SHELLS WITH AXISYMMETRIC
IMPERFECTIONS

FOR $\bar{\xi}_1 < 0 ; \bar{\xi}_2 \neq 0$

FOR $\bar{\xi}_1 > 0 ; \bar{\xi}_3 \neq 0$

PLOT OF EQ. (5.8)

PLOT OF EQ. (5.16)

$\lambda_{BIF.}$

λ_M

C_1

C_4

ξ_1

ξ_2

ξ_3

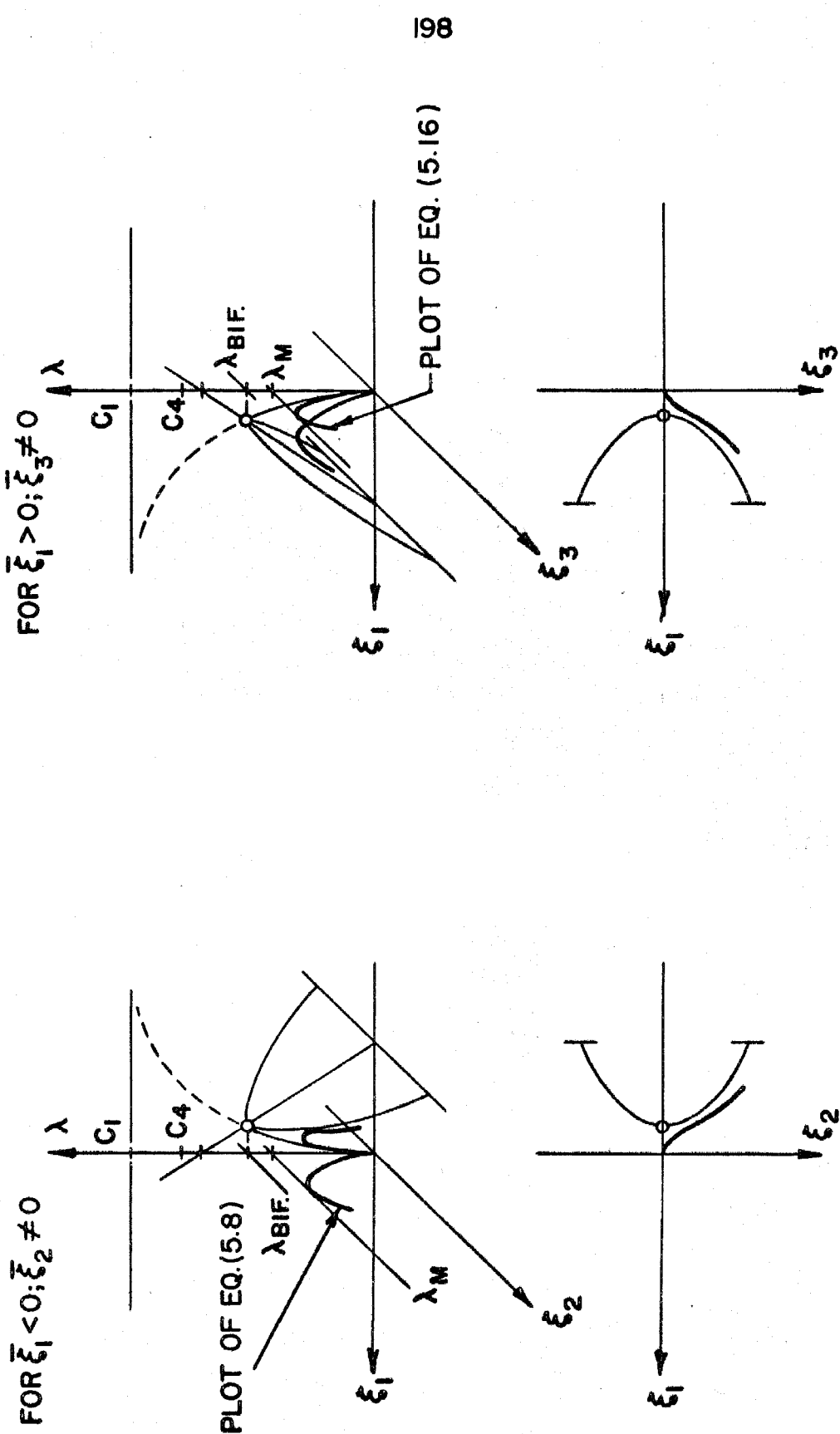FIG. 48 POST- BUCKLING EQUILIBRIUM PATHS FOR SHELLS WITH BOTH AXISYMMETRIC AND ASYMMETRIC IMPERFECTIONS